

Electronics: Microwave Antennas:

MODIFICATIONS OF SECONDARY REFLECTOR ANTENNA
PATTERNS DUE TO SHAPED BEAMS FROM
FLANGED PRIMARY HORN FEEDS

A Thesis Submitted by
P R A V I N K U M A R P . A .

in partial fulfilment of
the requirements for the degree of

DOCTOR OF PHILOSOPHY

of
THE UNIVERSITY OF COCHIN

Microwave Laboratory, Department of Physics
UNIVERSITY OF COCHIN
COCHIN 682 022
INDIA

1985

DEDICATED TO MY PARENTS

FOR PROVIDING BEST POSSIBLE EDUCATION WITHIN THEIR LIMITED MEANS

CERTIFICATE

This is to certify that this thesis is a report of the original work carried out by Mr.P.A.Pravin Kumar under my supervision and guidance in the Microwave Laboratory, Department of Physics, University of Cochin, Cochin 682022, and that no part has been presented for any other degree.



Dr.K.G.Nair
(Supervising Teacher)
Professor & Head of the
Department of Electronics
University of Cochin

Cochin 682022,
March 18, 1985.

DECLARATION

I hereby declare that the work presented in this thesis is based on the original work done by me under the supervision of Dr.K.G.Nair, in the Department of Physics, University of Cochin, and that no part thereof has been presented for any other degree to the best of my knowledge and belief.



P.A.Pravin Kumar.

Cochin 682022,
March 18, 1985.

ACKNOWLEDGEMENTS

The work presented here has been carried out under the guidance and supervision of Dr.K.G.Nair, Professor and Head of the Department of Electronics, University of Cochin. His help and inspiration were indispensable for the progress and completion of the thesis.

The author is very much grateful to Dr.K.Sathianandan, the former Head of the Department of Physics and Dr.M.G.Krishna Pillai, Professor and Head of the Department of Physics for providing all facilities and help during the course of the work. The faculty of the Department of Physics and Department of Electronics were very co-operative and the author acknowledges his profound thanks to them. The author places on record his sincere thanks to the administrative and technical staff of the Department of Physics and Department of Electronics for the support he has received from them. The University Services and Instrumentation Centre (USIC) were instrumental in the fabrication and assembly of the equipment which were indispensable for the completion of the work. The author recalls with deep gratitude the help rendered by USIC authorities and technical staff towards this goal.

The Director of Naval Physical and Oceanographic Laboratories, Cochin was very considerate by giving all help and encouragement to complete the work at the earliest.

For the first three years of the research the author has worked as a JRF in the DST sponsored project entitled "Design and development of high gain microwave antennas". Later

he was awarded the DAE Junior Research Fellowship for two years. For some time the author has been a recipient of University Research Fellowship also. All the above financial helps are gratefully acknowledged here.

The author is very thankful to Mr.S.Babu Sundar of the Department of Mathematics & Statistics, Cochin University for his invaluable help in preparing the computer program.

Mr.S.Kedarnath Shenoi, formerly of BARC was instrumental in running the computer program. The author is very much indebted to him for his timely help without which the theoretical expression might not have been numerically evaluated.

His colleagues Mr.P.Mohanan, Mr.C.K.Aanandan, Mr.P.Venugopalan, Mr.Stephen Rodrigues and Mr.Jose of the Microwave Laboratory were extremely helpful to him in preparing the thesis. Late Mr.P.O.Paul of Bharatha Matha College helped the author by having useful discussions. The author remembers the kind help and guidance provided by Dr.E.J.Zachariah, Centre for Earth Science Studies, Trivandrum and Dr.K.Vasudevan, Department of Electronics, University of Cochin during the initial stages of the work.

Finally this thesis is brought out in this form in a short time by the active help of Mr.C.B.Muraleedharan, Mr.K.P.Sasidharan and Mr.V.M.Peter. The author acknowledges his gratitude to all of them.

CONTENTS

| | <u>Page</u> |
|---|-------------|
| Chapter I BASIC MICROWAVE ANTENNA SYSTEMS AND OUTLINE OF THE PRESENT WORK | .. 1 |
| Chapter II REVIEW OF THE PAST WORK | .. 22 |
| Chapter III EQUIPMENT USED, EXPERIMENTAL SET UP AND MEASUREMENT TECHNIQUES | .. 40 |
| Chapter IV EXPERIMENTAL DATA AND RESULTS | .. 72 |
| Chapter V THEORETICAL EXPLANATIONS | .. 124 |
| Chapter VI CONCLUSIONS AND SUGGESTIONS FOR FURTHER WORK | .. 144 |
| APPENDIX I DEVELOPMENT OF A MICROWAVE ABSORBING MATERIAL | .. 150 |
| APPENDIX II DESIGN, DEVELOPMENT AND PERFORMANCE EVALUATION OF AN ANECHOIC CHAMBER | .. 158 |
| APPENDIX III AXIALLY SYMMETRIC RADIATION PATTERNS FROM FLANGED E-PLANE SECTORAL HORN FEEDS | .. 166 |
| REFERENCES | .. 180 |

MODIFICATIONS OF SECONDARY REFLECTOR ANTENNA

PATTERNS DUE TO SHAPED BEAMS FROM

FLANGED PRIMARY HORN FEEDS

Chapter I

BASIC MICROWAVE ANTENNA SYSTEMS AND AN OUTLINE OF THE PRESENT WORK

Introduction

Reflector antennas have been used since the radio pioneering era of Lodge, Hertz and Marconi. The Second World War was mainly responsible for the spectacular growth and development in reflector antenna art. Subsequent interest in the science of radio astronomy and the inception of microwave ground communication links were also reasons for the progress in the reflector antenna field. The design principles of prime focus-fed systems were well established in 1940s and 1950s. Cassegrain, or secondary focus system and horn reflectors came into prominence in the early 1960s with the advent of satellite tracking and communication networks. The desire to maximise gain led to the development of sophisticated techniques for properly shaping the illumination over the reflector aperture in order to maximise efficiency and minimise spill over. It is particularly noted that all reflector antennas do not utilize paraboloidal

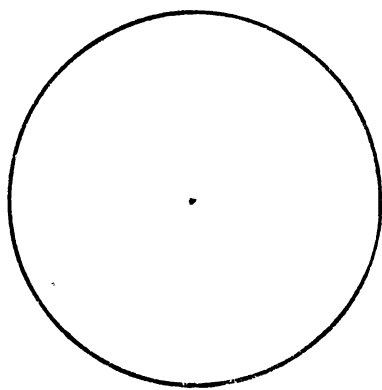
surfaces. Spherical reflector, elliptical reflector, hyperbolic reflector, plane sheet reflector, corner reflector etc. are some of the other surfaces used for special applications.

1.1 The reflectors that are of most interest in the antenna field are all derived from the conic sections. The geometric properties of these figures are well known and have been used in optics for centuries. The basic relationship for these reflectors is

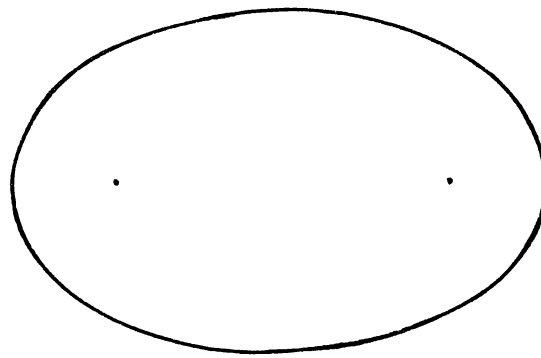
$$\frac{r}{f} = \frac{1 + e}{1 + e \cos \theta}$$

where f is the focal length and the pole is at one focus, r and θ are the co-ordinates of any point on the curve with focus as the centre. They differ only in respect to the eccentricity 'e'. The different conic sections are shown in fig.1.1.

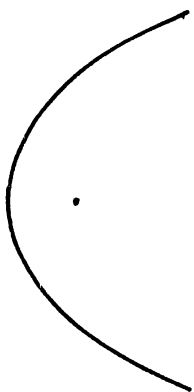
The reflecting surfaces are generated by the rotation of the curves around the focal axis, which is called the figure of revolution. Such reflectors are truly wideband devices capable in principle for operation from radio to optical frequencies.



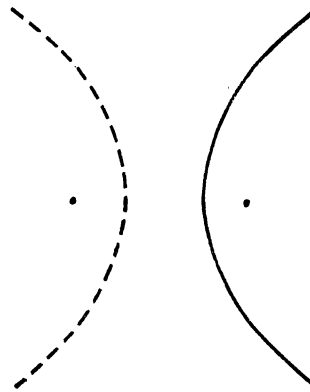
(a) Circle ($e=0$)



(b) Ellipse ($e<1$)



(c) Parabola ($e=1$)



(d) Hyperbola ($e>1$)



(e) Straight line ($e=\infty$)

Fig.1.1 : The various conic sections.

1.2 Hertz's experiments

It was Prof. Heinrich Hertz who experimentally demonstrated the existence of the electromagnetic waves that had been predicted theoretically by James Clerk Maxwell some fifteen years earlier. In his experiments, Hertz used simple adjustable spark gaps (fig.1.2a) as microwave transmitter and receiver.

The transmitter is a spark coil feeding V.H.T. to the adjustable spark gap, and the receiver is a single turn of wire, broken at one point by an adjustable spark gap. It was possible to produce small sparks in the receiving loop whenever there was a sparking at the transmitting spark gap.

Prof. Hertz was able to reflect waves by plane metallic sheets much in the same way as optical beams are reflected by mirrors. In his experiments he used a cylindrical parabolic mirror of zinc with a spark gap excited dipole placed in line with the focal line. A similar dipole mirror combination served as a receiver. The arrangement is as shown in fig.1.2(b).



Fig. 1.2(a): Hertz's Experiment.

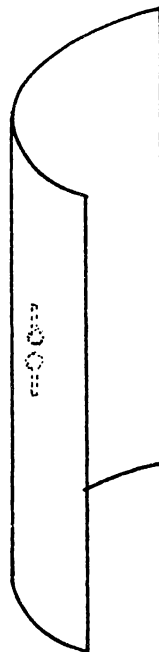


Fig.1.2(b): The first reflector antenna constructed by Hertz in 1888.

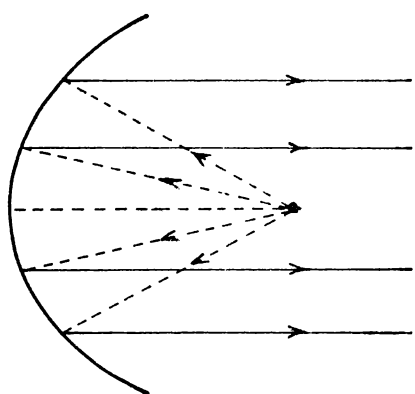
With this arrangement, Hertz has shown that microwaves can also be focused just like optical rays. This is the underlying principle of all metallic reflector antennas.

1.3 Different types of reflector antennas

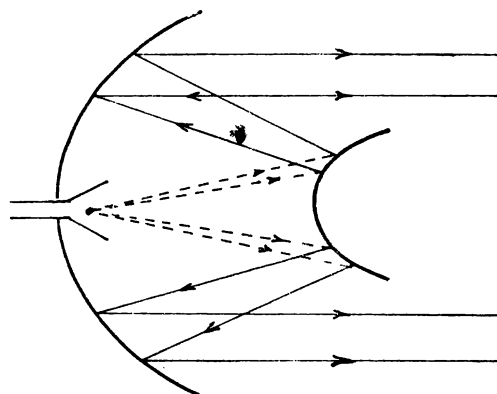
As stated earlier, there are a number of types of reflector antennas. The frequently used paraboloid is just one of them.

Paraboloid is the most extensively used reflector antenna. This is because, compared to others, it is relatively simple to make and adjust and it has got good gain and it is free from spherical aberration which is the main defect of spherical reflector, its nearest competitor. But for practical purposes, the paraboloid is used only above 1 GHz or around it, since for efficient gain the aperture of the reflector should be at least 10 times the wavelength. A sketch of paraboloid is shown in fig.1.3(a).

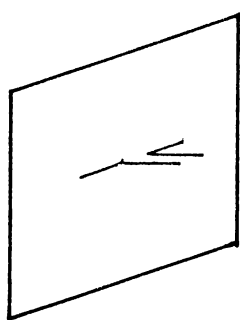
A modification of the paraboloidal reflector is the Cassegrain reflector. In this system, a hyperboloidal sub-reflector is placed near the focus of the main paraboloidal reflector. The feed horn is placed at the virtual



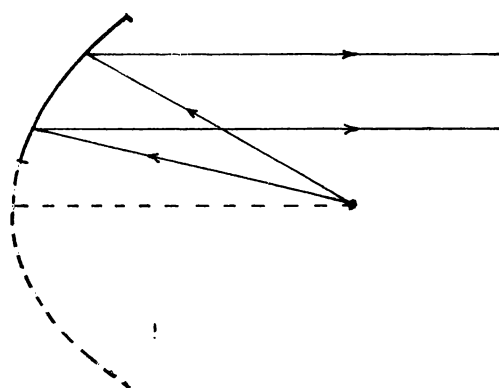
(a) The Paraboloid



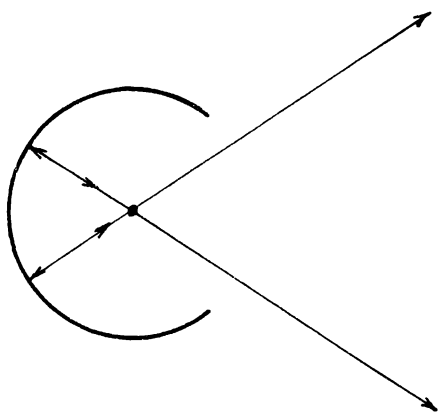
(b) The Cassegrainian



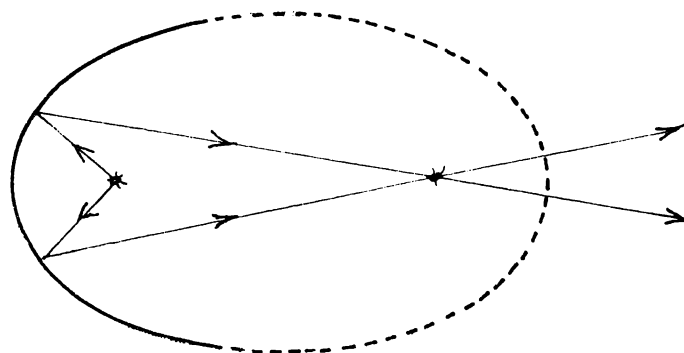
(c) Half wave Dipole with plane metal sheet as reflector



(d) The Offset paraboloid



(e) The spherical reflector



(f) The Ellipsoidal reflector

Fig.1.3 Different types of reflector antennas in use

focus of the hyperboloid through a hole at the centre of the main reflector as shown in fig.1.3(b). Main advantage of this system is its high efficiency and low noise because the feed horn is well shielded. The Cassegranian systems suffer more from aperture blocking than ordinary prime focus-fed systems because the sub-reflector blocks the plane wave generated from the main reflector, while the feed horn blocks the spherical wave coming from the sub-reflector. For this reason, Cassegranian antennas are usually considered only for those applications requiring a half power beam width of less than about one degree.

A useful variation of the paraboloidal reflector is the offset paraboloid. Here, only a portion of the paraboloid is used and the feed horn is displaced tilted as shown in fig.1.3(d). This avoids aperture blocking due to feed, which is a major drawback of ordinary paraboloidal reflectors.

Plane mirrors also find great utility in the antenna art. The arrangement as shown in fig.1.3(c) has a large flat sheet reflector near a linear dipole. This reduces the backward radiation. With small spacing between antenna and sheet, this arrangement yields a substantial gain in the forward direction.

Spherical reflectors are used when beam scanning has to be performed with a stationary reflector by moving the feed only. A main drawback of spherical system is the spherical aberration. To overcome the difficulty, the illumination is confined to the paraxial zone of the sphere, that is to a region over which the sphere does not differ from a paraboloid by more than one eighth of a wavelength. This practice however leads to a large value of f/D and the poor area of utilization. A sketch of spherical reflector is shown in fig.1.3(e).

Ellipsoidal reflectors are used whenever the need arises to focus the antenna's radiation pattern to a small region in the Fresnel zone. An outline of the ellipsoidal reflector is shown in fig.1.3(f).

Corner reflector antenna consists of a driven radiator normally a halfwave element associated with a reflector constructed from two flat conducting sheets which meet at an angle to form a corner. Fig.1.3(g) shows the configuration of the corner reflector antenna.

1.4 Feeds for a paraboloid

Almost all types of primary antennas can be used as feeds for secondary reflector antennas. Dipoles, horns,

helical antennas, waveguides etc. are some of the commonly used feeds. In almost all the cases, the feed is placed at the focus of the reflector. To obtain maximum efficiency from the paraboloidal antenna, it requires a close control of amplitude, phase and polarisation of the field incident on the reflector. This requires the primary source or 'feed' to be small and of a configuration that gives a spherical phase-front, ie., from a distance it must appear as though the energy is radiated from a point. The amplitude of the radiation from the feed should be uniform over a wide angle to illuminate adequately the entire reflecting area. The incident field should be of such a nature that, after reflection, the waves will be properly polarized. To make effective use of the area of the paraboloidal reflector, the energy must be distributed over the surface with the same degree of uniformity. But it is very important to avoid loss of energy by waves radiated from the feed which fail to strike the reflector. This energy is called 'Spill-over' and to obtain the optimum gain efficiency from a paraboloid, it is necessary to design the combination of reflector and feed to compromise between the loss due to spill-over and loss due to non-uniformity of illumination.

Simple halfwave dipole antenna radiates uniformly in a plane perpendicular to its length as shown in

fig.1.4(1)(a). If a paraboloid is made to subtend a solid angle of 180 degrees at the focus, half of the energy will be radiated into space without striking the reflector. This energy which does not strike the reflector is wasted. To reduce this loss and increase the radiating efficiency of the overall system, it is necessary to direct most of the energy from the feed into the paraboloid. The half wave dipole feed can be made more directional by simply placing a reflecting element such as another dipole, a plane sheet, a half cylinder, or a hemisphere. The arrangement using a disc which is most popular is shown in fig.1.4(1)(b).

The dipole antenna is not ideal for feeding paraboloids in that the polarization characteristics are poor. Beyond 90° in the E-plane, the polarization actually reverses, and extending a paraboloid beyond 90° in this plane would result in a decrease in gain.

Open-ended waveguide feeds are used when the wavelength is of the order of a few centimeters. The radiation characteristic of a waveguide aperture is dependent upon the size and shape of the aperture and the mode or modes of propagation within the guide. For getting a circularly symmetric radiation pattern, a circular TE_{11} waveguide is

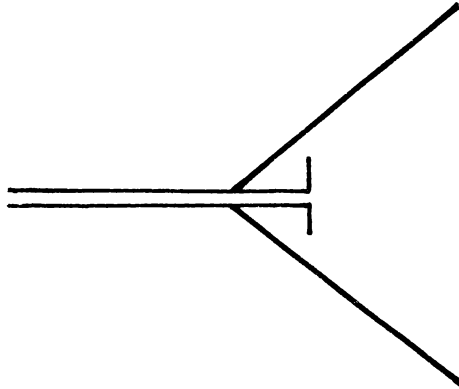
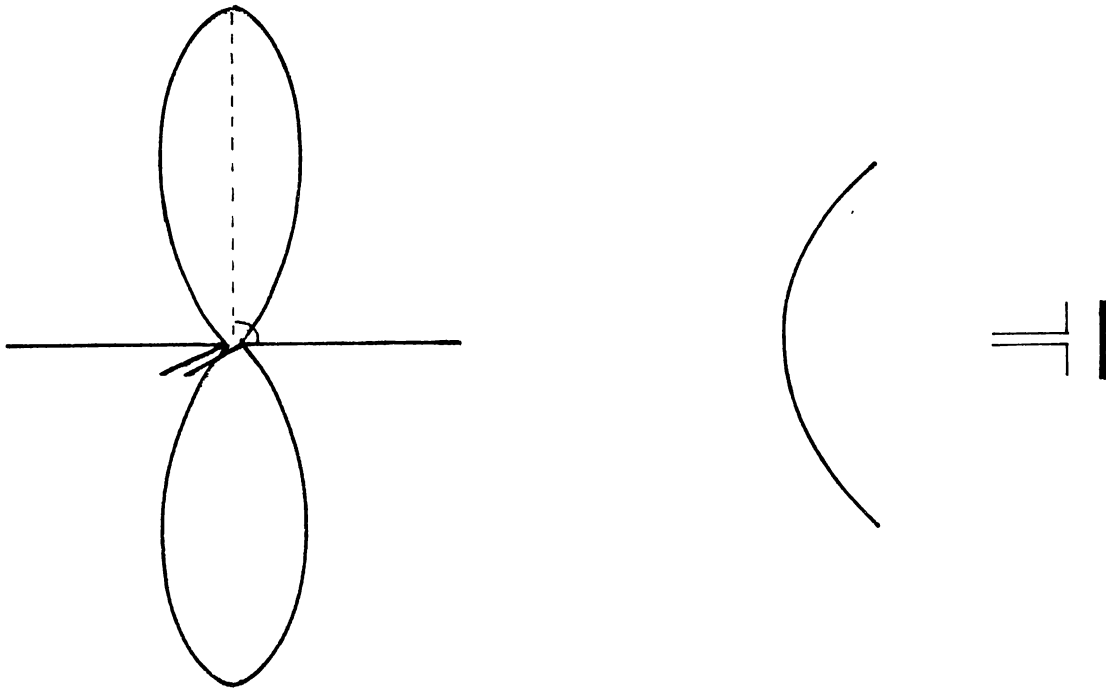


Fig.1.3(g): The Corner reflector antenna .



(a) Radiation pattern of the half wave dipole

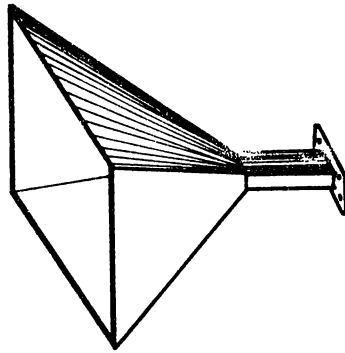
(b) The dipole disc pair used as the feed to a reflector

Fig. 1.4(i)

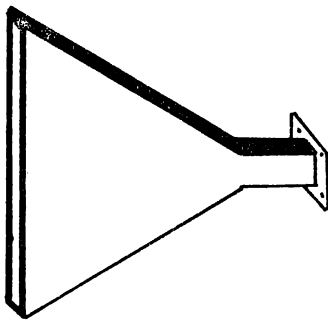
used as feed. A rectangular TE_{10} waveguide does not generally give a circularly symmetric radiation pattern, but it is suitable for feeding a paraboloidal section which is out to subtend a wide angle in one plane and a narrow angle in the other plane. The directivity in the electric and magnetic planes can be controlled independently by altering the respective apertures.

When more directivity is required in the feed than that can be obtained with a simple aperture waveguide, e.m. horns are used. There are several types of horn antennas. These can take either circular or rectangular cross section for their apertures. The circular ones are usually fed by a matching circular waveguide and rectangular ones by rectangular waveguides.

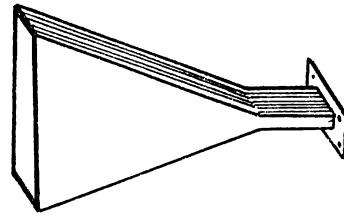
There are three types of rectangular horns as shown in fig.1.4(2)(a). If the horn is made by flaring in a plane perpendicular to the TE_{10} wave electric field, it is called a H-plane sectoral horn and if the horn is flared in the plane of the electric field, it is called an E-plane sectoral horn. A rectangular horn with flare in both planes is called pyramidal horn.



(a) Pyramidal horn



(b) H - plane sectoral horn



(c) E - plane sectoral horn

Fig.1.4(2): Different rectangular aperture horns

Helical antennas are also used as feeds for paraboloids, when the need for a circular polarization arises. Helical antennas are very easy to manufacture and extremely light in weight. But they are not so directional as horn feeds.

1.5 Sectoral horn feeds

Horns flared only in one plane are called sectoral horns. There are two types of sectoral horns. In one type, the flare increases the aperture in the direction of the E-vector called E-plane sectoral horns, and in the other type the flare increases the aperture in the direction of the H-vector, called H-plane sectoral horn.

The radiation patterns in the flared plane are narrow and focused. But the radiation patterns in the orthogonal plane are very broad and same as that of an open ended waveguide of the same dimensions. The energy radiated by a sectoral horn is distributed in a fan shaped beam. Such a pattern is useful only for such special applications like tracking radar antennas etc. For other applications like point to point communication, illuminating circular aperture paraboloids etc., an identical pattern shape in both principal

flares is required. Hence it was felt that the pattern shape in the unflared plane should be modified. Many workers have tried to modify the pattern shape of sectoral horn antennas in both the principal planes. The 'grill technique' developed by K.G.Nair^{23,27,53,55,57} and Hariharan is found to be effective in controlling the E-plane radiation pattern of the E-plane sectoral horns. Here, conducting grills were attached to the aperture of the E-plane sectoral horn. Optimum performance of the system is found by varying the dimensions and by changing the positions of the grills. The arrangement is as shown in fig.1.5(1)(a).

Owen and Reynolds⁴ are pioneers in the field of 'flange technique'. Their technique is developed and investigated in detail by later workers.^{20,42,45,46,48,60,63,75,80,83,84} The plane flanges are known to have good control in the E-plane pattern of the H-plane sectoral horns.

The important parameters of a system with plane flanges mounted on sectoral horn are:

- (1) Flange angle
- (2) Flange width
- (3) Flange position, and
- (4) Amplitude of excitation of the flange elements.

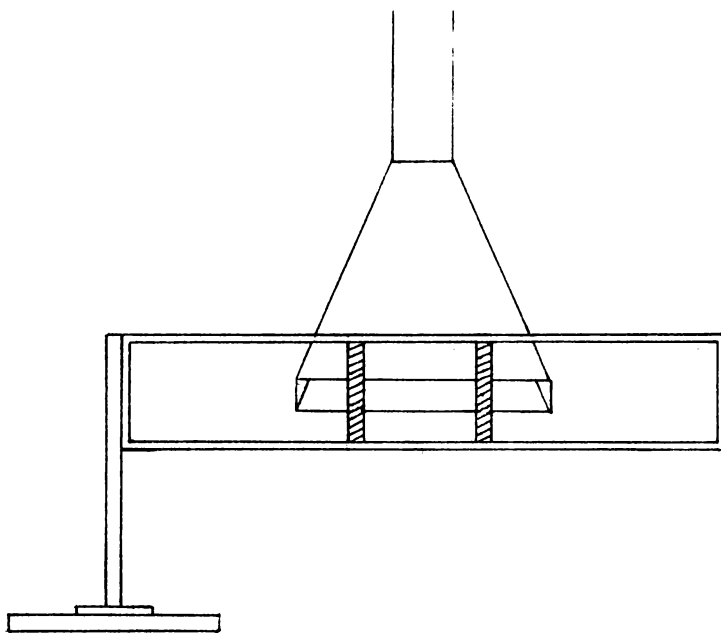


Fig.1.5(1) (a) Schematic representation of a sectoral horn attached with Grills.

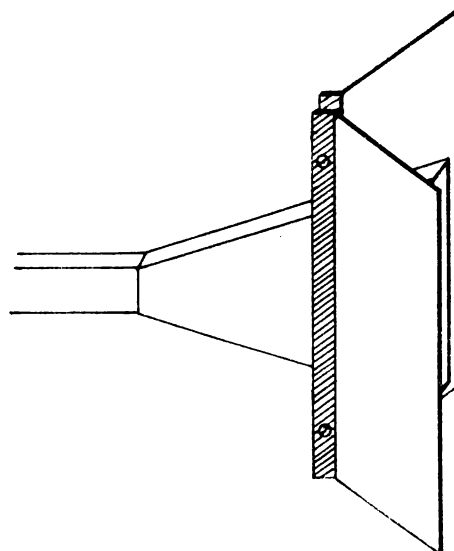


Fig.1. 5 (2) (a) Schematic representation of a sectoral horn attached with plane flanges.

By this technique the pattern in any one plane can be conveniently modified without seriously affecting the radiation pattern in the other plane. By introducing assymetries in the flange system the beam can also be made assymmetric to suit specific applications. A diagram of a H-plane sectoral horn attached with plane flanges is shown in fig.1.5(2)(a).

1.6 Outline of the present work

With the advent of satellite communication and radio astronomy, the need for large and efficient reflector antennas had triggered a widespread investigation in reflector feed design techniques. Major improvements sought are reduction in spill-over, cross polarization losses and the enhancement of aperture efficiency. The search for such a feed culminated in the corrugated horn. A large amount of work has already done in this field and the properties of corrugated horns are now well known.

Some workers^{83,84} used corrugated surfaces as flanges on H-plane sectoral horns and found that an H-plane sectoral horn can also be modified to give a circular symmetric radiation pattern far more easily and with more flexibility

than a corrugated horn. The properties of corrugated-flanged H-plane sectoral horn were studied in detail by Nair and Zachariah^{83,84}.

The main idea behind the present work is to use the H-plane sectoral horns fitted with corrugated flanges as feeds of a paraboloid and see how the secondary pattern of the reflector antenna varies with different parameters of the feed. An off set paraboloid is used as the secondary reflector in order to avoid the adverse effect of aperture blocking by the feed horn structure on the secondary radiation pattern. The measurements were repeated for three different H-plane sectoral horns with the same set of corrugated flanges at various X-band frequencies. The following parameters of the whole system were studied: (a) Beam shaping, (b) Gain, (c) Variation of VSWR and (d) Cross polarization.

Theoretical explanation to the effects of the feed horn parameters on the secondary reflector antenna patterns is attempted.

The scheme of the present work is as follows:

Chapter 2 gives a comprehensive review of the research work done in this field. The review deals with papers on secondary reflectors and modifications of feed structures to get suitable illumination beams. This chapter is intended to provide an understanding about various theoretical and experimental techniques employed in reflector antenna design.

Chapter 3 describes the experimental set up and methods of measurement used in the present study. The main equipment used is described in detail. Fabrication and other details of antenna components and accessories used here are also described.

Chapter 4 is mainly meant to discuss the experimental results relating to pattern modification, gain measurement and variation of VSWR and cross polarization.

A theoretical treatment of the corrugated flanged H-plane sectoral horn fed off set paraboloid is attempted in Chapter 5. Theoretical and experimental patterns are compared.

Chapter 6 contains the conclusions derived from the above study. Suggestions for further work to improve the overall antenna performance is also included in this chapter.

During the initial course of the work on secondary reflector antenna, the impedance characteristics of the feed horn system were also studied in some detail. For this purpose, a specially designed anechoic chamber was used.

For the purpose of chamber lining, a natural rubber based absorbing material was developed and a note on this is given in Appendix I.

A brief discussion on the design, development and performance evaluation of microwave anechoic chamber constructed in the Department, is given in Appendix II. The author actively participated in this work during the tenure of his research fellowship.

Another experimental work done on flanged E-plane sectoral horns is described in Appendix III.

Chapter II

REVIEW OF THE PAST WORK

This chapter presents a review of the past work that has already been done in the field of microwave reflector antennas in general and paraboloidal reflectors in particular. A detailed review of the feed horns used with reflectors is also included.

2.1 Microwave reflector antennas

The first reflector antenna was constructed by Prof. Heinrich Hertz¹⁹. He used a cylindrical parabolic reflector with a dipole as feed. It had a rectangular aperture of 2m height and 1.2m breadth. He worked with 66cm waves and obtained an aperture efficiency of 10%.

Indian Physicist Jagadish Chandra Bose constructed plane and cylindrical mirrors and gave a lecture demonstration at the Royal Institution in London¹⁹. He used his reflectors down to 5mm wave length.

Jansky¹ discovered extra terrestrial radio emission, which is now known as the birth of radio astronomy.

The first large paraboloidal reflector was constructed by Reber². This reflector was 9.6m in diameter and operated in the region of 1.9m waves.

Ashmead and Pippard³ were the first to point out that beam scanning can be performed with a stationary spherical reflector by moving the feed alone.

It was Spencer⁶ who initiated investigations of the aperture phase errors on the gain of the antenna.

Ruze¹¹ showed that for any reflector there is a wavelength at which the gain reaches a maximum. This wavelength depends on the r.m.s. deviation of the reflector surface from the ideal paraboloid.

Through a theoretical analysis Jones¹³ showed that low amplitude cross-polarized radiation and high gain factors can be obtained from a paraboloidal reflector excited by a plane wave source.

Cheng¹⁴ obtained simple expressions for predicting maximum loss in antenna gain when the peak value of the aperture phase deviation is known.

Carter¹⁵ developed expressions for the accurate prediction of phase centres of microwave antennas.

Robieux¹⁶ emphasized the influence of the precision of the surface on the ultimate performance of the antenna.

Cheng¹⁷ established a method to determine proper amount of defocuss necessary to simulate Fraunhofer radiation pattern in the Fresnel region which had become the usual practice in testing of large antennas.

Brown and Lovell¹⁸ had given an excellent account of the radio astronomical telescope design. They had reported that the first really large telescope built and put to practical use at Jodrell Bank was having a gain of 31 dB at 100 MHz.

For the first time the concept of equivalent parabolas in cassegrain antenna systems was introduced by Hannan²².

For large paraboloidal antennas Bracewell²¹ had proved that the deterioration in directivity is found to depend on the mean square departure of the surface from the paraboloid of the best weighted least-squares fit and on the two-dimensional autocorrelation function of the departure. The variation of directivity with wavelength of a particular paraboloid is deduced by leaving out of account those two-dimensional Fourier components of the departure with spatial periods less than a wavelength.

Rusch²⁵ calculated the scattered field from a hyperboloidal reflector and established that at radio frequencies, Geometrical Theory of Diffraction (GTD) is far superior to ray optics method.

It was Schell²⁶ who showed that the field along the axis of a spherical reflector is determined from geometry of the system rather than from each term of the aberration taken separately. He further showed how the field distribution changes from the case of small aberration where there is a well-defined focus to the geometric optics limit.

Galindo³¹ demonstrated that with a two reflector system, it was possible to achieve arbitrary phase and amplitude distribution over the main aperture.

Holt and Bouche²⁹ showed how an auxiliary Gregorian Reflector can be used for getting wide angle scanning from a spherical reflector without the adverse effect of spherical aberration.

It was Watson³² who devised a method to find the field distribution at the focal plane of a symmetric paraboloidal reflector.

Ruze³⁵ presented a set of formulas to determine the axial loss of gain and pattern degradation as a function of the reflector surface r.m.s. error and the surface spatial connection. He had also presented a correlation between the theoretical predictions and performance of actual large antenna structures.

The Bao Vu³³ studied in detail the effect of random phase errors on the forward gain of the reflector antennas.

Williams³⁴ described a modified cassegrain system to which the approach of Galindo³¹ was applied and an improvement of about 25% in aperture efficiency was observed.

Koffman³⁶ established that a combination of crossed electric and magnetic dipoles can be adjusted to eliminate

cross-polarized radiation in any reflector formed as a surface of revolution from a conic section. He found that it is only necessary to impose the condition $A = eB$ where 'e' is the eccentricity of the conic section and 'A' and 'B' are the electric and magnetic dipole strengths.

Zarghamee⁴⁰ extended the theory of Ruze to account for the uneven distribution of surface irregularities of reflections. He derived a correction term to the theory of Ruze³⁵.

McCormick⁴¹ has given a detailed description about the correct excitation of a line feed for a spherical reflector. He also derived expressions for the field components in the focal region.

Evans⁵⁰ made a computer study of spill-over, cross-polarization and illumination efficiency of paraboloids of various focal length paraboloid diameter ratios (F/D), fed by rectangular, square and circular wave guides in their lowest order modes. The results showed that the figure of merit of a low F/D ratio system is about 0.8 dB less than that of a large F/D ratio system.

Nair et al⁶⁰ derived expressions for the radiation pattern of a flange mounted sectoral horn antenna, treating the primary horn as an aperture antenna and taking into consideration its radiation pattern. In the earlier works the primary horn antenna was considered to be an isotropic linear source.

Chu and Turin⁶⁶ investigated the cross-polarized radiation for linearly polarized excitation and beam displacement for circularly polarized excitation and established a valuable design procedure for reflector antennas.

Leonard Tsai et al⁶⁴ analysed a number of two dimensional reflectors using both geometrical theory of diffraction (GTD) as well as integral equation formulation (IEF) and showed that while GTD is accurate for large structures, IEF is good only for small structures.

James and Kerdelidis⁶⁷ analysed the reflector antenna radiation pattern using the method of equivalent edge currents and established that it shows better agreement with measured values than those obtained by other methods.

Cogdell and Davis⁶⁹ studied the characteristics of the astigmatic phase error in large parabolic reflector

antennas and outlined a procedure for focusing and diagnosing the presence and degree of astigmatism.

Rudge⁷¹ described two simple mathematical models for the prediction of the vector radiation fields from off-set parabolic reflector antennas with off set feeds. Experimental verification of the models and comparisons with surface current techniques had indicated that reliable predictions can be obtained by the use of these models over a moderate range of angles about the antenna bore sight.

Kauffman et al⁷³ developed a numerical technique for a rapid calculation of the far-field radiation patterns of a reflector antenna. They showed that this technique can be used to calculate the radiation patterns of even off set paraboloids.

Bennet et al⁷⁴ developed a microwave holographic technique for the determination of amplitude and phase of the principal and cross polarized aperture fields of large reflector antennas. Their technique describes the means used to obtain vital information on the antenna structure such as E- and H-plane phase centres of the feed and r.m.s. values of the reflector surface profile errors.

Ghobrial⁷⁷ derived equations for the copolar and cross-polar fields in the focal plane of a paraboloidal reflector excited by a plane wave.

Safak and Delogne⁷⁸ put to an end the controversy about the relative susceptibility of cassegrarian and front fed antennas to depolarisation effects by showing that the cross-polarization in reflector antennas is closely related to the feed design.

Nair and Mathew⁸⁰ were using a flanged sectoral horn as feed to a paraboloidal reflector. They showed that the position and geometry of the flanges determine the nature of the secondary patterns.

Agarwal et al⁸² published a numerical method to calculate the radiation properties of even very large spherical reflectors. They verified the method by comparing the calculated and measured results from a 120 wavelength spherical reflector.

Raj Mittra et al⁸⁵ presented a method to compute rapidly the vector secondary pattern of an off set paraboloidal reflector where the feed was displaced. They showed that the

Jacobi-polynomial series method can also be extended to the case of an off set paraboloid without compromising base and speed of computation.

Bucci et al⁸⁶ gave an analysis of the behaviour of the reflector antennas loaded by a surface impedance along a peripheral rim. Both single and dual (Cassegrain) reflector antennas were considered and it was shown that an effective control on the radiated field can be achieved by the proper choice of the loading characteristics.

Cha and Bathken⁹⁰ have achieved a 85% aperture efficiency using a dual reflector antenna. They claim that this to be the most efficient reflector antenna ever designed.

2.2 Reflector antenna feeds

Owen and Reynolds⁴ attached metal flanges to the aperture of H-plane sectoral horns and studied their E-plane patterns. They found that the flanges are very effective in controlling the E-plane pattern. They explained this with the help of line source theory, which considers the horn aperture as the primary source to the line source which in turn excite the two tips of the flanges. The total radiation is considered to be the resultant of all these three radiators.

Cutler⁵ showed qualitatively that the ideal feed should radiate a spherical wave with proper polarization characteristics, if the reflector as a whole is to radiate with linear polarization in fixed direction. Spencer⁷ was first to suggest that a line source can be used to correct the spherical aberration.

Butson and Thomson²⁰ continued the studies of Owen and Reynolds⁴ on the effects of metal flanges on the radiation patterns of sectoral horns and waveguides. After exhaustive studies, they came to the conclusion that there was no change in the H-plane pattern of E-plane sectoral horns.

Hariharan and Nair²³ investigated about the effect of a shorting grill system on the near field radiation pattern of E-plane sectoral horns. They found that the system can make the E-plane beams more sharper. The same authors in 1962²⁴, studied the effect of shorting grills on the VSWR of the system. They established that at certain positions of the grills, the VSWR is decreased and the axial power density is increased.

Potter²⁷ introduced a step discontinuity in the diameter near the throat of a conical horn, which converted

a part of the dominant mode, into higher order mode. A correct combination of these two modes at the horn aperture gave rise to almost identical E- and H-plane patterns.

The above technique of Potter²⁷ was applied by Jenson²⁸ to a square pyramidal horn in which the dominant mode is the TE_{10} . He showed that the correct higher modes are the hybrid mixture of TE_{12} and TM_{12} .

In the United States, Kay³⁰ used grooved walls in a wide flare angle horn which was called 'Scalar feed' because its properties are independent of polarization.

Minnett and Thomas³⁷ gave an analytical description of the synthesis of hybrid HE_{11} mode.

Rumsey³⁸ showed that a linearly polarized horn that has the same power pattern in all planes through the axis can be made from a synthetic material for which the boundary conditions on E and H are the same.

Laurie and Peters (Jr)³⁹ of USA designed a horn antenna with significantly reduced backlobes over nearly a two-to-one frequency band. This horn has a well defined

phase centre at its apex, and the E- and H-plane patterns are nearly identical over the frequency band if the horn has a square or circular aperture.

Nair and Srivastava⁴² were first to report that the position of flanges relative to the horn aperture affected the radiation property of the system drastically. They found that if the flanges were moved back, the radiation pattern can be focused or broadened. They defined those positions of the flanges which gave a sharp beam and a broad beam as optimum or (O) position and minimum or (M) position respectively.

Jull⁴⁴ made some accurate microwave horn gain measurements with revised proximity connections. These results established that edge diffraction is the major source of error in Schelkunoff's¹² gain expression and suggested a value for its accuracy.

Nair et al⁴⁵ studied in detail the effect of metal flanges on the H-plane radiation patterns of E-plane sectoral horns. The effect of the flange position and its geometry on the radiation pattern of the H-plane sectoral horns was also studied later⁴⁶.

Hamid⁴⁷ analysed the radiation from a conical horn by extending Brillouin ray tracing techniques to the three-dimensional case.

Yu and Ruddock⁵⁴ calculated the H-plane radiation pattern of pyramidal horns by considering the diffraction from the aperture edges.

Jeuken⁵² carried out experimental study on small flange angle corrugated conical horn. He found that small flange angle horns with large aperture diameters had a bandwidth of only 1:1.3.

Narasimhan and Rao⁵⁸ found a simple solution to the corrugated conical horn using the spherical hybrid modes. Their results are fairly accurate for small flange angles of the horns. Later on the same authors analysed the case of wide flare angle horns and the computed patterns were in good agreement with experimental results.

Cohn⁵⁹ described a new method of generating and controlling the hybrid modes by changing the flare angle at appropriate points in the horn.

Koshy et al⁴⁹ made an experimental investigation on the effect of flanges on the radiation patterns of horn antenna. The same authors published a report⁶⁰ on the theoretical analysis of the flanged sectoral horn antenna. The theoretical results are in good agreement with experimental results.

Clarricoats and Saha⁶² investigated on the propagation and radiation behaviour of circular corrugated waveguides. They showed that the radiation pattern of a corrugated waveguide exhibits nearly perfect symmetry over a 1.5:1 frequency band, and when corrugations are approximately $\lambda/4$ deep, the pattern is symmetric and there is no cross-polarized component in the radiated field. The attenuation is also found to be less than that of a uniform waveguide for the dominant mode. They extended their work to cover the conical corrugated horns and their theoretical predictions were justified well by experimental results.

Mizusawa and Kitsuregawa⁶⁵ described about a beam waveguide feed system in which the receiver and the Cryogenics can be housed in a fixed location beneath the main reflector without incurring excessive line losses.

Love⁶⁶ developed a leaky cylindrical waveguide feed to be used for the correction of spherical aberration.

Truman and Balanis⁷⁰ devised a method to determine the optimum dimensions of a horn feed for a parabolic reflector using the power transferred to the feed as a criterion.

Adatia and Rudge⁷² developed new primary feed types for off set reflectors that offer significant improvements in the cross polar and beam squinting properties, without adding significantly to the complexity or mass of the primary feed system.

Srivastava et al⁷⁵ reported a slotted flange system which produced a square radiation pattern. They got an almost ideal 10 dB taper with sharp 10 dB fall off beyond the 10 dB points. The resultant beam is very much suited for feeding deep paraboloids.

Nair et al⁷⁶ used dielectric flanges on sectoral horns instead of metal flanges and succeeded in reproducing all the effects observed with metal flanges. They even tried a hybrid system with one flange element of metal and other identical flange element of dielectric. It was found that the resultant beam was tilted towards the metallic flange element.

Nair and Mathew⁸⁰ established the similarities between a flanged sectoral horn and corner reflector antenna. After a detailed study of their properties they concluded that the corner reflector theory could be more suited to explain the behaviour of flanges.

Dragon⁸¹ fabricated a corrugated conical horn feed which successfully operated in the 17 GHz - 29 GHz band. In this region the radiation has got good polarization purity.

Zachariah et al^{83,84} found that corrugated metal flanges fitted on sectoral horn antennas are more superior to conventional plane metal flanges in all respects. This is established theoretically and experimentally by authors.

Vasudevan and Nair⁸⁷ analysed the effects of corrugated reflector elements on the radiation characteristics of corner reflector antennas. They found that the radiation patterns and half power beam widths of the system, show remarkable agreement between theory and experiment.

Kildol⁸⁸ presented a formula for the numerical calculation of the combined phase centre. He had also given theoretical aspects of the feed position tolerances and efficiency loss due to differences in the principal plane phase patterns.

Huang et al⁸⁹ used the uniform GTD to determine the near and far field patterns of a pyramidal horn which they used as the feed for an off set parabolic reflector.

From the above review it is clear that enormous amount of work has already been done and still the field continues to grow indicates that the reflector antennas are vital for the development of communication and other purposes. From the later part of the review it is evident that corrugated horns are gaining more momentum as feeds for the secondary reflector antennas of all types by their superior radiation characteristics and impedance matching properties. But, no serious effort has been made so far to study how the secondary radiation characteristics will vary by using the flexible feed arrangement of sectoral horn fitted with corrugated flanges as feed to a paraboloid. The work presented in this thesis is oriented precisely towards this aim.

Chapter III

EQUIPMENT USED, EXPERIMENTAL SET UP AND MEASUREMENT TECHNIQUES

In this chapter, the various equipments used and the experimental set up is described in detail. The methods of measurement of different antenna parameters which are of primary importance in reflector antenna field are also extensively covered.

3.1 Description of the equipment used

The whole work of this thesis was conducted at different X-band frequencies. The frequencies of 8.25 GHz, 9 GHz, 10 GHz, 10.6 GHz and 11 GHz were used for the study of the off set parabola.

3.1(i) Microwave source

Gunn diode was used as microwave source throughout the experiment. The source includes a stabilized power supply (0 to 10V) capable of supplying a current of 1 amp. The power supply was also having provision for supplying a 1000 KHz

square wave signal for the purpose of modulating the microwave source. A PIN diode mounted in a suitable waveguide cavity connected between source and load acts as the modulator.

The Gunn diode is mounted inside a X-band waveguide section, one end of which is terminated in a precisely calibrated movable shorting plunger. The waveguide section between the plunger and the diode acts as the resonant cavity. When the plunger is moved towards the diode, the volume of the cavity decreases and the frequency of the generated wave increases and vice versa. The manufacturer has supplied a calibration curve by which the approximate frequency corresponding to the micrometer reading can be noted. The Gunn diode used here is having a rating of 160 mA at 10V. The useful maximum microwave power output available is 20 milliwatts. This corresponds to a D.C. to A.C. conversion efficiency of 1.25%. Whenever the Gunn diode is used, an isolator is placed immediately after the oscillator and other components are connected only to the output port of the isolator. This is necessary for the safety of the Gunn diode because the reflections from the load may disturb the operation of the device. The Gunn source used with the above precaution worked very smoothly and its output power and frequency were exceptionally stable and reliable. The frequency range of the device

is 8.2 GHz to 12.4 GHz. But towards the upper end of the band, i.e., after 11 GHz, the output power is not enough for the radiation experiments, using only a crystal as detector. So the experiments are carried out only upto 11 GHz. The CW mode operation is adopted throughout the work.

3.1(ii) Waveguide components

As stated earlier, the Gunn diode is housed in a X-band waveguide cavity so that the pulses of the Gunn diode can be converted into sinusoidal oscillations with an adjustable frequency range. A three port circulator with one port terminated in a matched termination as dummy load is used as the isolator. A precision X-band cavity frequency meter with direct reading facility is used for monitoring the frequency accurately.

The microwave power output from the oscillator can be monitored at regular intervals using a directional coupler, detector mount and a sensitive micro ammeter to ensure that there are no R.F. power fluctuations. An adjustable vane type attenuator is used to keep the microwave power level at the receiving end to a minimum, in order to ensure that the detecting crystal follows square law. Waveguide slotted section carriage is used for calculating the voltage standing wave ratio of the system accurately.

Waveguide twist is used for studying the cross polarization patterns of the system. Using the waveguide twist either receiver or transmitter can be made to receive or transmit cross polarized waves relative to each other.

Waveguide to co-axial adapters were used when the offset paraboloid was used as the transmitter for VSWR studies. The adapter couples a RG/U cable through a N-type female connector to the waveguide system.

Crystal detector mount is used to detect received power. Since CW R.F. power was used, the detected output was pure D.C. signal. The crystal detectors used are IN21C, IN23C, IN415B type Schottkey diodes. One side of the crystal mount is terminated at an adjustable shorting plunger. The plunger can be adjusted for maximum detected power.

3.1(iii) Offset paraboloid

Offset paraboloid is the only secondary reflector used in the present study. The paraboloid is made out of aluminium sheet. It is a part of a full paraboloid of aperture diameter 2 meters and focal length 1 meter. The offset portion used is circular in shape with a diameter of

97 cms. A two dimensional diagram of the offset paraboloid is as shown in fig.3.1(iii)(a).

The offset paraboloid was made using the method of the sheet metal extrusion. A template of solid aluminium sheet was first made. For this purpose, the equation of parabola $y^2 = 4ax$ is plotted on a big graph sheet and the resulting parabolic curve is cut and pasted on the aluminium sheet. The sheet is then cut out exactly along the curve and a template is obtained as shown in fig.3.1(iii)(b). This template is rotated about the axis of the proposed paraboloid while the process of sheet metal extrusion is in progress. The resulting figure of revolution is the full paraboloid of 2 metres in aperture. Every effort was made to see that the manufactured paraboloid surface followed the parabolic curve as closely as possible. The paraboloid is then cut and a circular portion shaded as shown in fig.3.1(iii)(c) was taken out. Precautions were taken to see that there is no deformation of the curve while the offset portion was cut out. This cut out portion is the offset paraboloid used for the study. It is having a surface accuracy of $\lambda/16$.

The offset paraboloid is supported from the back by a rigid aluminium structure. A few iron nuts and bolts fastened the reflector securely to the aluminium support structure

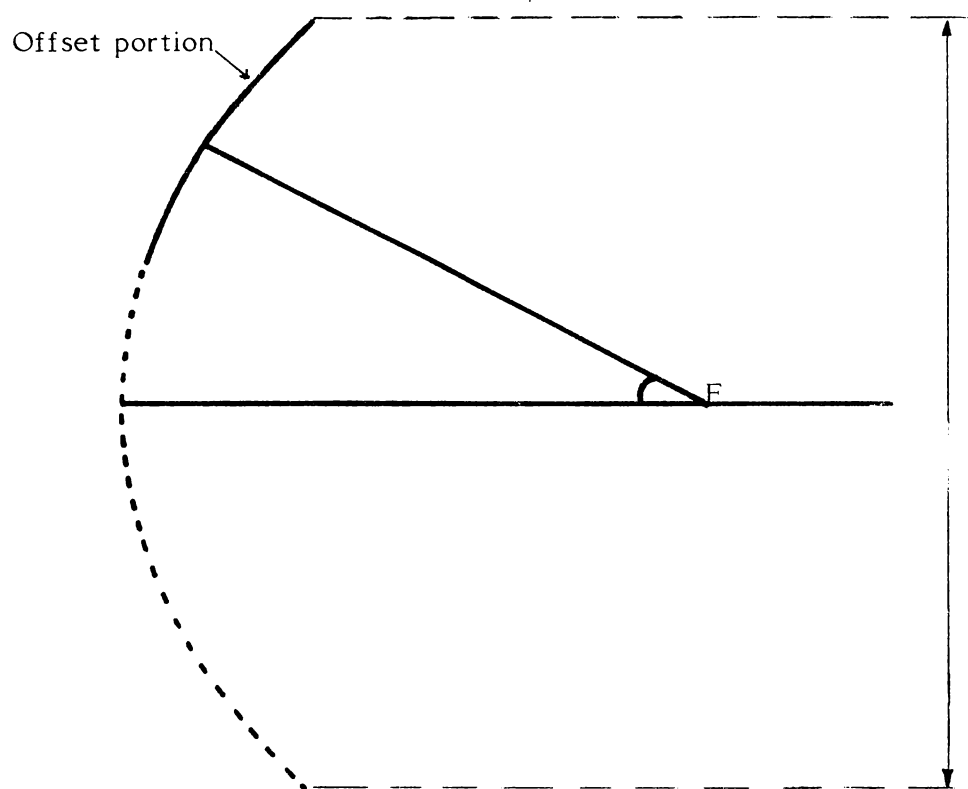


Fig.3.1(iii)(a):The cross section of the offset paraboloid.

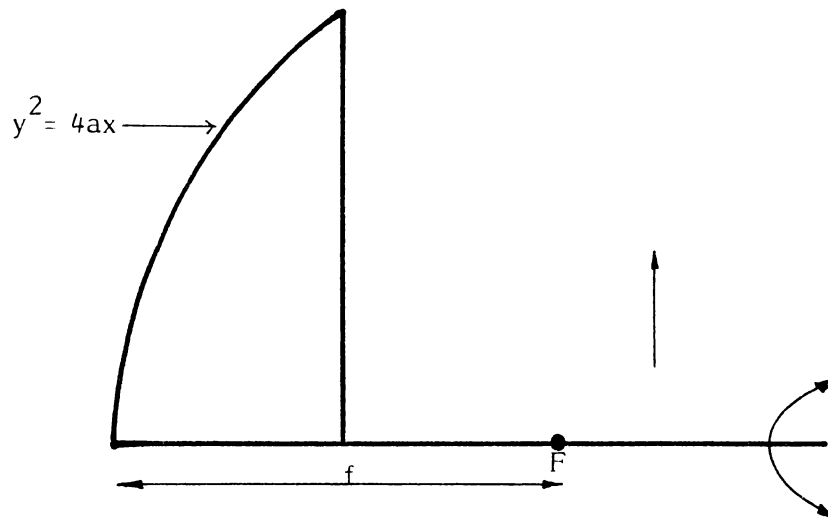


Fig.3.1(iii)(b): The template used to generate the paraboloid.

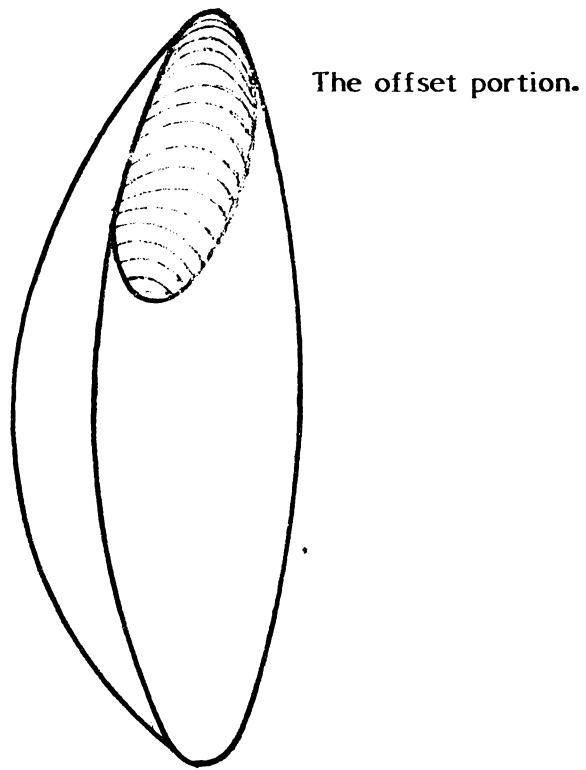


Fig.3.1(iii)(c): The cutout offset portion with the parent paraboloid.

without any distortion to the curve. A photograph of the structure is shown in fig.3.1(iii)(d).

After the offset paraboloid was properly supported, the mirror method of test for the focus of the paraboloid is conducted. For this, a number of small and thin ($\frac{1}{2}$ cms x $\frac{1}{2}$ cms) plane reflecting mirrors were pasted to different spots all over the reflector surface and the reflector was placed to face the evening sun directly so that a plane beam of light was incident on the mirrors. It was found that roughly the light was focused about a point (focus) on the axis at 100 cms away from the vertex (not a part of the offset paraboloid) of the original full paraboloid. This established, that the offset paraboloidal reflector is made exactly according to the original design.

3.1(iv) Sectoral horns as feeds

H-plane sectoral horns are used here as the basic feeds. The sectoral horns are made of copper. Sheets are cut into required shape and soldered together to form a sectoral horn. The inside walls of the horn are polished and silver plated to a high accuracy. Extreme care was taken to avoid mechanical imperfections during the process of

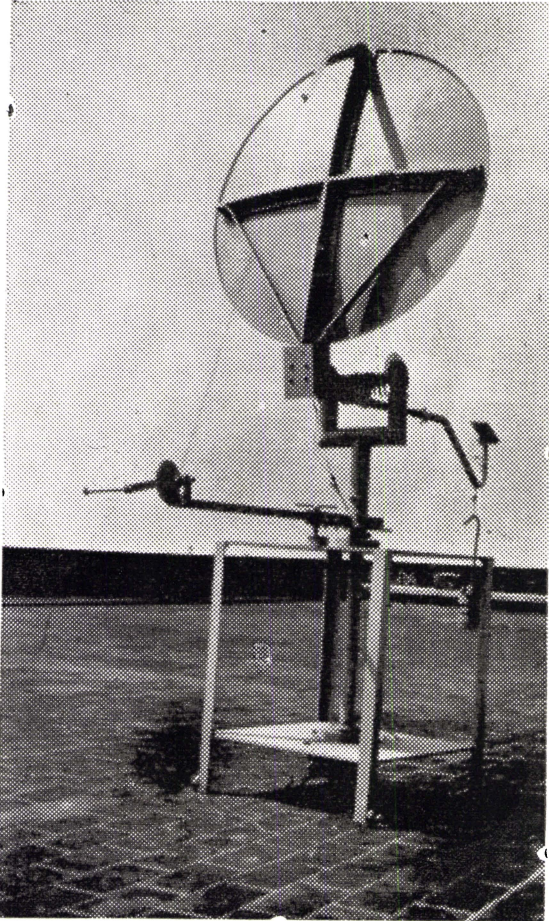


Fig 3.1 (iii) (d) The supporting structure of the offset paraboloid as seen from the rear.

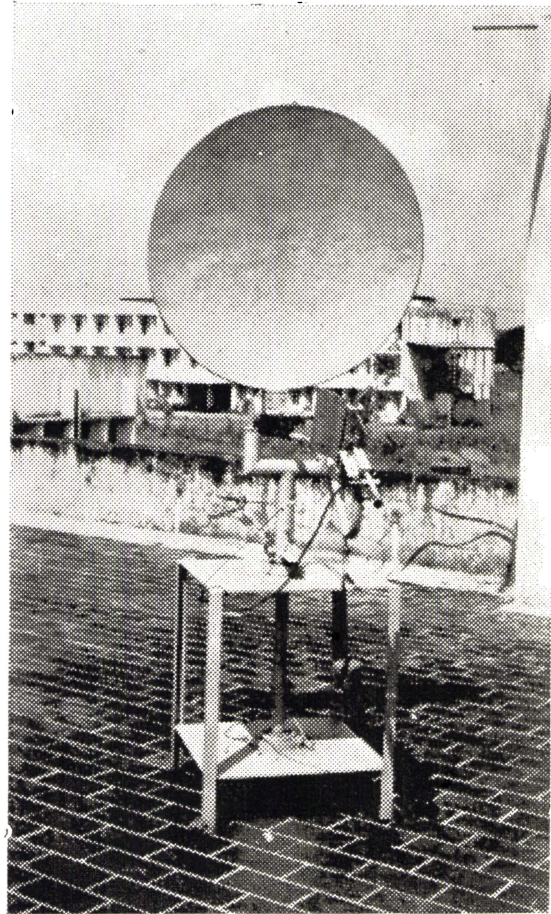


Fig 3.1 (vi) (a) The offset paraboloid as mounted on the turn-table.

fabrication of the horns. Standard waveguide flanges WG16 supplied by reliable manufacturers were soldered to the horns carefully. The various sectoral horns fabricated and used for the experiment are shown in the photograph of fig.3.1(iv)(a). The different parameters of the sectoral horns used are given in table 3.1(i).

3.1(v) Flanges on the feed

Metallic flanges are used to shape the E-plane pattern of the H-plane sectoral horns which were used as the basic feeds. A pair of identical flanges are attached on the external sides of the horn with provision to adjust the included angle and the relative position with respect to the horn aperture. A photograph of the arrangement is as shown in fig.3.1(v)(a). Two types of flanges are used in the study:

(i) Plane sheet flanges

(ii) Corrugated flanges with corrugations perpendicular to the E-vector

Fig.3.1(v)(b) is a photograph of the different flanges used in this experiment. It is established by earlier workers that for a given set of flanges and a horn at a given frequency

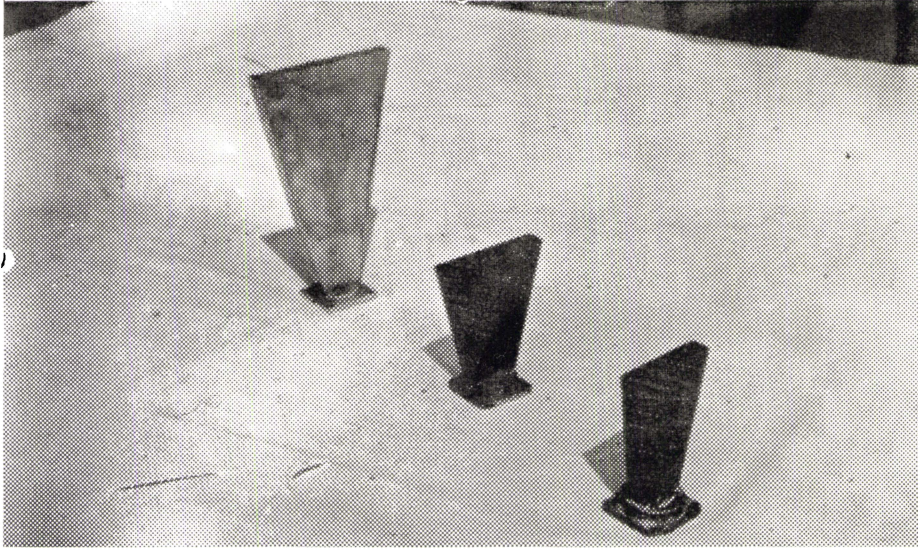


Fig 3.1 (iv) (a) The three different X - band H - plane sectoral horns used in the study.

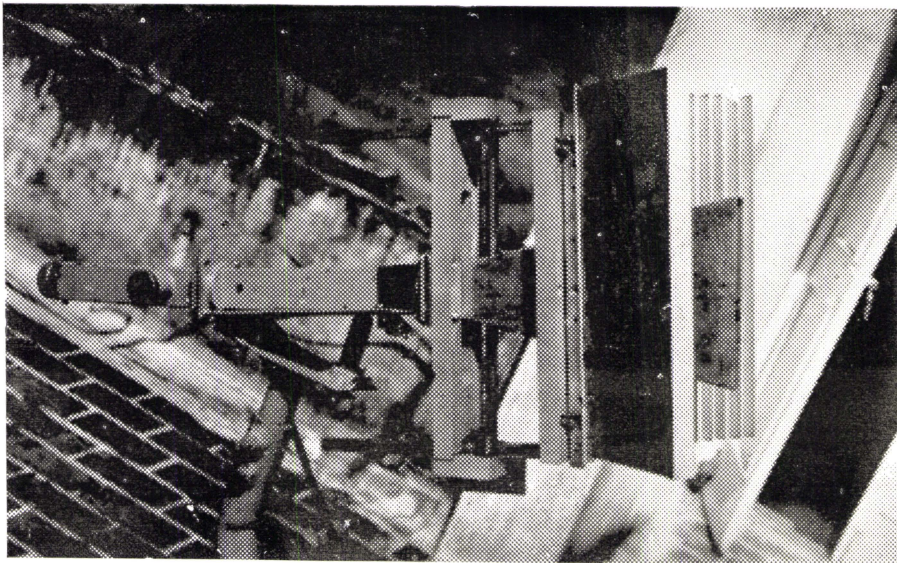


Fig 3.1 (v) (a) Flanged feed horn arrangement

Table 3.1(i)

| Sl. No. | HORN | Aperture in cms. | Flare angle in Degrees |
|---------|----------------|------------------------|------------------------------|
| 1 | H ₁ | 5.6 | 20° |
| 2 | H ₂ | 7.3 | 30° |
| 3 | H ₃ | 6.5 | 22° |

the included angle between the flanges and flange position relative to the aperture are two vital parameters which directly affect the radiation patterns of the basic primary feed horn. Hence arrangements were made to vary these parameters very precisely and to study the resultant effect on the secondary reflector characteristics. The flanges are attached to a frame which is capable of moving back and forth over the length of the horn by a rack and pinion arrangement. The distance of the flanges from the aperture of the horn is noted from a scale attached to the horn. Since the number of discrete angles necessary for the study, were not very large, strips with definite angles were prefabricated from 3mm thick aluminium sheets. The angles were bent carefully and adjusted using a high accuracy 'Universal Bevel Protractor'. Suitable holes were drilled to attach the flange-pair symmetrically. The flange elements are then screwed to the angle-strip.

3.1(vi) Antenna positioner

Plotting of the secondary radiation patterns is a very important part of the problem. For calculating the absolute gain of the system, it is necessary to have the patterns both in E and H planes. For this purpose the offset reflector was mounted on a turn table which is capable of rotating independently on both azimuthal and elevation axes. These mutually perpendicular

axes should pass through the centre of the aperture of the full paraboloid of which the offset reflector forms a part. It is absolutely necessary to have the system completely free of wobbling or jerks since the secondary patterns will be having 3 dB beam widths of the order of 1 to 2°. Even a slight wobbling will displace the beam from the target by twice the amount. It was possible to carry out the experiment only on the open-roof terrace of the building, since the distances involved are large, ruling out the comfort of indoor rooms like the anechoic chamber, already available in the department. Winds with speed of the order of 40 to 60 km/hr are frequent in the area. The turn-table together with the solid paraboloid mounted on it should be able to withstand this wind. Taking all these into account, a very sturdy and heavy but simple and manually operated turn-table was designed. A photograph of the turn-table with the offset paraboloid in position is shown in fig.3.1(vi)(a). The entire rotating mechanism is housed in an iron frame of dimensions $2 \times 2 \times 2\frac{1}{2}$ feet which forms the body of the set up. The top and bottom portions are made of 10mm thick mild steel plates. One and a half inches angles are welded to the two plates so as to form a frame. Two circular holes are cut at the centre of the steel plates so that a $1\frac{3}{4}$ " diameter steel rod can pass through it. This is the main shaft on which the whole

structure of the reflector with feed is mounted. The rod is held in position by two heavy ball bearings attached to the two plates right at the centre. The paraboloid is fitted in such a way that the straight line passing through the centre of the shaft is collinear with the aperture diameter of the full paraboloid. This line is the vertical axis on which the reflector antenna is rotated to get the azimuthal pattern.

Another rod perpendicular to the main shaft but passing through the centre of the aperture of the parabola forms the horizontal axis. The reflector can be tilted up and down through an angle of more than 45° on either side by the action of a string and counter weight round this axis. A schematic diagram showing the axes and the direction of rotation is given in fig.3.1(vi)(b). As noted earlier, the reflector can be rotated around any of the two axes independently, keeping one axis fixed by a clamping arrangement. When the azimuthal pattern is required, the elevation system is arrested by a screw arrangement at the handle in the normal position and the paraboloid is rotated around the vertical shaft. Similarly when the elevation pattern is required, the vertical axis is fixed using a nut and bolt arrangement. With the transmitter in the normal position, the clamp of the handle is released and the handle is slowly rotated so that the reflector is tilted

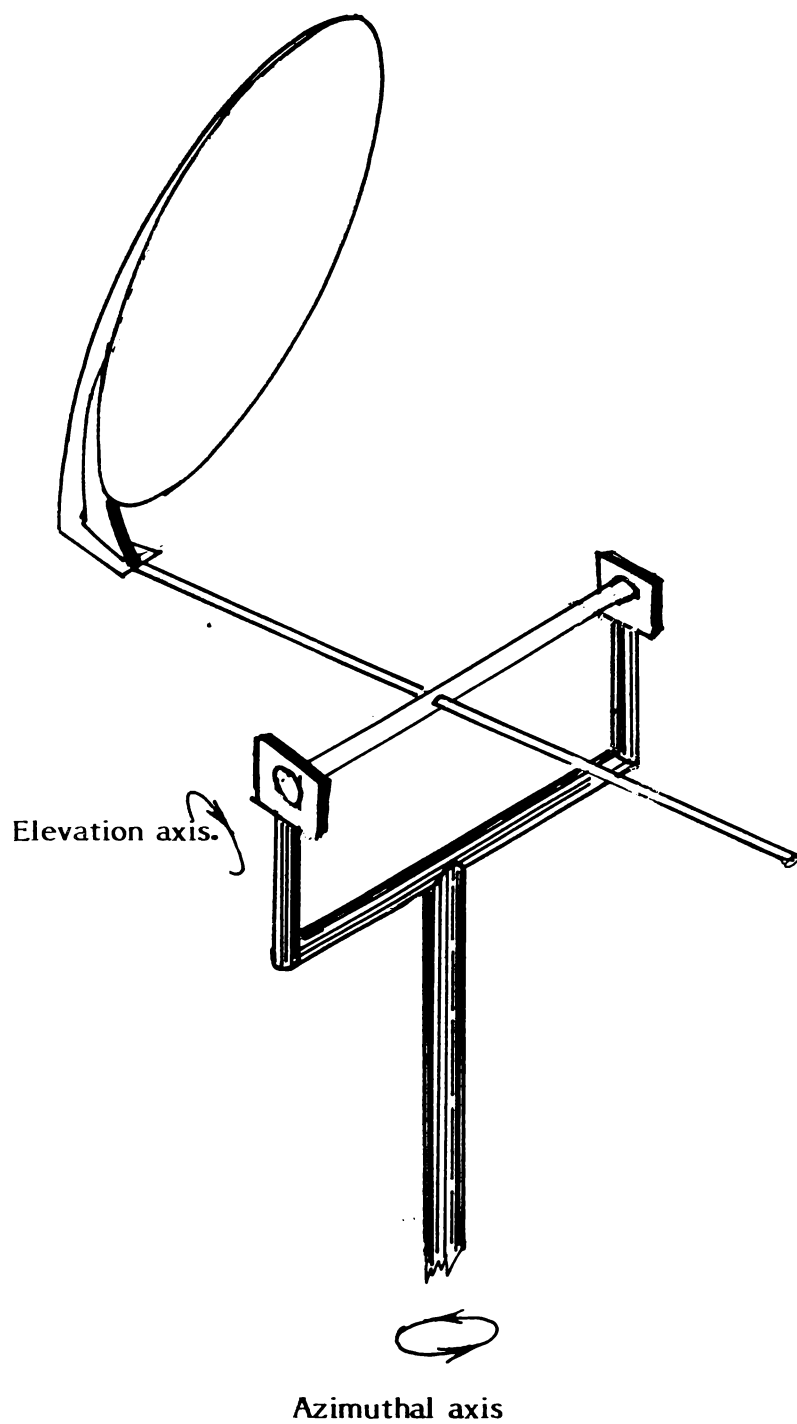


Fig.3.1(vi)(b): The schematic diagram showing the two orthogonal axes and their direction of rotation.

as required. The counter weight just below the feed horn keeps the reflector balanced in any position of tilt. By the combined action of horizontal and vertical clamps, the paraboloid can be made to point towards any desired direction.

The arrangement described above was used to plot semiautomatically the E- and H-plane patterns of the offset reflector one after the other. For the semiautomatic plotting, an X-Y plotter (H.P 7047A) having a maximum sensitivity of 2 micro volt/mm was used. To plot a pattern, it requires a D.C. signal corresponding to the position of the paraboloid on the X-axis. This signal was derived from a linear potentiometric voltage divider arrangement attached to the corresponding axis of the system. The movable contact of the potentiometer moves exactly at the same speed as the axis so that the D.C. signal is proportional to the angle through which axis has turned. Two wire wound linear potentiometers together with a highly stabilized D.C. power supply are used for this purpose. By a switching arrangement, any one of the two potential dividers can be connected to the X-axis of the plotter. When the arrangement is finally used for plotting, it is rotated in the same direction as at the time of calibration on both the axes. This is done in order to prevent the error due to backlash of the potentiometers. This rule was followed throughout

the work. The speed of rotation is kept at a steady minimum value of about 0.25 rpm in order to get the sharp peaks and nulls of the pattern recorded properly.

3.2 Plotting of the radiation patterns

Radiation pattern is a graphic record showing the spatial distribution of radiated energy from a source. The radiation characteristics can be presented either as power patterns or as intensity patterns. Usually it is easy to plot power patterns than intensity patterns. Throughout this work, all patterns plotted are power patterns. Whenever it was necessary to calculate antenna gain, the power patterns were changed into intensity patterns and the method of pattern integration was employed. Fig.3.2(1)(a) show the typical radiation power patterns in both polar co-ordinates and rectangular co-ordinates. Their corresponding intensity patterns are also shown.

Usually two methods are employed to plot radiation patterns. In the first method, the test antenna is used as the transmitter of microwave power. A receiving antenna is moved along the circumference of a circle with the aperture centre of the transmitting antenna as its center. The received signal

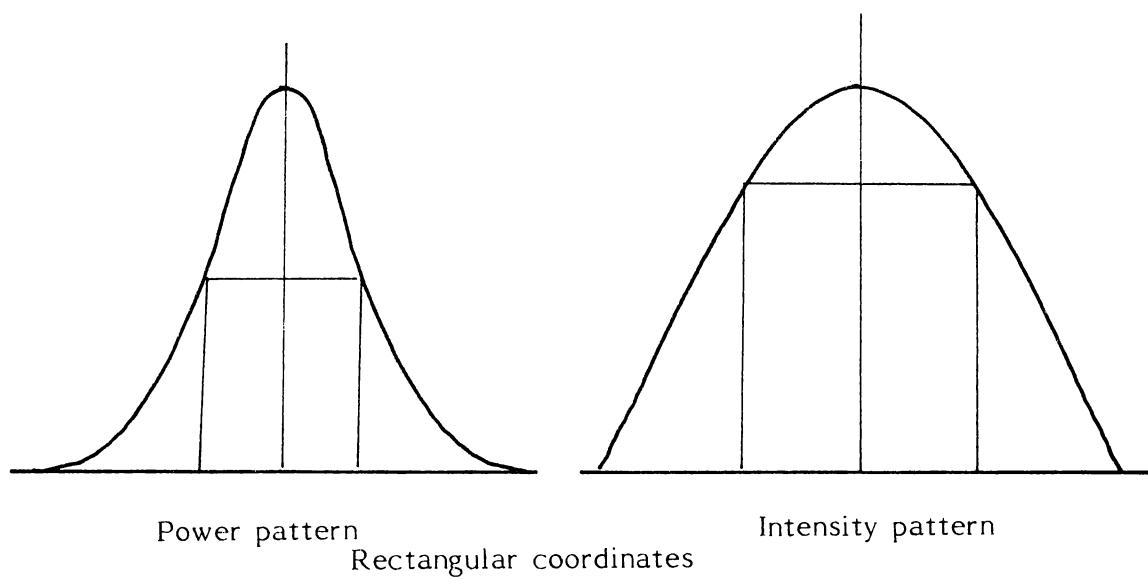
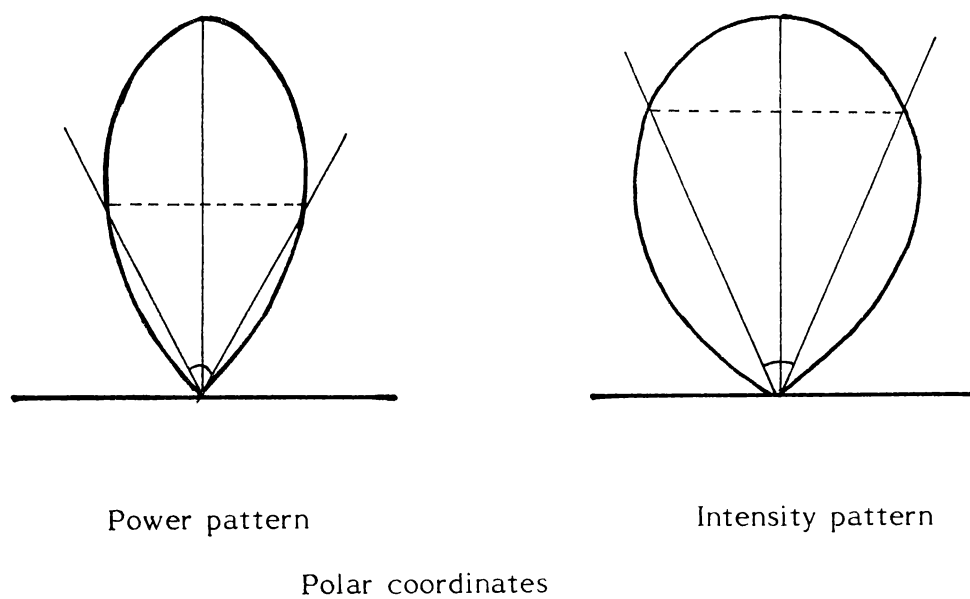


Fig. 3.2 (i) (a) : Typical radiation patterns in polar and reangular coordinates .

is plotted against the angular position of the receiving antenna with respect to the transmitter. The method is very cumbersome and requires a lot of space.

In the second method, the antenna under test is used as the receiver and it is rotated keeping a standard transmitting antenna fixed. A plot of the signal from the receiving antenna against the angle through which the test antenna has rotated gives the radiation pattern.

According to the theorem of reciprocity in antennas, the radiation characteristics of an antenna is same in both transmitting and receiving modes. In the present work, the second method which is simpler and convenient than the first method is used for plotting the radiation patterns. A standard pyramidal antenna is used as the transmitter. The test antenna here consists of the secondary offset paraboloid together with the flanged sectoral horn as the feed at the focus. The receiving antenna and transmitting antenna were kept at a distance greater than $2D^2/\lambda$. This ensured that the patterns plotted are those in the radiation field and not in the induction field. This is an important point in antenna measurements technique since almost all practical antennas we use are used to transmit or receive far field (radiation region) signals.

For this purpose, the experiment was set on the flat roof top of the department building. The transmitter and receiver were placed at the two ends of the 'L' shaped portion of the three storeyed building. A photograph of the set up is shown in fig.3.2(i)(b). A deep "valley" between the two wings of the L-shaped building ensured that no ground reflected ray reached the receiver. Two photographs in fig.3.2(i)(c) and fig.3.2(i)(d) show the transmitter as seen from the receiving end and receiver as seen from the transmitting end.

The transmitter set up consisted of a standard pyramidal horn, an isolator and the Gunn diode oscillator. The whole set up is pictured in fig.3.2(i)(e). The system shown is supported on a tripod stand specially built for the purpose. The transmitter horn is nearly 2 meters high from the roof's ground level and it is so oriented that its E plane is parallel to ground. A regulated D.C.power supply kept at the bottom of the tripod stand provided the working voltage to the Gunn diode.

In the receiving system, the feed horn is kept on the axis of the parent paraboloid with the centre of the horn aperture coinciding with the focus of the paraboloid. A crystal detector mount connected to the horn by a straight waveguide

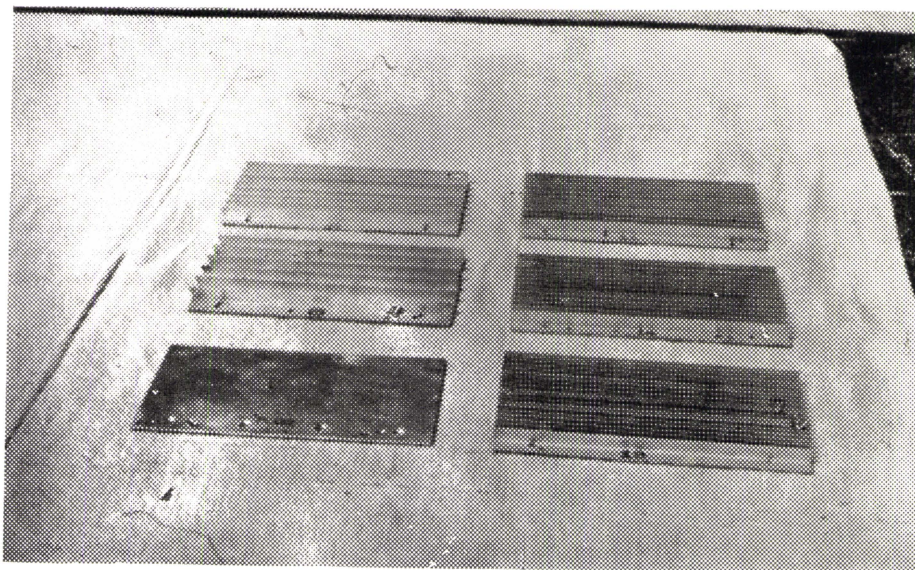


Fig 3.1 (v) (b) Different flanges used to modify the feed.

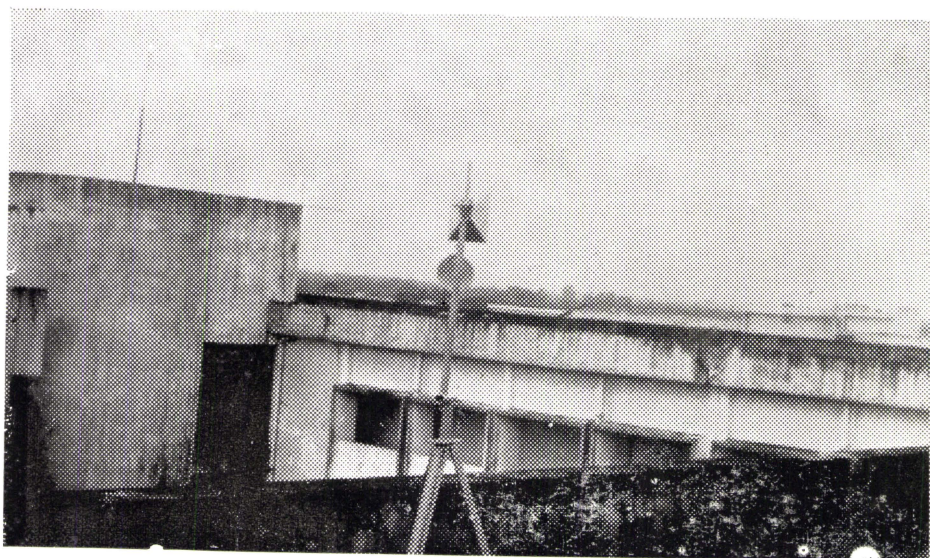


Fig 3.2 (i) (b) The experimental arrangement of the transmitter and receiver as viewed from the transmitting end.



Fig 3.2 (i) (c) The transmitter (pyramidal horn) almost indistinguishable from the background as viewed from the receiving end.

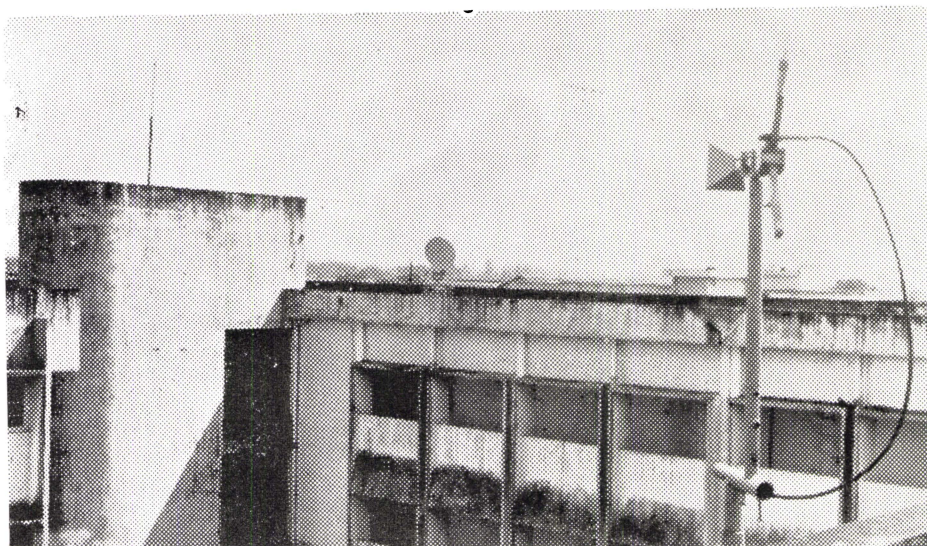


Fig 3.2 (i) (d) The paraboloidal receiving antenna as seen from the transmitting end.

section rectified the received microwave power and the resulting D.C. signal is taken out via well shielded co-axial cable to the Y-input of the recorder. A moving frame arrangement on the feed horn is used to carry the flanges. The H-plane sectoral horn was fitted in such a way that its E-plane is parallel to the ground (the horn is kept vertical). A photograph of the arrangement used to plot the radiation pattern is shown in fig.3.2(i)(f). As stated elsewhere, the flange pair can be moved back and forth along the length of the horn and can be clamped at any position. To plot E-plane pattern, the axis of the parent paraboloid is kept parallel to the ground and the offset reflector is rotated about the vertical shaft. To plot H-plane pattern, the vertical shaft is locked such that the offset antenna points straight towards the transmitter and maximum on-axis power is received. Now the clamp of the horizontal (elevation) axis is released and is brought to the extreme position. The handle is then rotated so that the offset paraboloid scans the vertical plane (H-plane) in the pre-calibrated direction. The signals corresponding to the angular position of the offset reflector are taken out using coaxial cables and connected to X-axis of the recorder. Care is taken to see that no external noise reached the recorder.

In plotting cross polarization patterns, almost the same experimental set up and procedure is followed. The only difference is that the transmitting horn is made at the cross

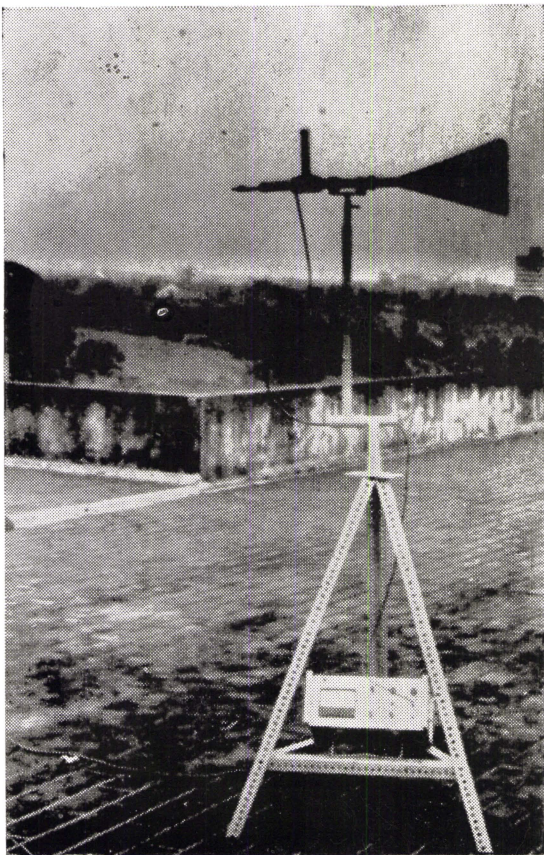


Fig 3.2 (i) (e) The transmitting set up consisting of the pyramidal horn, the isolator with matched load and Gunn-diode oscillator with power supply at the base of the tripod stand.

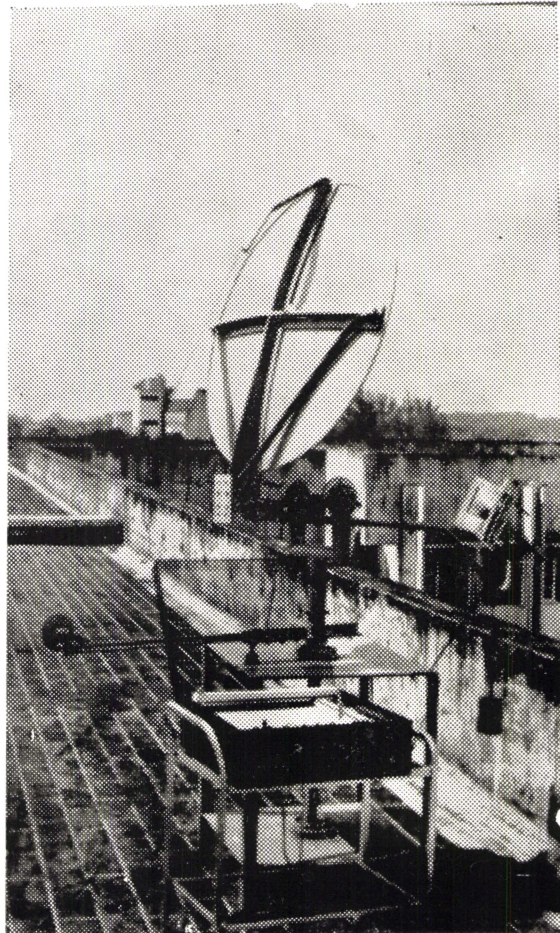


Fig 3.2 (i) (f) The experimental arrangement used to plot the radiation patterns. Here the test antenna (paraboloidal reflector with modified feed) is used as the receiver.

mode to the receiving feed horn. This is achieved by using a 90° waveguide twist at the transmitting end. Thus the E-plane of the transmitting horn was perpendicular to the ground while at the receiving end the feed horn was kept with E-plane parallel to the ground. This ensured that the amount of power received is proportional to the degree of cross polarization of the system.

3.3 Measurement of VSWR and On-axis power density

The VSWR of any antenna is proportional to the degree of impedance mismatch. No antenna design is complete without investigating its voltage standing wave ratio. If the antenna is not properly matched to the transmission line, a portion of the energy is reflected back to the source. The advancing wave from the source and the reflected wave interact to set up standing waves in the system analogous to mechanical waves on a stretched string. At the maximum position (antinode) of the standing wave, the voltage may be so high that the equipment may be damaged. Moreover, the transmission efficiency is deteriorated by backward reflection.

The VSWR is defined as the ratio of the electric field intensity at the voltage antinode to that at the node.

$$\text{VSWR (S)} = \frac{E_{\text{MAX}}}{E_{\text{MIN}}}$$

For ideal matching, there should not be any reflected power and hence no standing waves.

So,

$$E_{\text{MAX}} = E_{\text{MIN}} \quad \text{and} \quad S = 1$$

In the other extreme case of total reflection, all the energy is reflected back and the nodes will be at zero potential, i.e., $E_{\text{MIN}} = 0$.

$$S = \frac{E_{\text{MAX}}}{E_{\text{MIN}}} = \frac{E_{\text{MAX}}}{0} = \infty$$

So if there is total mismatch, the VSWR tends to an infinite value.

The 'on-axis power density' is the power radiated per unit area along the axis of the antenna. Since in almost all practical systems, the power radiated along the main axis only is used, the measurements are also confined to on-axis direction only.

Measurement of VSWR and on-axis power density were carried out simultaneously using an experimental set up shown in fig.3.3(i)(a). The test antenna is used in the transmitting mode with a slotted section carriage inserted in series with the

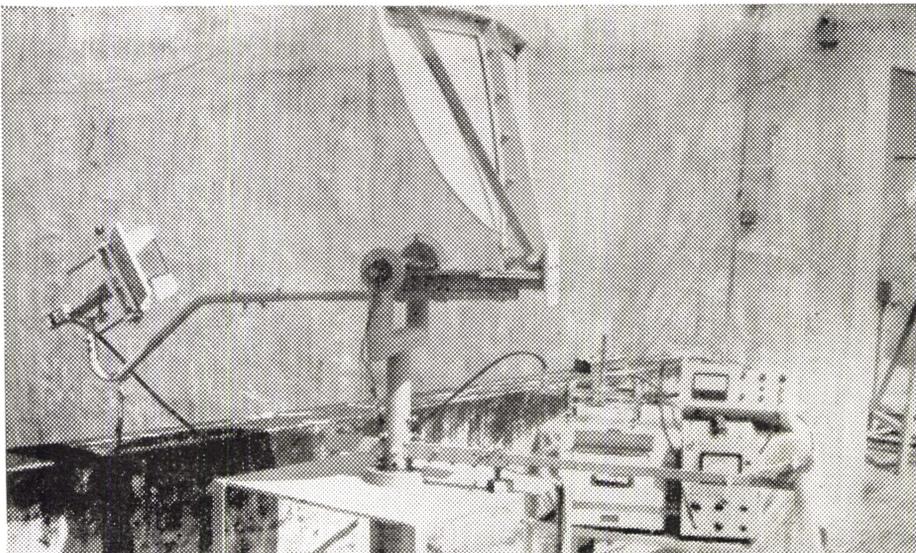


Fig 3.3 (i) (a) The VSWR and on-axis power density measurement is carried out simultaneously using the arrangement shown in the above photograph. Here the test antenna (paraboloidal reflector) is used as the transmitter.

Gunn diode and test antenna. The on-axis power received using a small pyramidal horn kept at a distance greater than 35 metres (far field) is detected and brought back to the transmitting end using good quality shielded cable so that simultaneous measurements of VSWR and on-axis power density can be carried out. The detected outputs of the slotted line carriage and the receiver horn are fed to two sensitive microammeters and the readings are noted manually.

$$\text{VSWR} = S = \sqrt{\frac{I_{\text{MAX}}}{I_{\text{MIN}}}} \quad \text{where } I_{\text{MAX}} \text{ and } I_{\text{MIN}} \text{ are maximum}$$

position and minimum position readings on the slotted section microammeter respectively.

3.4 Directive gain and half power beam width

Directive gain of any antenna is defined¹⁰ as the ratio of the maximum radiation intensity in a given direction to the radiation intensity in that direction from an isotropic antenna with the same power input.

In this study, we are interested in the total gain of the system. For this purpose, both E-plane pattern and H-plane pattern are plotted. The respective gains can be

determined by pattern integration method⁸. Numerical integration of the intensity patterns in rectangular co-ordinates is employed to calculate the directive gains.

Gain in any plane is given by

$$G_{\text{plane}} = \frac{2\pi I_{\text{MAX}}}{\int_0^{2\pi} I_{\theta} d\theta}$$

In decibels it is expressed as

$$G_{\text{plane}} \text{ dB} = 20 \log_{10} \frac{2\pi I_{\text{MAX}}}{\int_0^{2\pi} I_{\theta} d\theta}$$

where I_{MAX} is the intensity in the direction of maximum radiation and I_{θ} is the intensity in any direction whose bearing angle is θ in the same plane.

$\int_0^{2\pi} I_{\theta} d\theta$ is the area between the intensity curve

and the θ -axis within the limits $\theta = 0$ and $\theta = 2\pi$.

Using this method the directive gains in the two orthogonal planes (E and H) are calculated separately. The

directive gain of the antenna is then given by

$$G = \frac{G_E G_H}{\pi}$$

where G_E = Directive gain in E-plane

G_H = Directive gain in H-plane

The directive gain can also be expressed in decibels as

$$G \text{ dB} = G_E \text{ dB} + G_H \text{ dB} - 20 \log \pi$$

G dB is the absolute directing power gain of the antenna system over an isotropic radiator.

This is the experimental value of the directive gain. The half power beam width of the radiation pattern also can be estimated from the patterns.

Chapter IV

EXPERIMENTAL DATA AND RESULTS

This chapter presents the results of the experimental investigations carried out on the offset reflector antenna using different feed configurations. The results obtained with different flanges on the feed horn are compared with those obtained when the horn alone is used as the feed. The experiments are carried out on three different H-plane sectoral horns with the same set of flange parameters. The response of the antenna at five X-band frequencies of 8.25 GHz, 9 GHz, 10 GHz, 10.6 GHz and 11 GHz with the above feed is studied in detail with stress on the following:

- 1) VSWR of the system
- 2) On-axis power density
- 3) Radiation patterns
- 4) Directive gain
- 5) Half power beam widths
- 6) Cross polarization

4.1 Voltage standing wave ratio (VSWR)

4.1(i) Dependence of VSWR on flange position

The flanges are attached to the H-plane sectoral horn as shown in fig. 3.1(v)(a). The position of flanges with respect to the aperture of the horn is adjusted using a rack and pinion arrangement. For measuring VSWR the standard method of slotted section carriage and sensitive spot galvanometer is used as it was found that this arrangement gave more accurate and reliable results than a VSWR meter.

The VSWR of the system is found to be depending very much on the position of the flange pair relative to the horn aperture. As the flange pair is moved along the length of the horn, the VSWR fluctuated between sharp maximas and minimas. For all horns fitted with flanges of various parameters operating at various frequencies, the same is found to be true as the graphs in fig.4.1(i)(a) to (h) show. The general pattern of VSWR closely resembles a damped sine wave. When we compare the flanged horn VSWR with horn alone as feed, it is found that at some positions the VSWR shoots up above the normal (i.e. when horn alone as feed) value and at some other positions it goes well below near to the ideal value of 1.

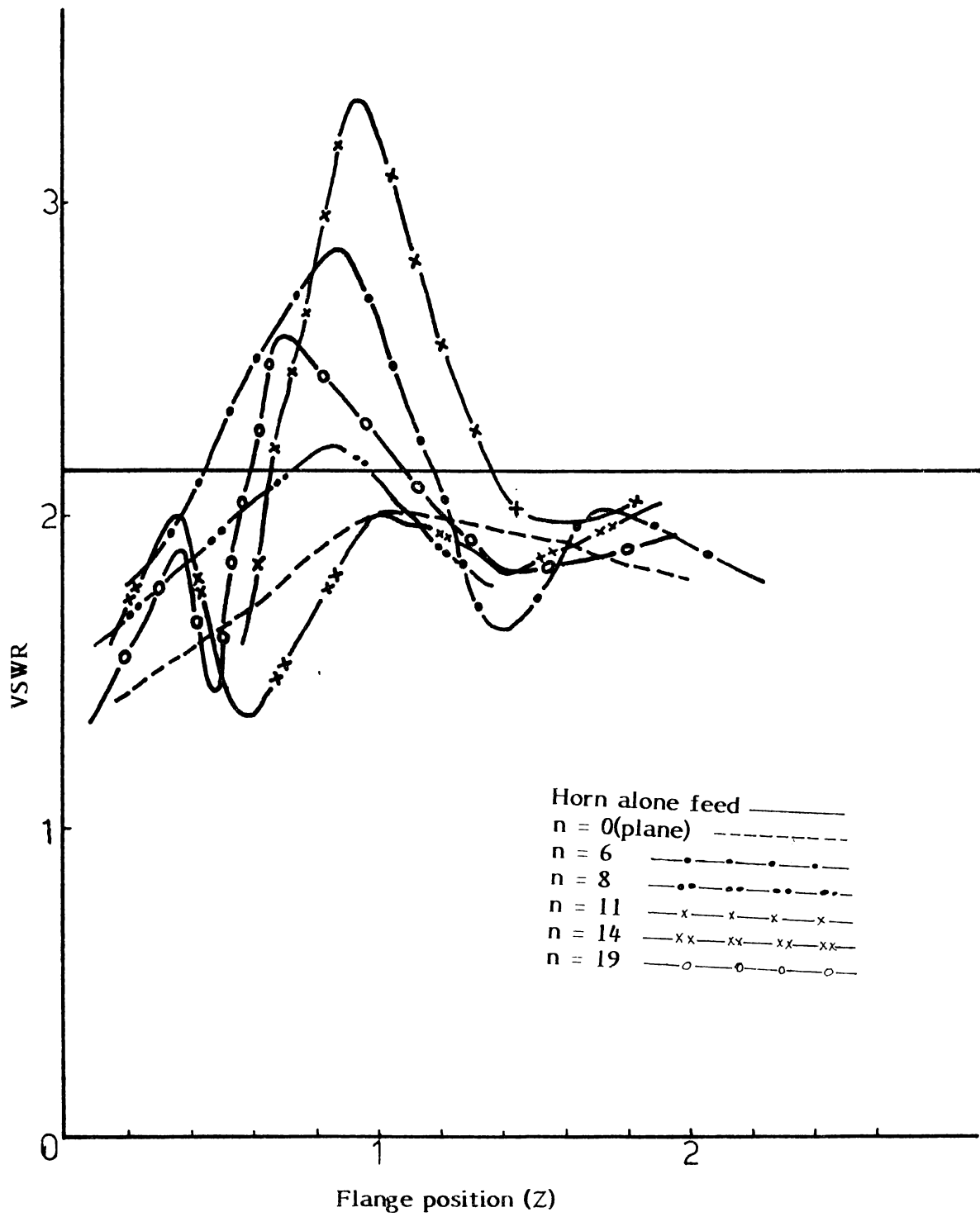


Fig. 4.1(i)(a): Variation of VSWR with flange position .

Horn H3 , F = 9 GHz , 2B = 60 .

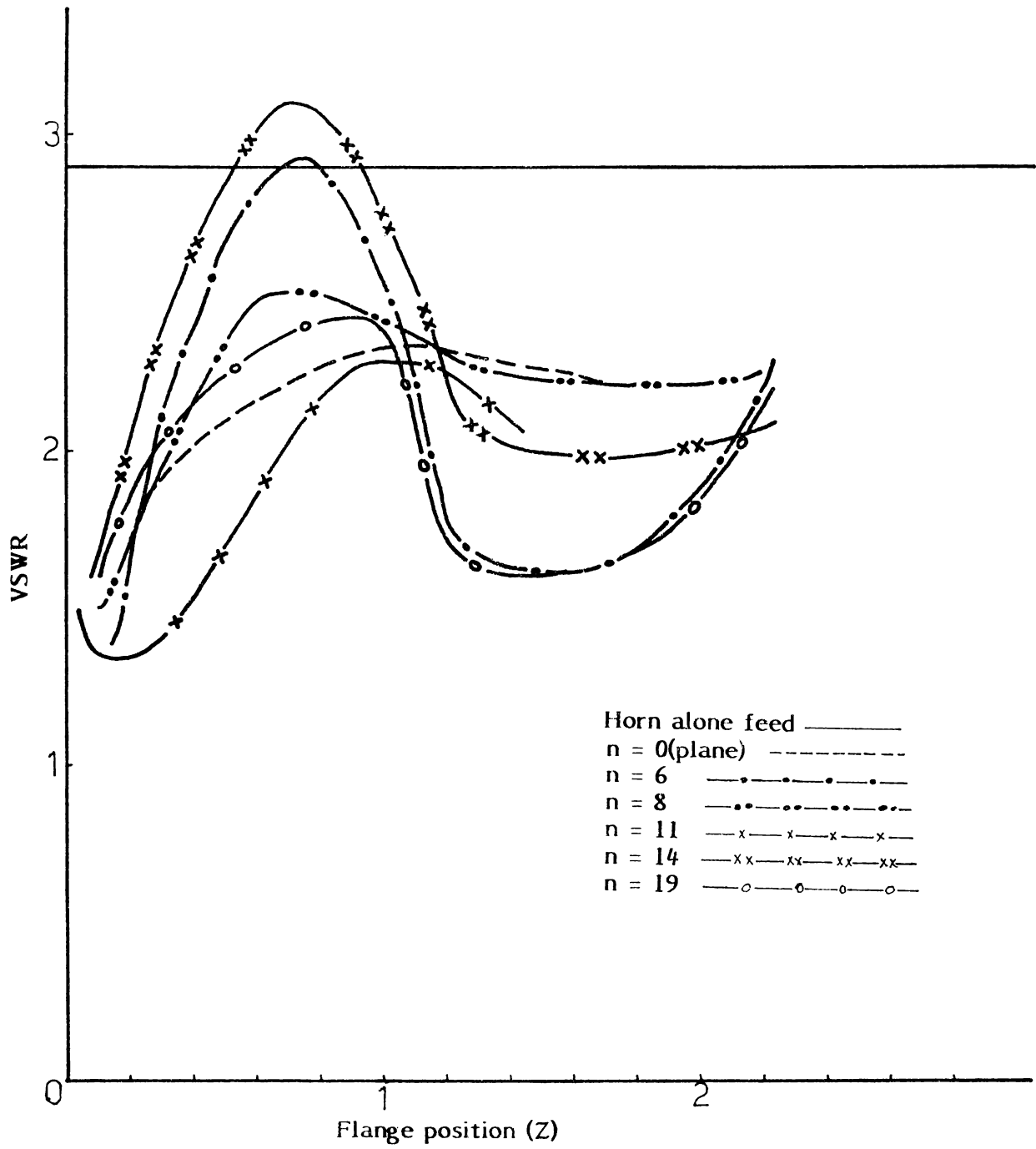


Fig.4.1(i)(b): Variation of VSWR with flange position .

Horn H3 , F = 8.25 GHz , 2B = 60 .

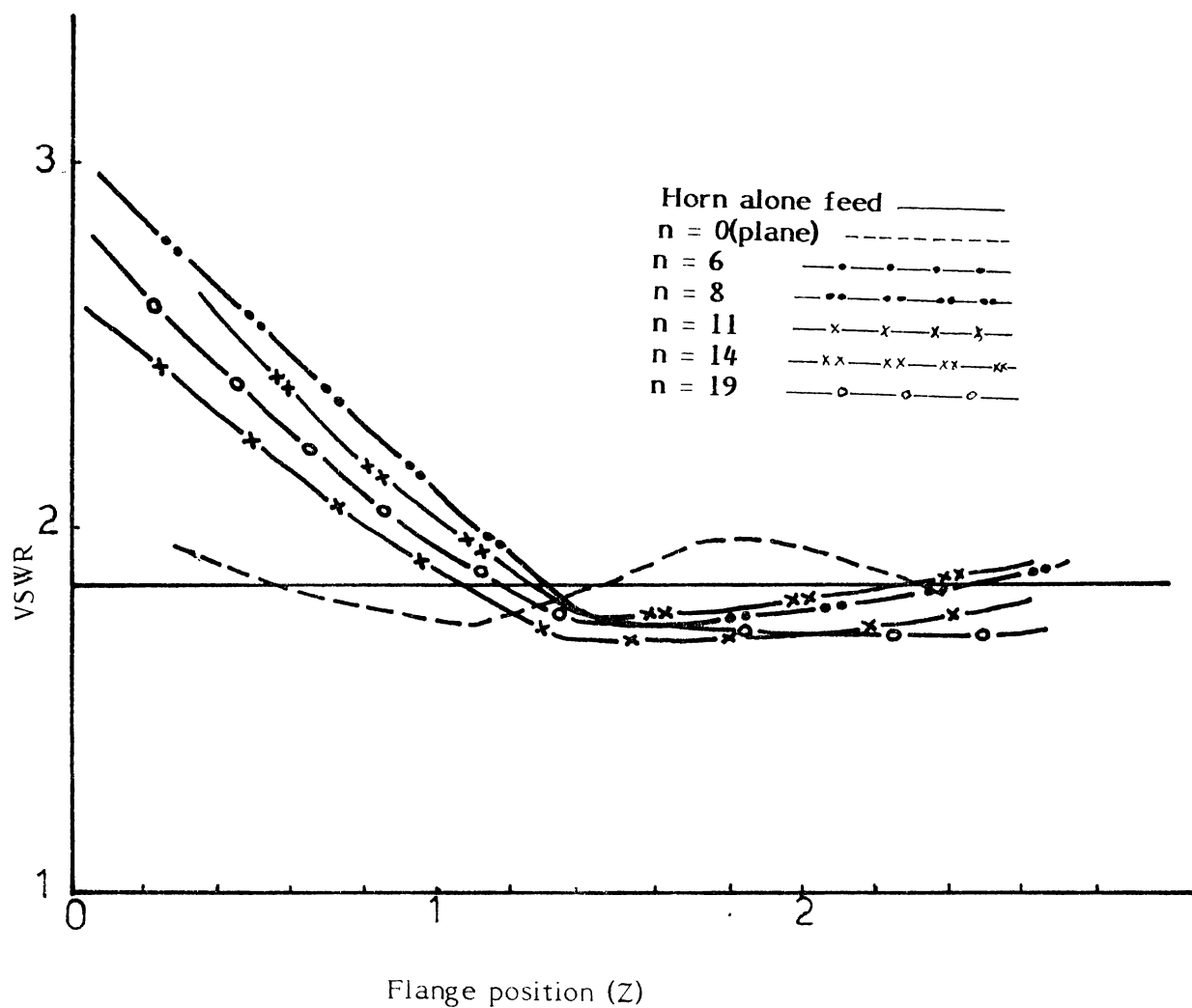


Fig.4.1(i)(c): Variation of VSWR with flange position.

Horn H3, $f=10.6$, $2B=60$.

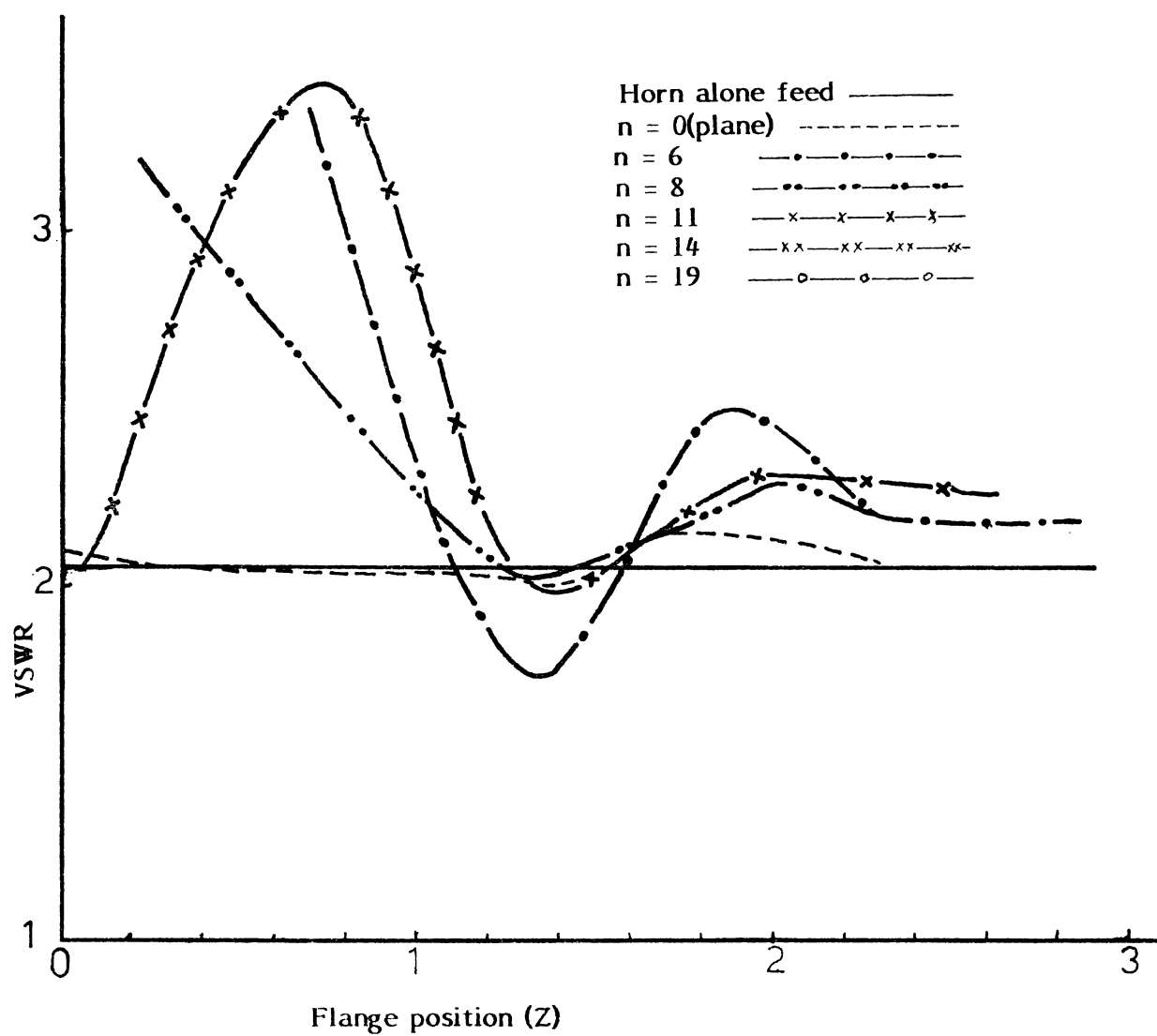


Fig.4.1(i)(d): Variation of VSWR with Flange position
Horn H3, $f=11$ GHz, $2B=60$.

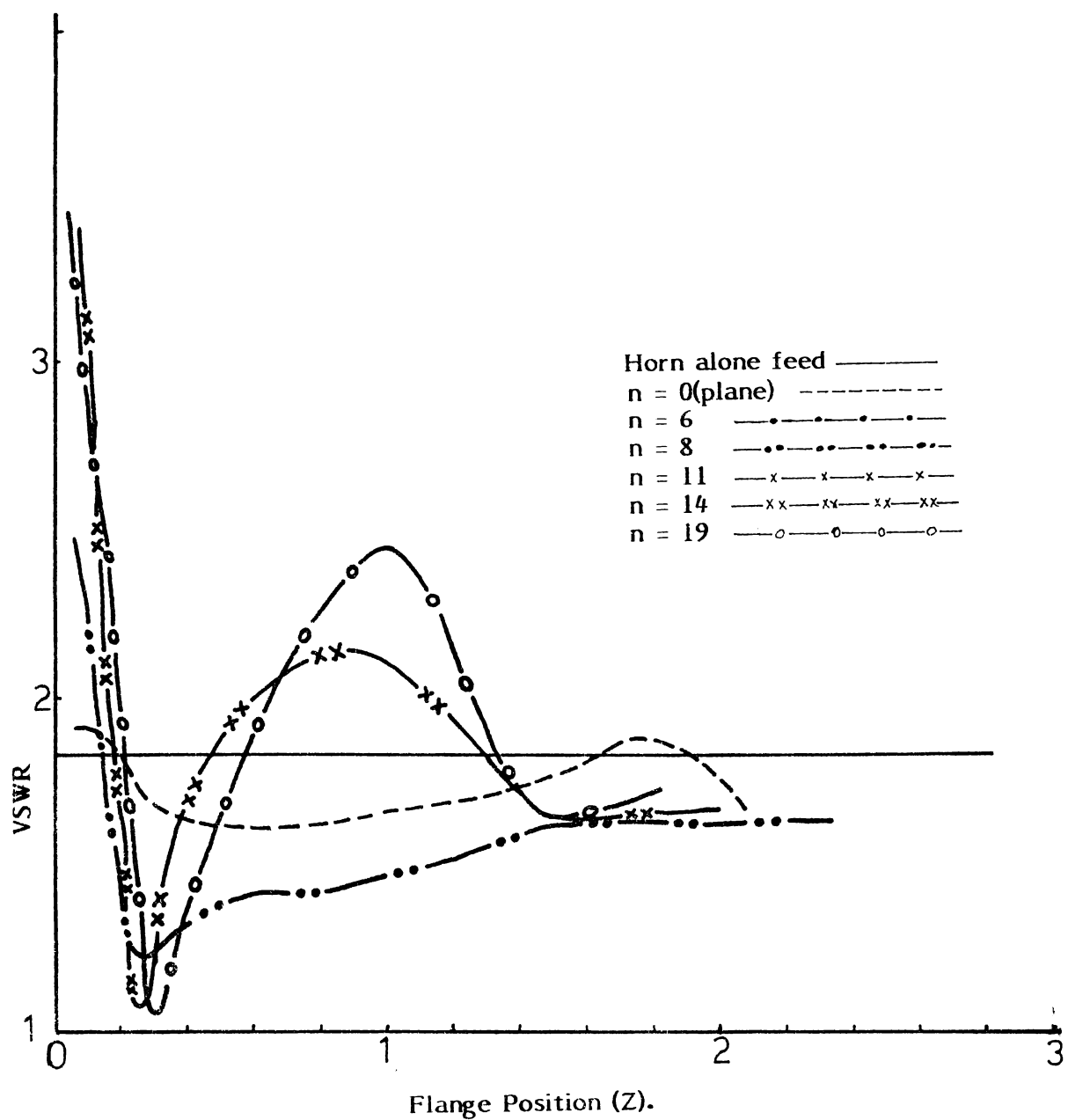


Fig.4.1(i)(e): Variation of VSWR with flange position.

Horn H3, $f=10$ GHz, $2B=60$.

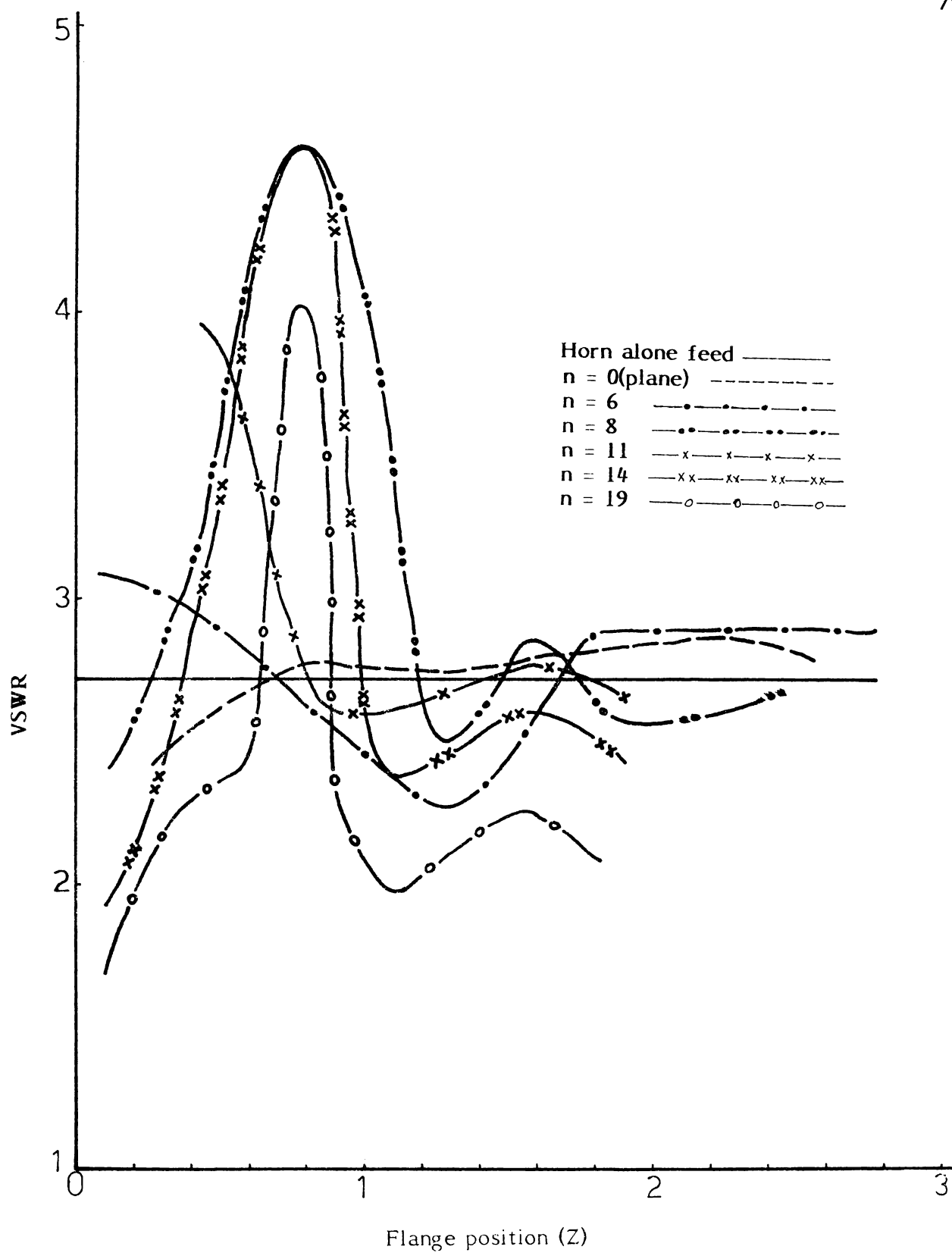


Fig. 4.1 (i) (f) ; Variation of VSWR with flange position .

Horn H3 , $F = 11 \text{ GHz}$, $2B = 90$.

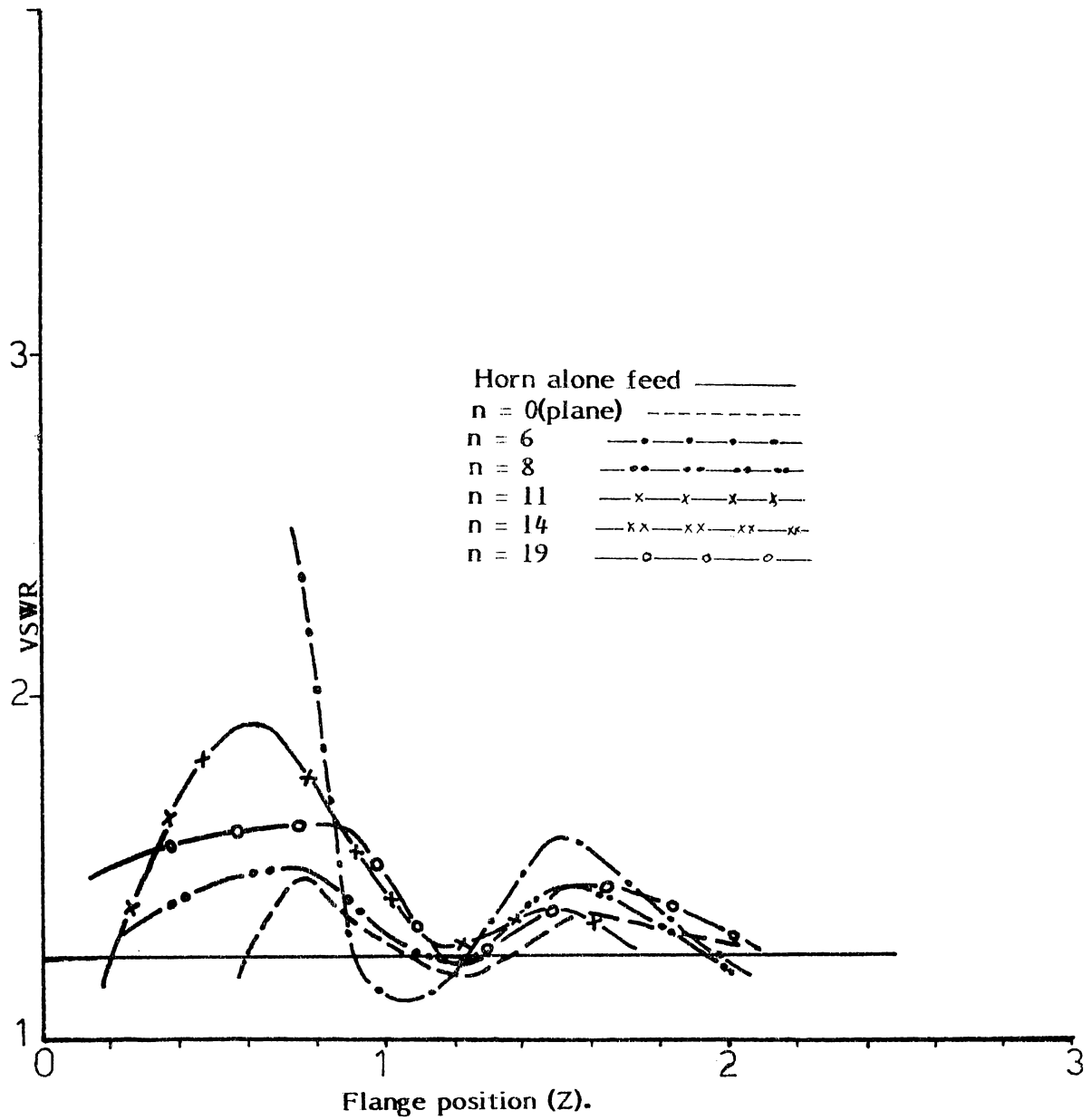


Fig.4.1(i)(g): Variation of VSWR with flange position.

Horn H3, $f=8.25$ GHz, $2B=90$.

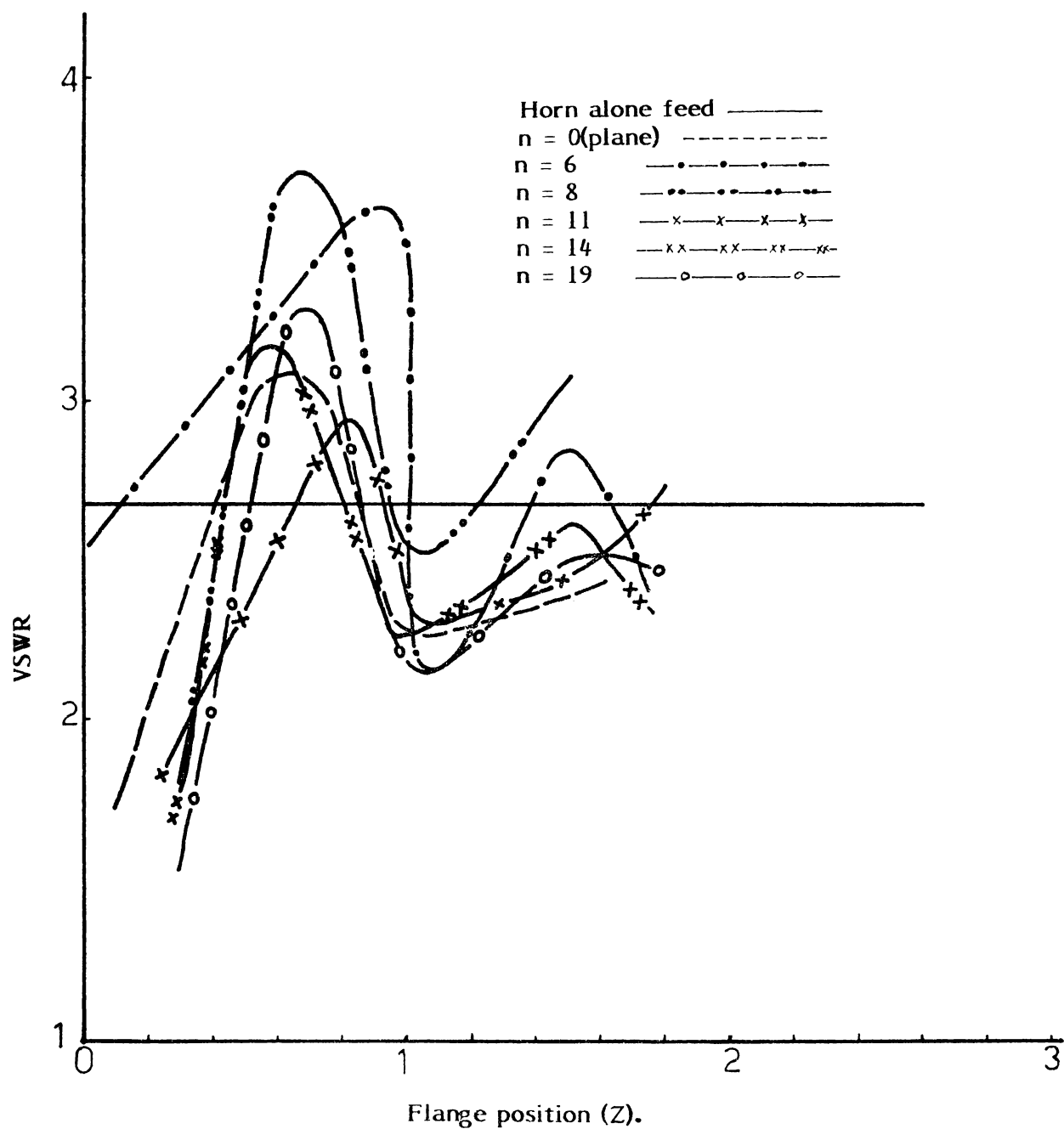


Fig.4.1(i)(h): Variation of VSWR with flange position.

Horn H3, $f=11\text{GHz}$, $2B=90$.

The second observation is very significant if we consider the on-axis power density at the corresponding positions. This aspect is discussed in next section. From the graphs, it can be inferred that corrugated flanges are superior to the plane flanges as far as impedance matching is considered.

4.1(ii) Dependence of VSWR on frequency

The VSWR is found to be depending very much on the frequency of operation, if other parameters are invariant. The VSWR of the system is determined by the phase and amplitude of the waves reflected from the primary feed horn and the secondary reflector. The two waves add up or reduce the effective reflection depending on the phase variation between them.

It is observed that for almost all frequencies the value of VSWR is less when corrugated flanges are used. Just the horn alone as feed or horn with plane flanges, are found to give a greater VSWR. The variation of VSWR with frequency is studied only at 'optimum' positions of the flanges where the on-axis power is maximum, since it is the only case of practical importance. It can be inferred from the graphs 4.1(ii)(a) to (e) that the variation of VSWR with frequency for different flanges is almost similar to the variation of the VSWR of the

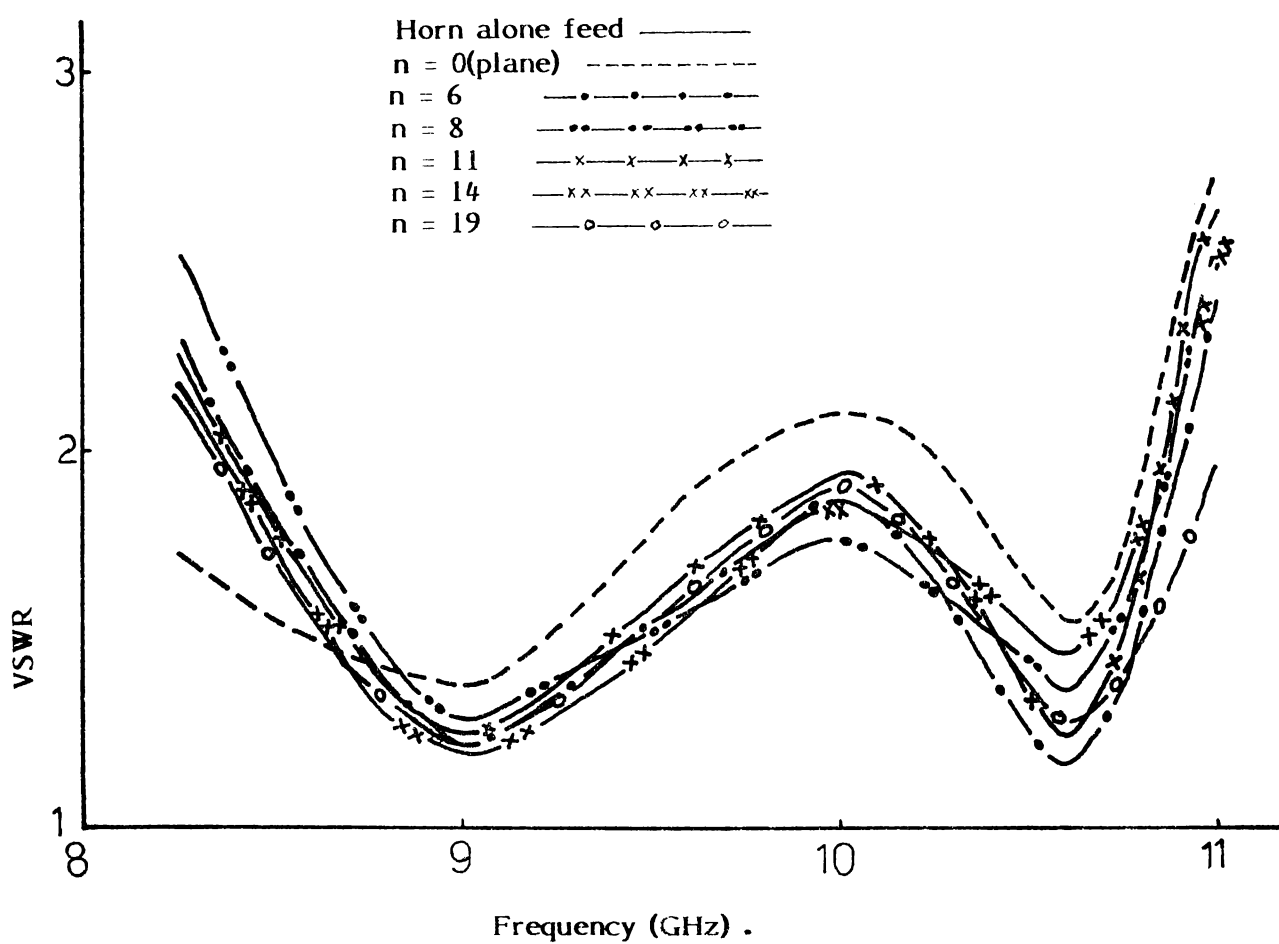


Fig.4.1(ii)(a): Variation of VSWR with frequency at Optimum position..

Horn H3, $2B=90$.

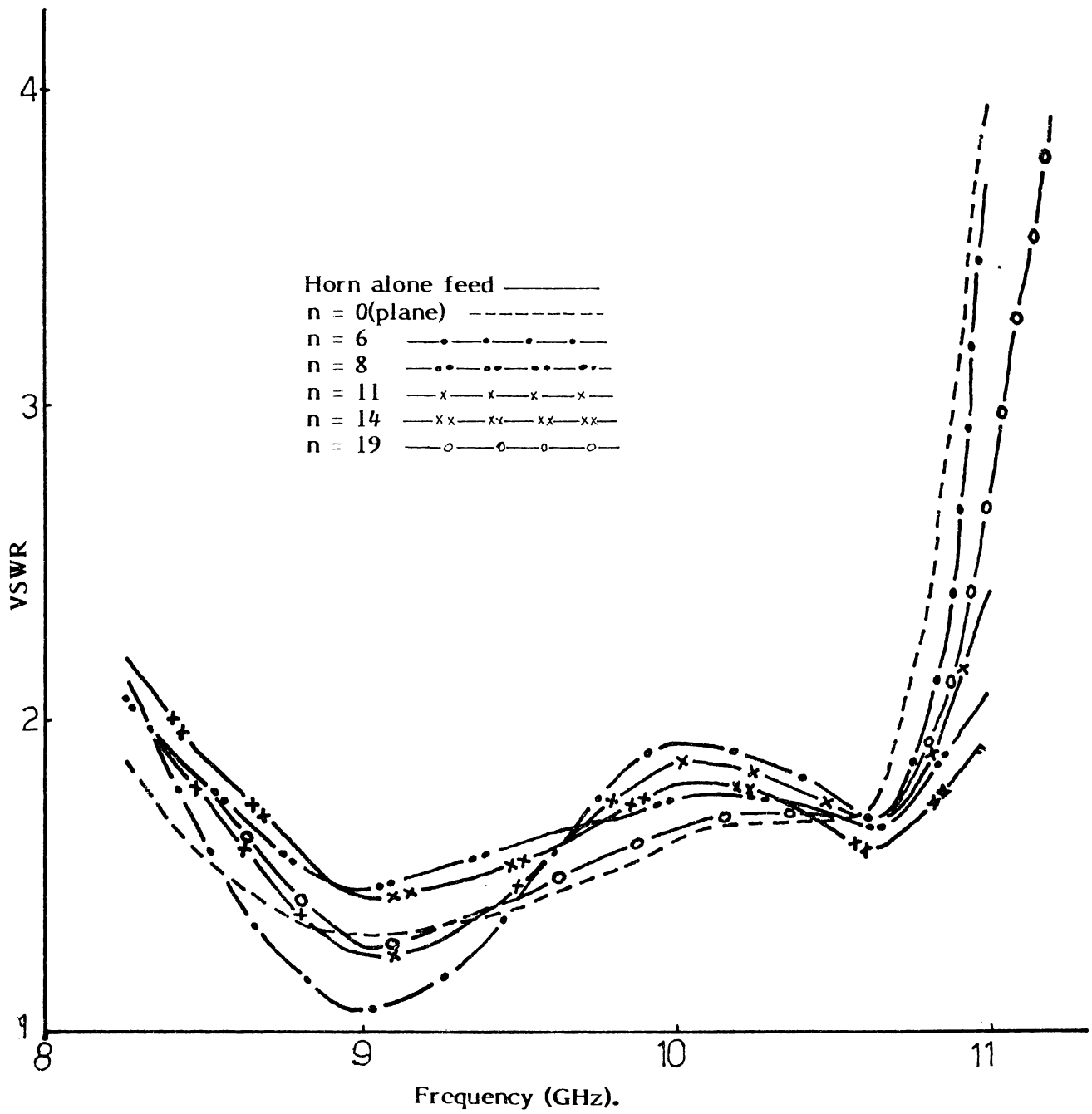


Fig.4.1(ii)(b): Variation of VSWR with frequency at the Optimum position .

Horn H3,2B=45 .

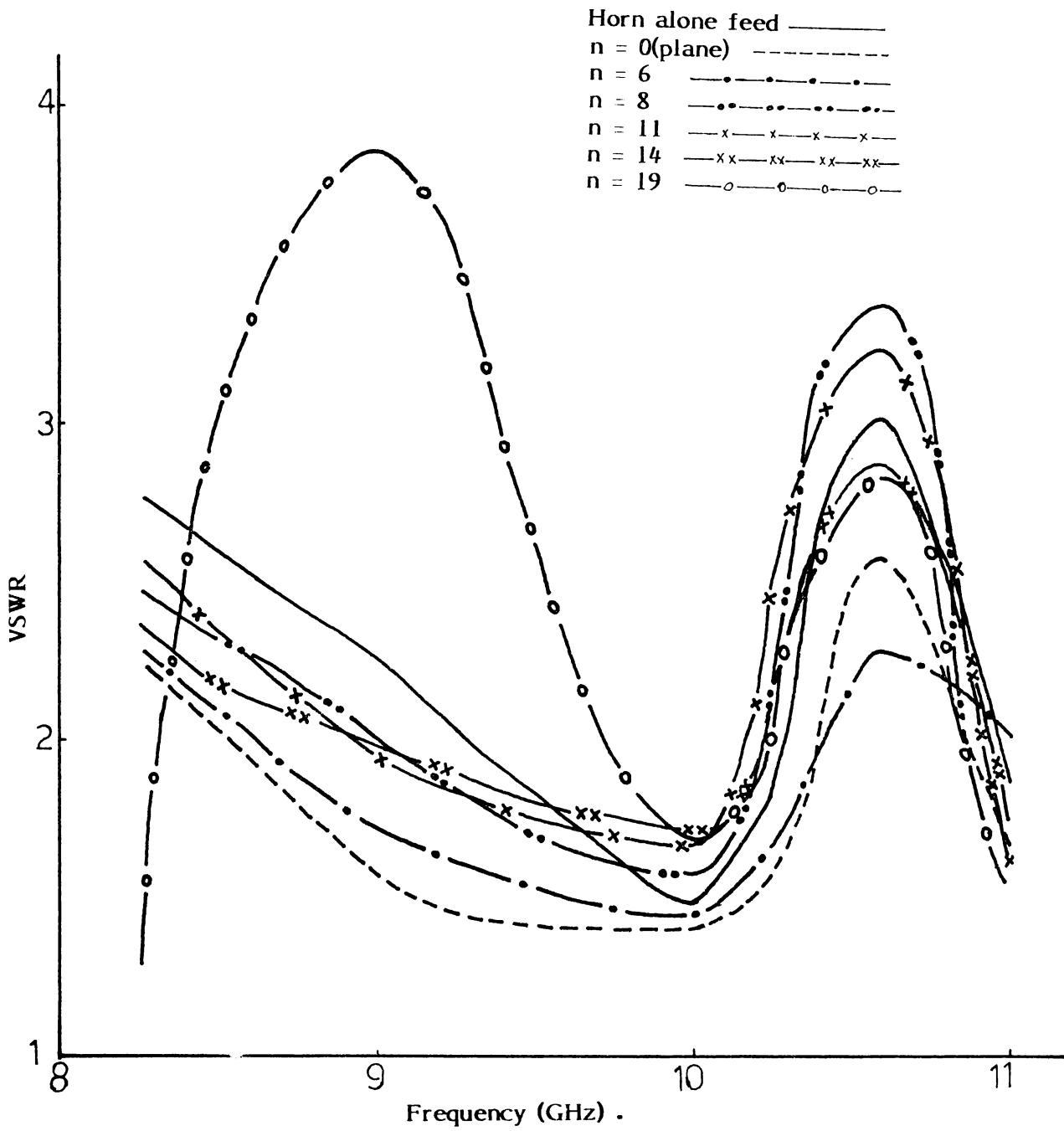


Fig.4.1(ii)(c) : Variation of VSWR with frequency at Optimum position .

Horn H2,2B=45 .

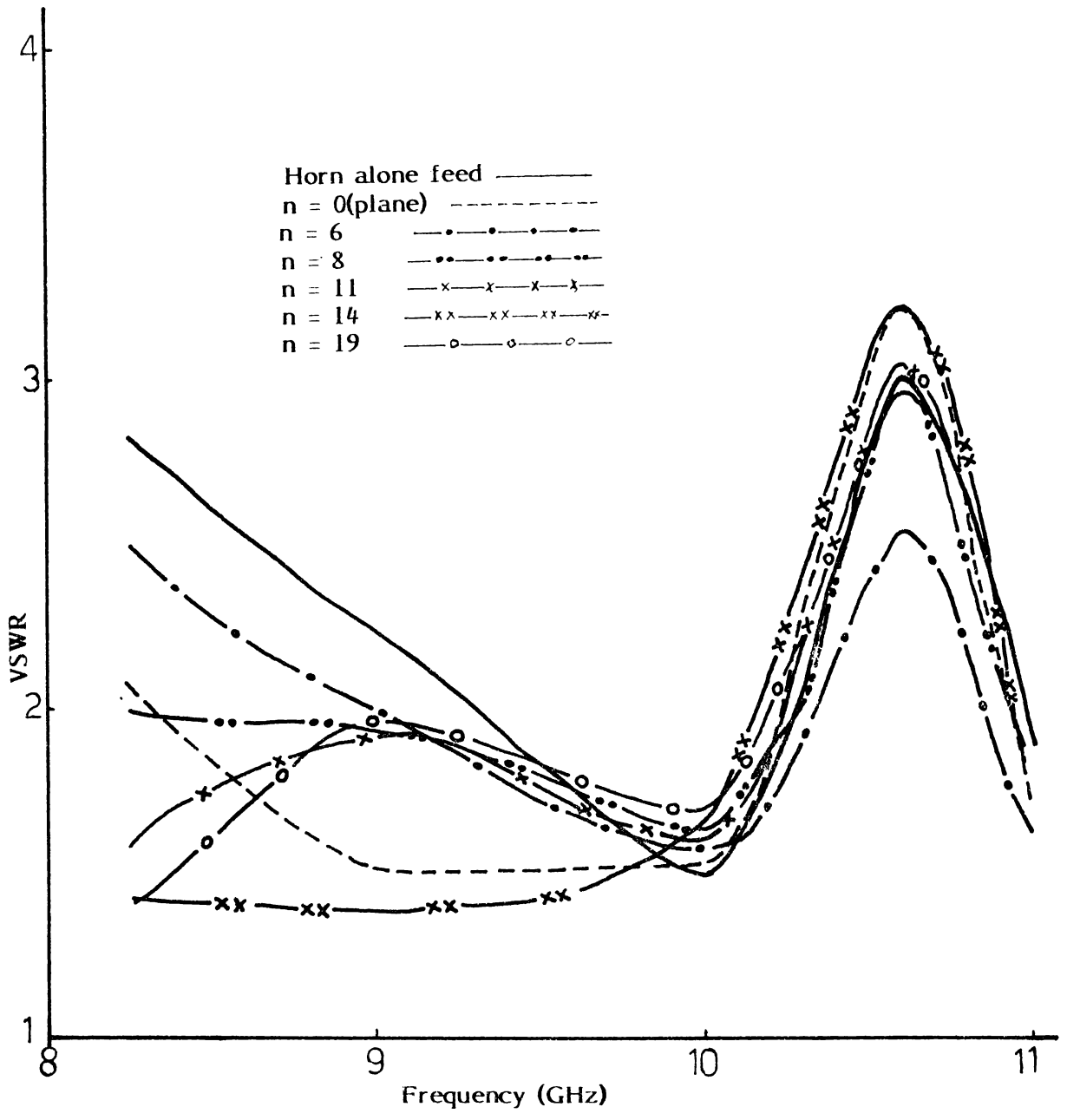


Fig.4.1(ii)(e): Variation of VSWR with frequency at Optimum position .

Horn H2 , 2B-90

feed horn without flanges. This fact reveals that certain flanges serve to lower the VSWR while maintaining the frequency characteristics of the primary feed horn. This means that if the primary feed is broad band, the addition of the corrugated flanges just lowers the VSWR, without adversely affecting the band width. The flanges with corrugation numbers 6, 8, and 11 with periods in the neighbourhood of $\lambda/2$ where λ is the wavelength of radiation are found to be most attractive.

4.1(iii) Dependence of VSWR on corrugation parameters

The corrugations are made of aluminium flats of thickness 1.2 cms, width 10 cms and length 20 cms, by machining grooves of equal width parallel to each other. The depth of the groove 'h' was kept constant for all flanges. The corrugation period or slot width 'a' depends on number of corrugations 'n'. The variation of VSWR with corrugation period 'a' is studied and results are presented here.

The curves in fig.4.1(iii)(a) to (d) show that the VSWR at optimum position of flanges depends on the corrugation parameters also. It can be inferred that all flanges help to lower the VSWR for all the frequencies in the X-band.

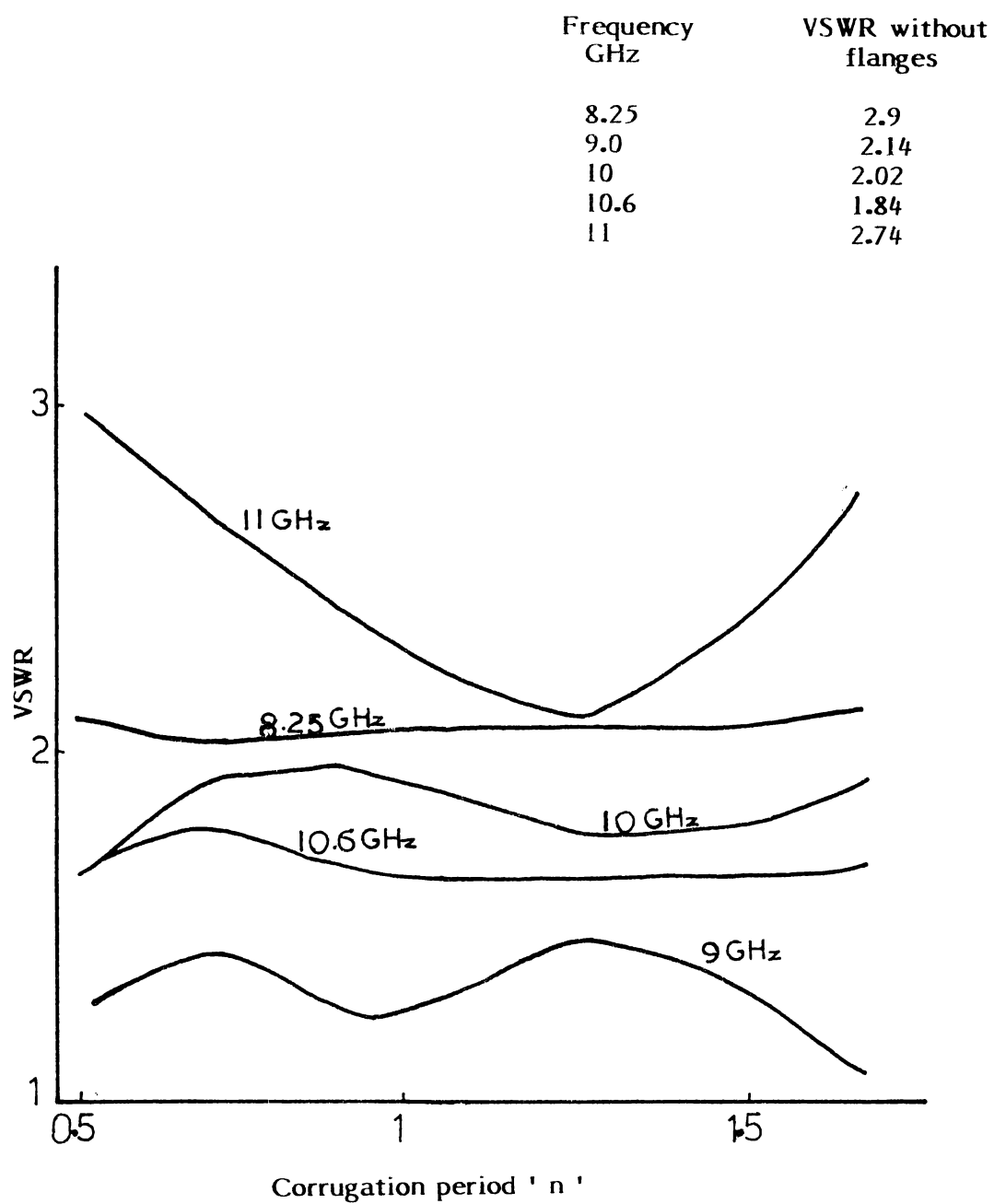


Fig.4.1(iii)(a): Variation of VSWR with corrugation period at the Optimum position .

Horn H3 , $2B = 45$.

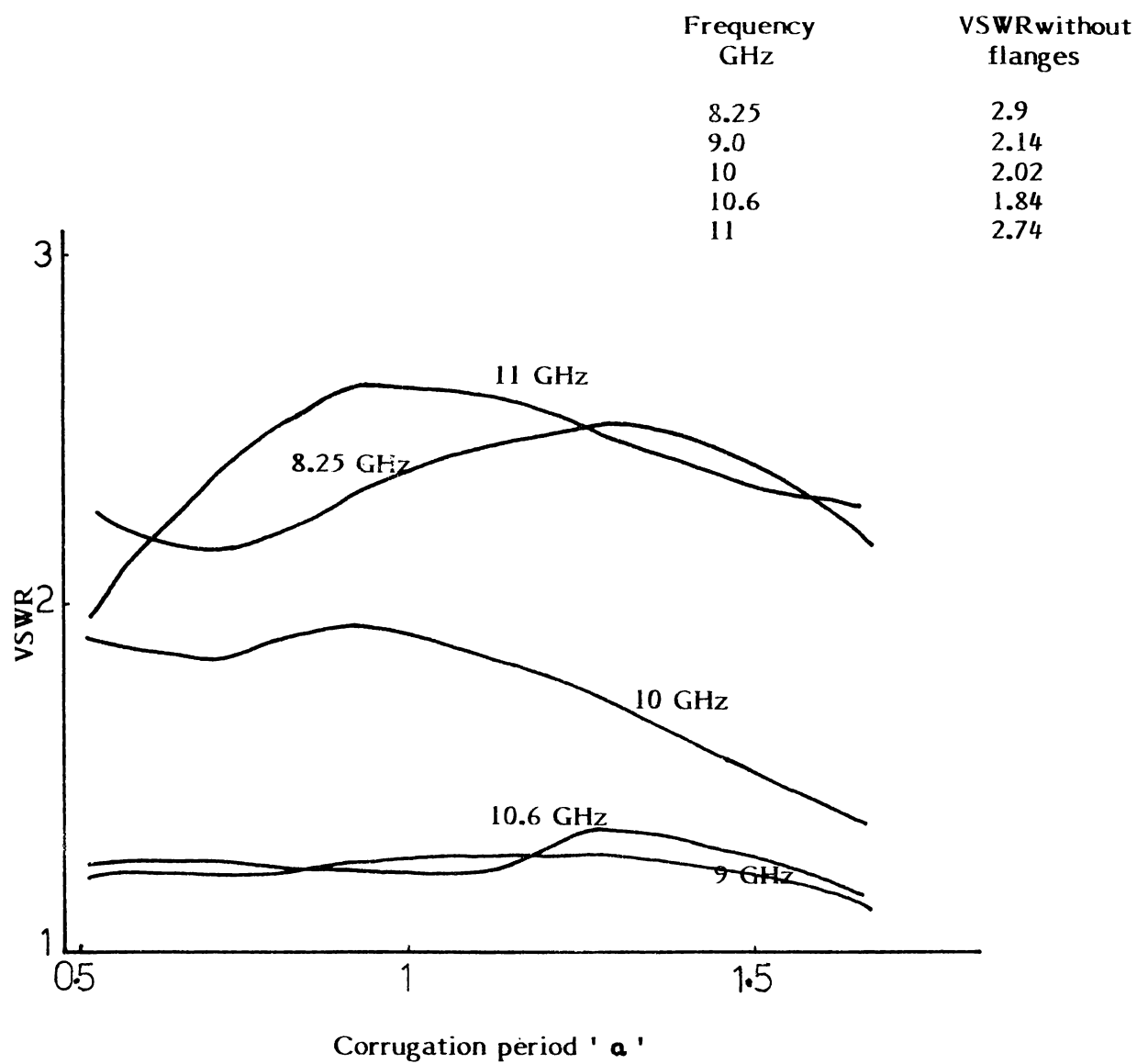


Fig.4.1(iii)(b): Variation of VSWR with corrugation period at the Optimum position .

Horn H₃, 2B = 90 .

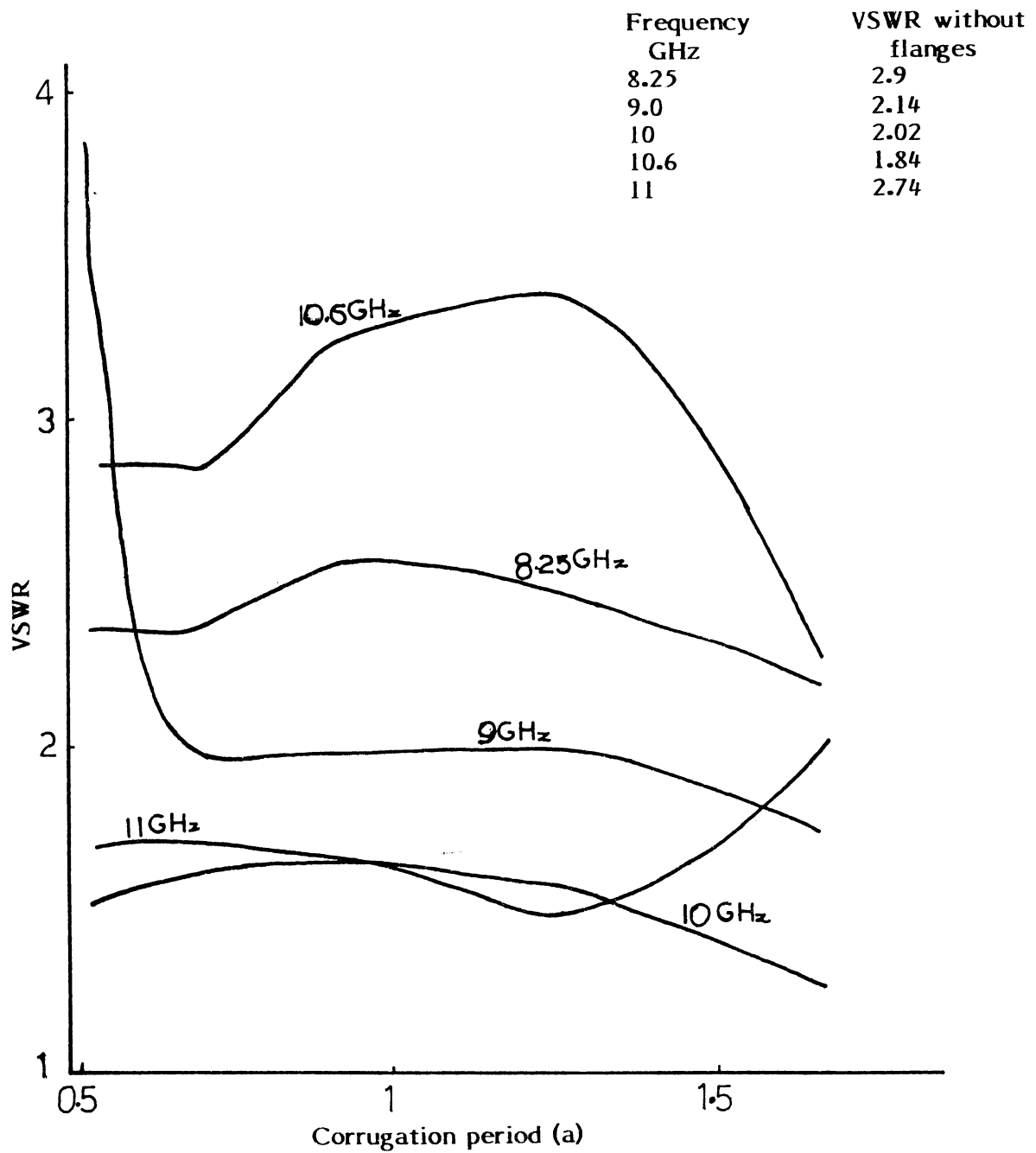


Fig. 4.1 (iii) (c) ; Variation of VSWR with corrugation period at the Optimum position .

Horn H2 , $2B = 45$.

4.1(iv) Variation of VSWR with the angle ' 2β ' between flanges

Here the flanges are kept at '0' position as usual and the effect of different flange angles on the VSWR of the system is studied. Observations were taken for different flanges at various frequencies.

The graphs of fig.4.1(iv)(a) to (h) show that for a given frequency the VSWR remains almost steady; without much variation as the angle is varied. The graphs further show that for a single frequency, all the flanges behave in the same way as far as VSWR is concerned. Here also in most cases, corrugated flanges show less VSWR than plane flanges or feed horn without flanges.

4.2 On-axis power density

As mentioned earlier, the main interest of practical importance in secondary antenna is to get as much power as possible on the bore sight or on-axis region of the system. Moreover the power distribution should be confirmed to a minimum area around the axis. In this context, the on-axis power density is defined as power distributed per unit area perpendicular to

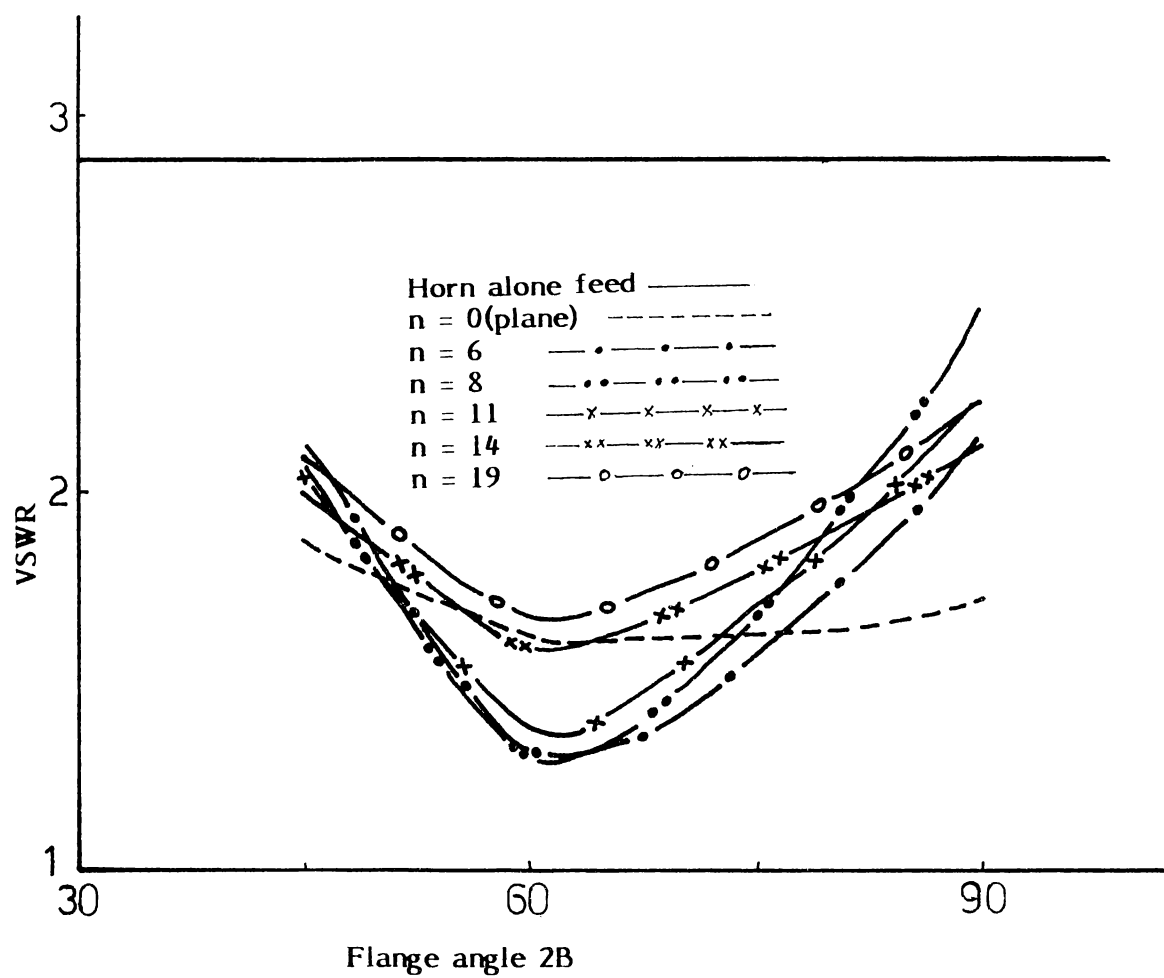


Fig.4.1(iv)(a): Variation of VSWR with flange angle $2B$ at the Optimum position .

Horn H3 , $f=8.25$ GHz .

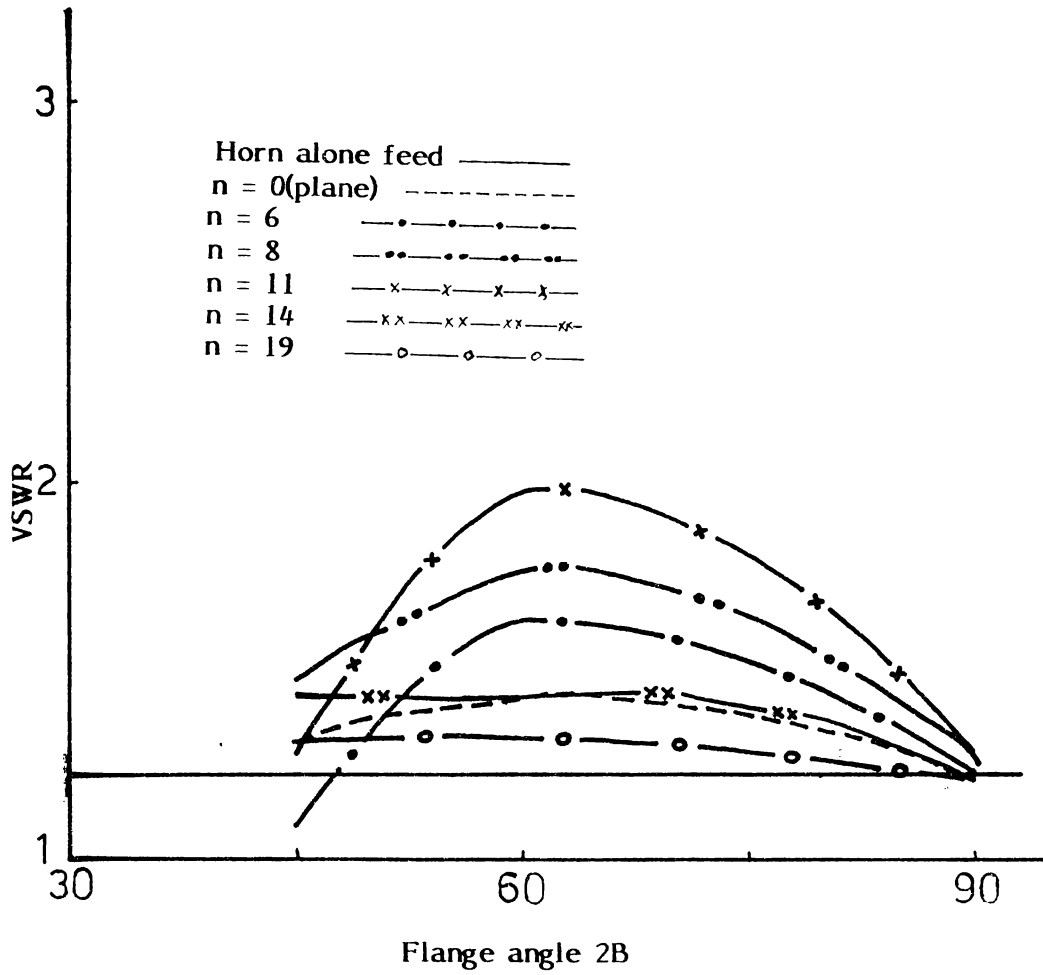


Fig. 4.1(iv)(b): Variation of VSWR with flange angle 2B at the Optimum position .

Horn H3 , f=9 GHz .

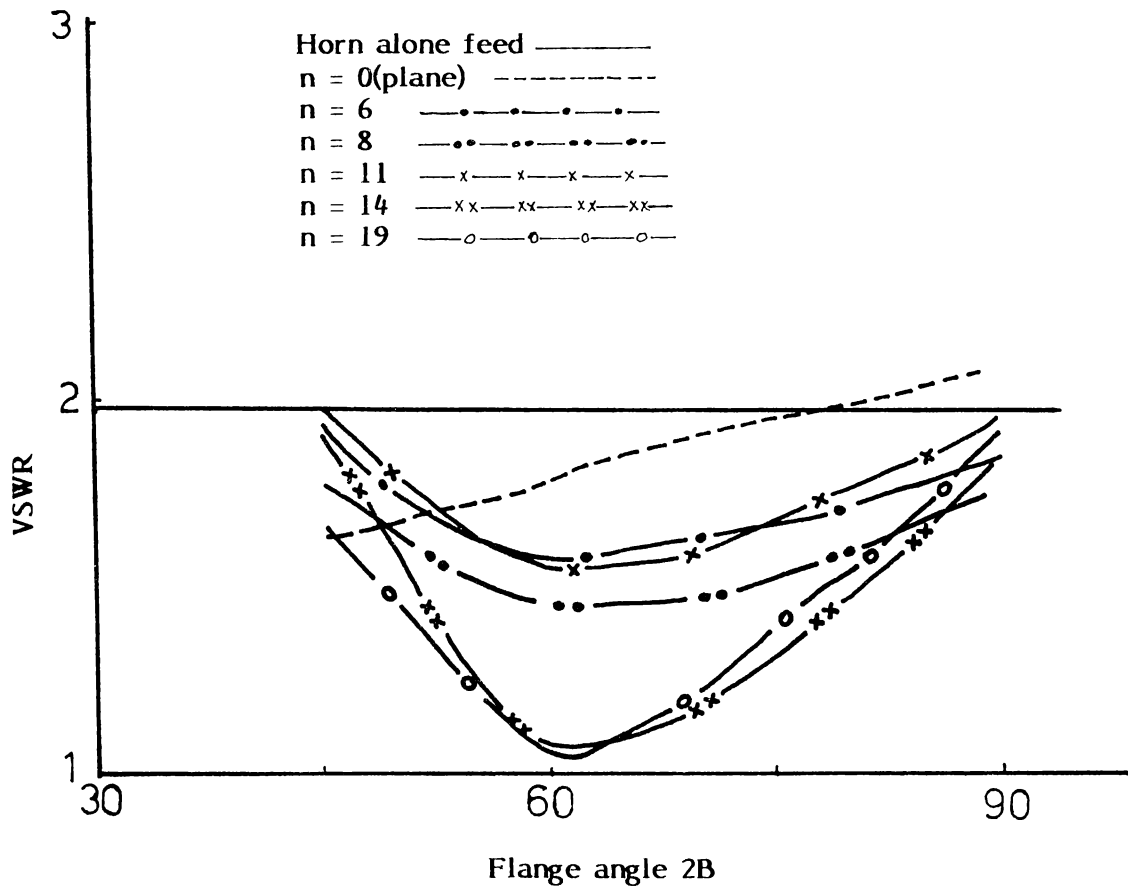


Fig.4.1(iv)(c): Variation of VSWR with flange angle 2B at the Optimum position .
 Horn H3, F=10 GHz .

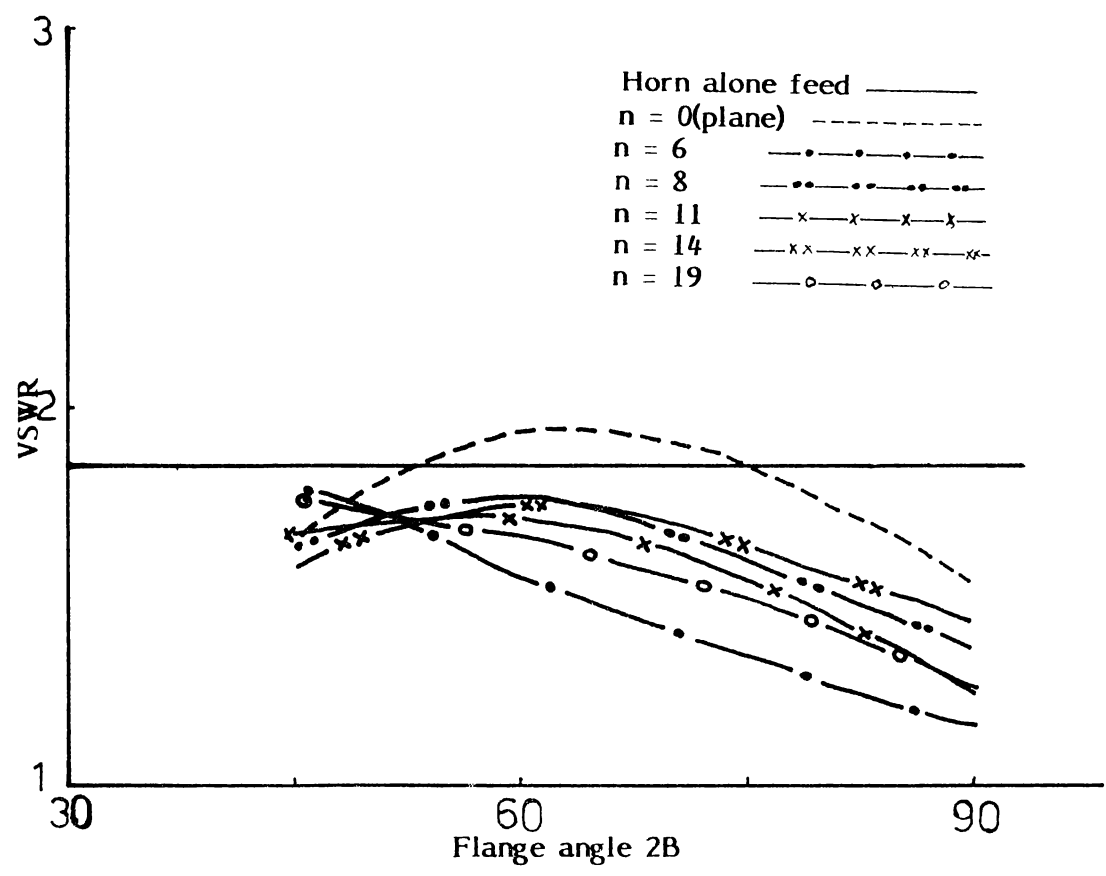


Fig.4.1(iv)(d): Variation of VSWR with flange angle 2B at the Optimum position .
Horn H3, F = 10.6 GHz .

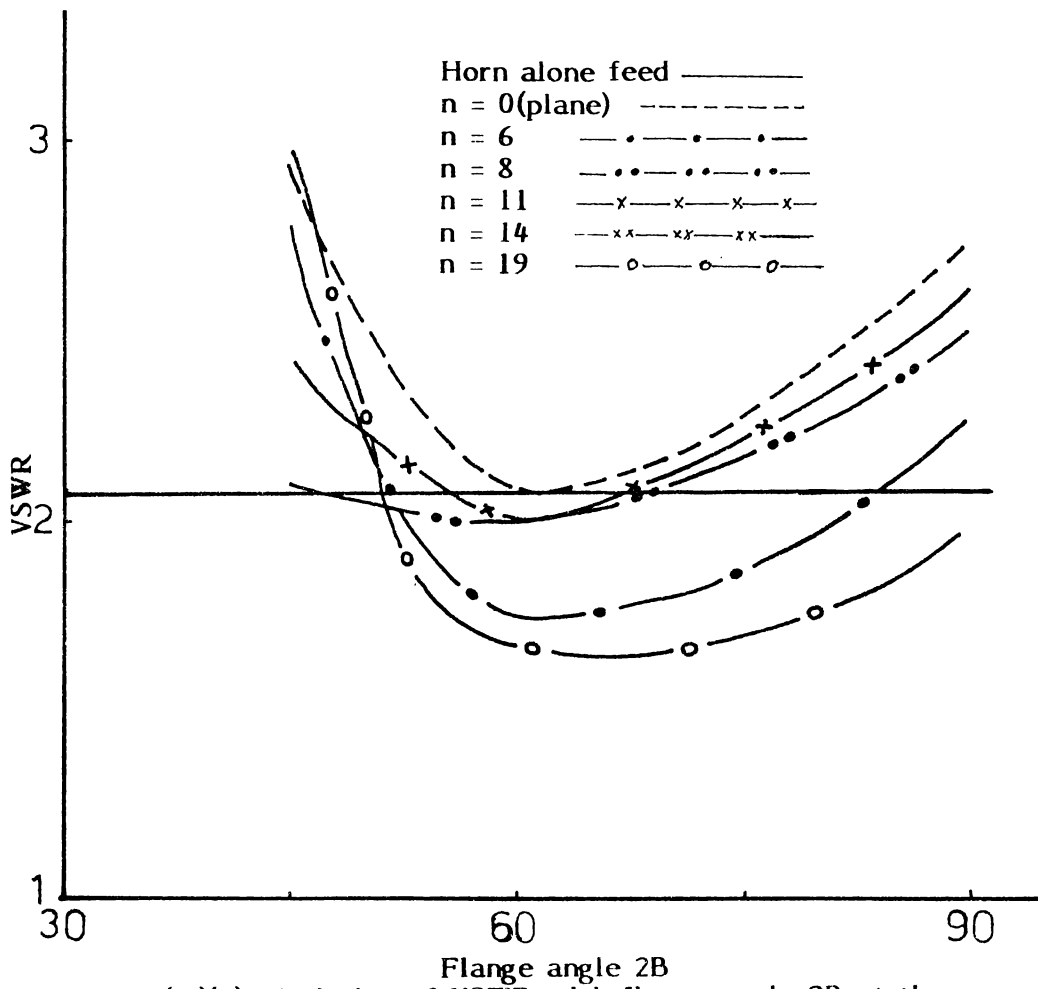


Fig. 4.1(iv)(e): Variation of VSWR with flange angle 2B at the Optimum position .

Horn H3 , F = 11GHz .

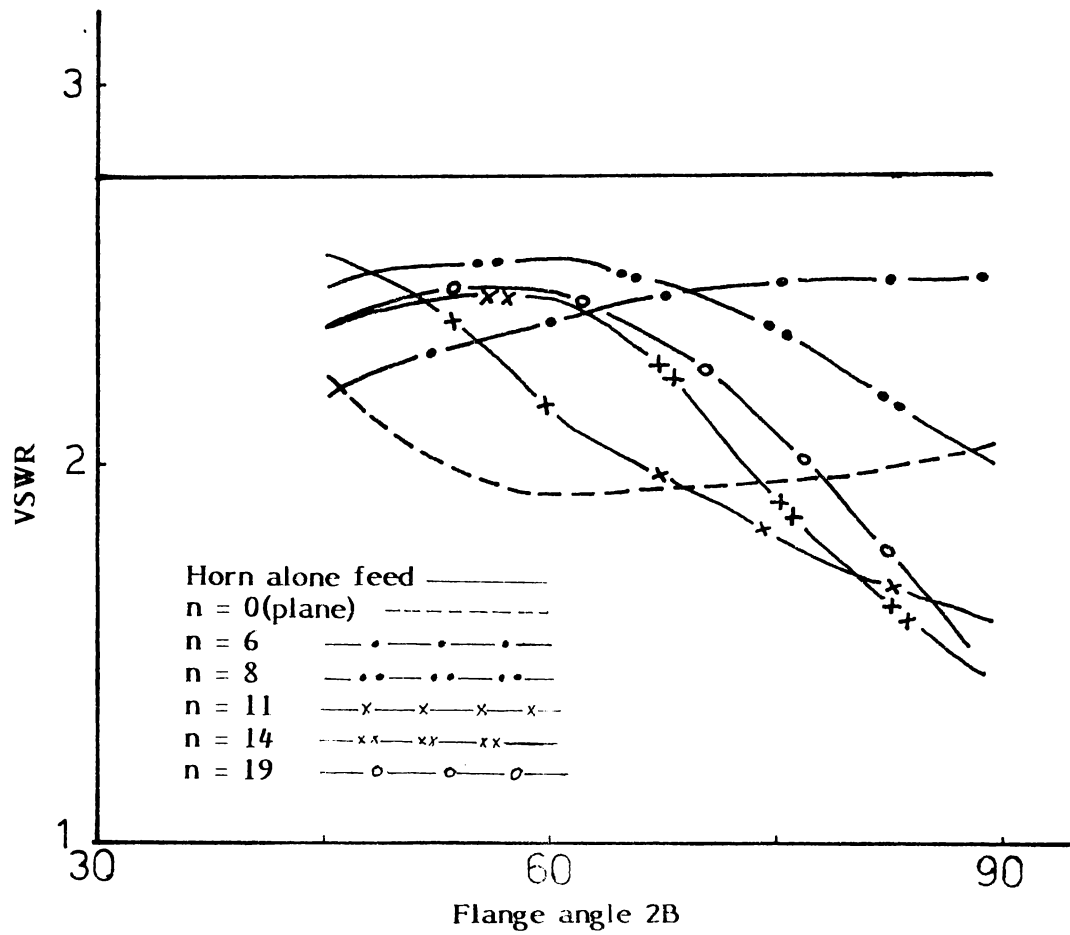


Fig. 4.1(iv)(f): Variation VSWR with flange angle $2B$ at the Optimum position .

Horn H2 , $F = 8.25$ GHz .

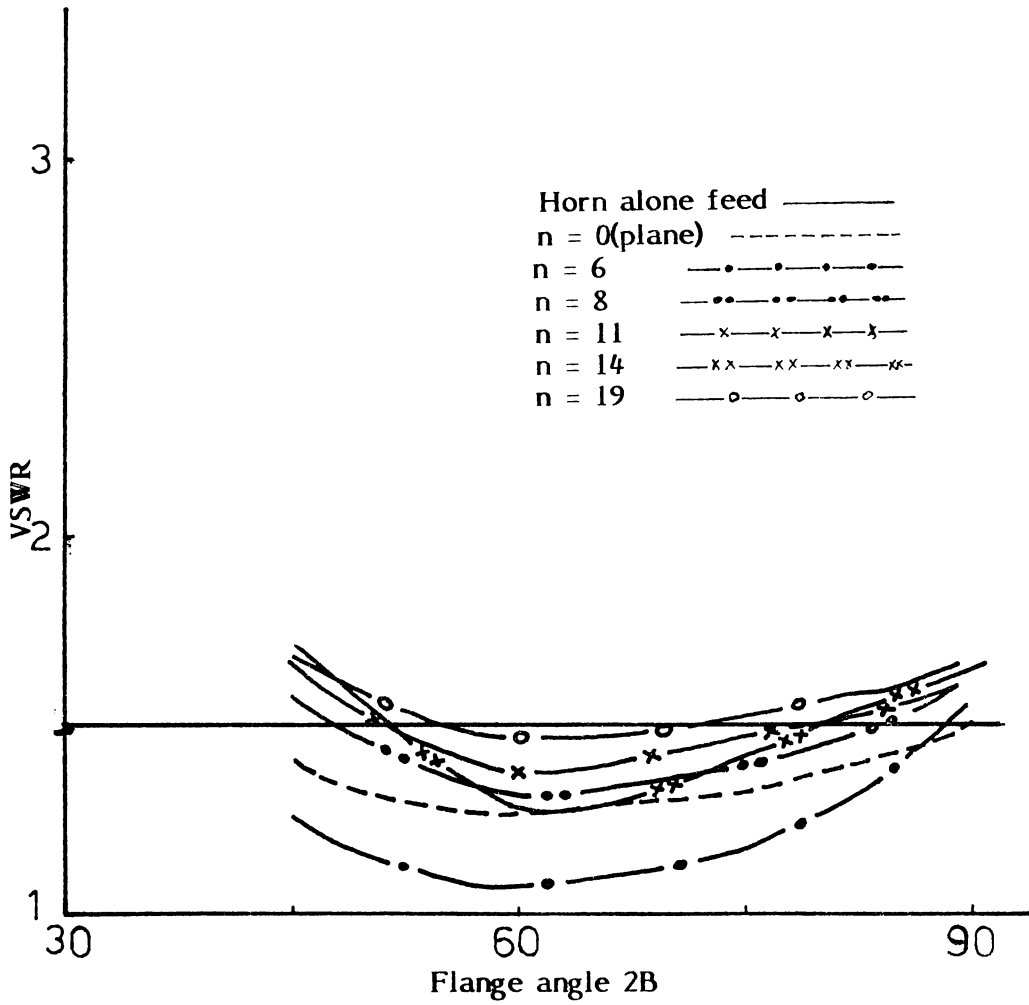


Fig.4.1(iv)(g): Variation of VSWR with the flange angle 2B at the Optimum position .

Horn H2 ,F = 10 GHz .

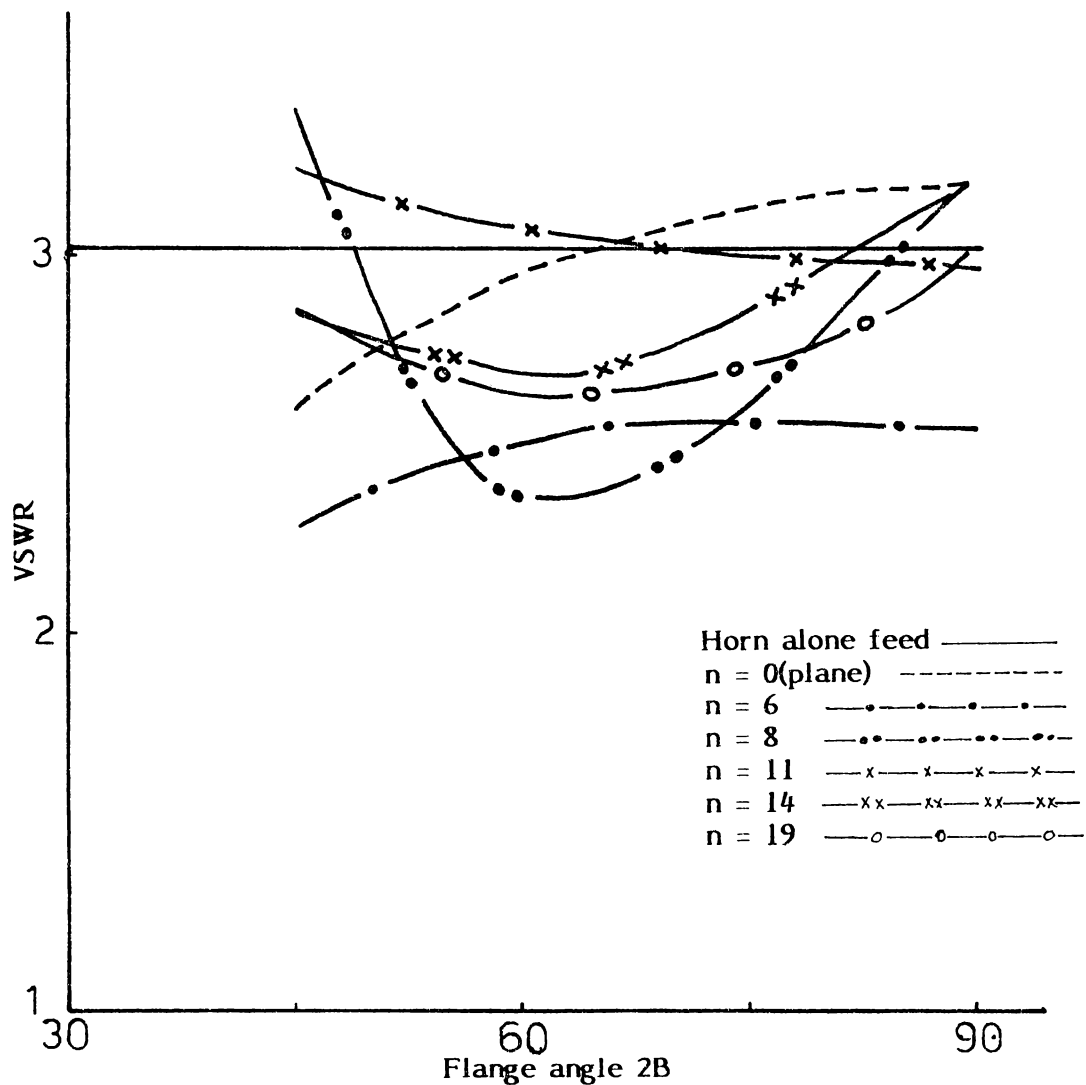


Fig. 4.1(iv)(h): Variation of VSWR with the flange angle $2B$ at the Optimum position .

Horn H2 , $F = 10.6$ GHz .

the axis. The on-axis power density measured with a standard pyramidal horn kept at a point along the axis at a distance greater than $\frac{2D^2}{\lambda}$ where D is the aperture dimension of the reflector antenna.

Optimum position (O-position) is the flange position corresponding to a maximum value of on-axis power and minimum position (M-position) is the flange position corresponding to the minimum value of on-axis power.

4.2(i) Dependence of on-axis power density on flange position

It is found that just like VSWR the on-axis power is also highly dependent on the position of the flanges relative to the horn aperture. The on-axis power varies approximately in sinusoidal fashion as the flanges are moved back from the aperture of the horn. At certain positions (M-positions) the on-axis power is reduced to very low value even to zero. There are some other positions (O-position) where the on-axis power reaches a maximum. This is clearly brought out by the graphs in fig.4.2(i)(a) to (e). As mentioned in the previous section 4.1(i), the VSWR is also position dependent. So a comparison is made between variations in VSWR and on-axis power density due to changes in flange position. The most

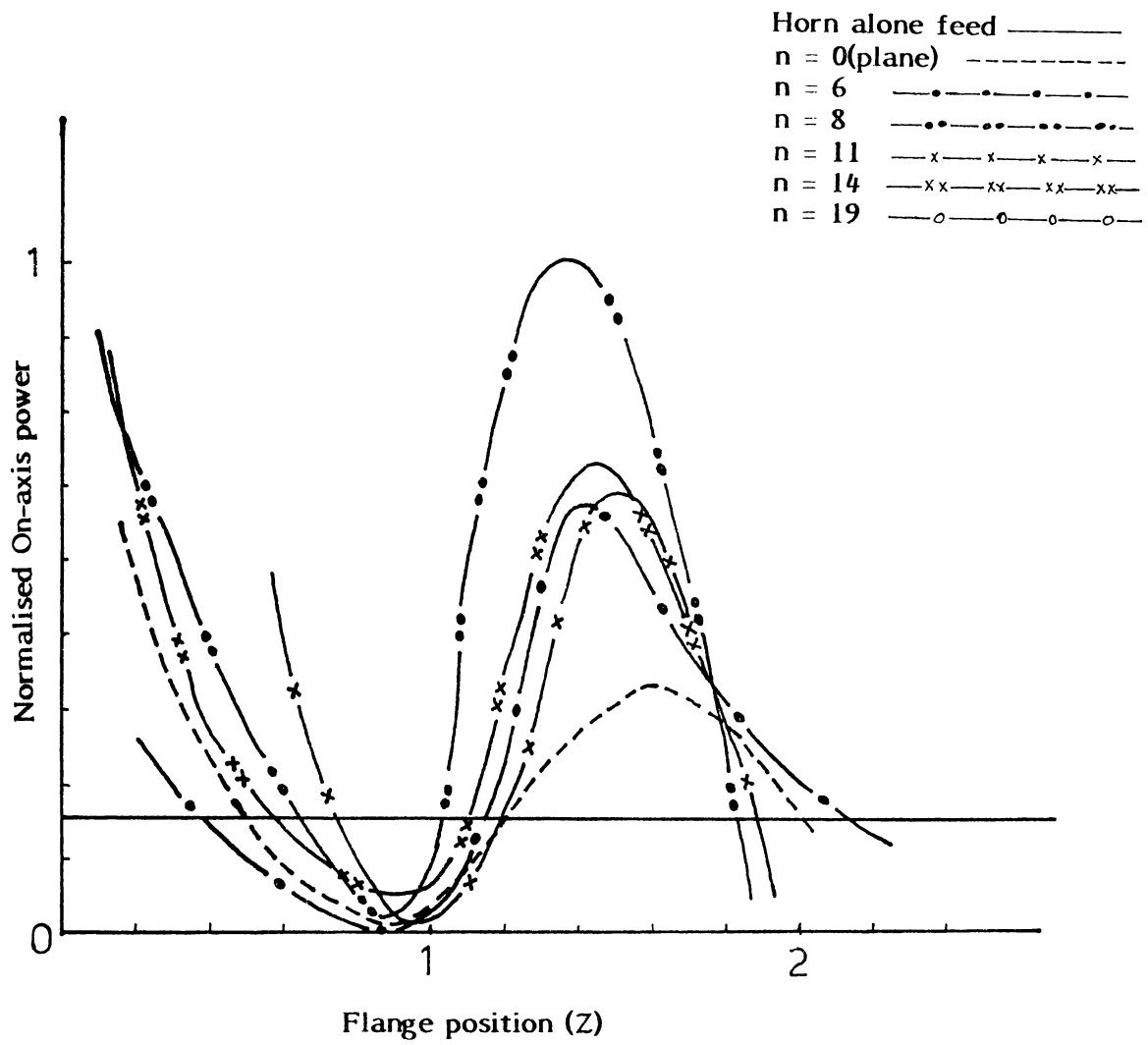


Fig.4.2(i)(a): Variation of On-axis power with flange position .

Horn H3 , $2B = 60$, $F = 9$ GHz .

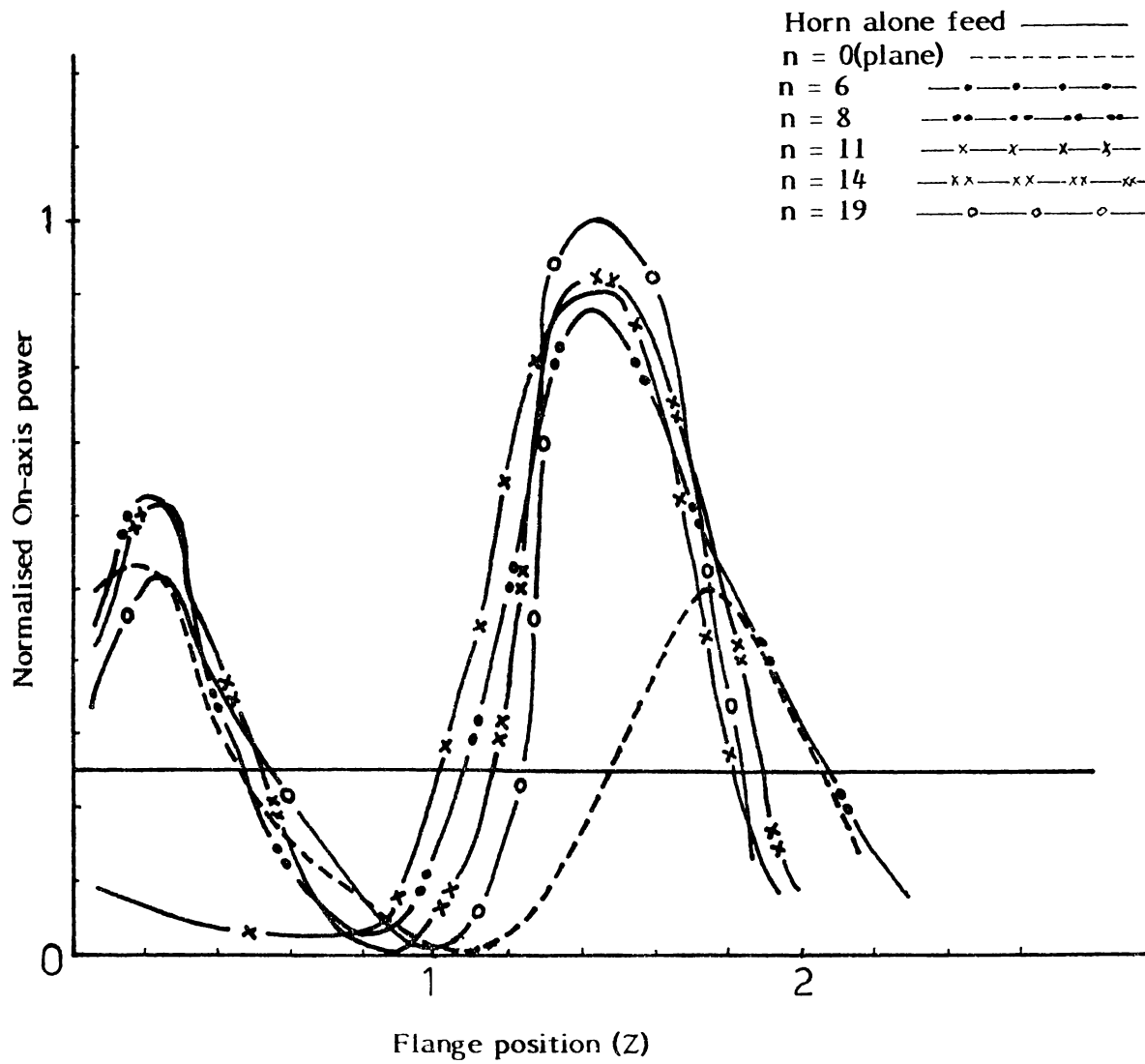


Fig. 4.2(i)(b): Variation of On-axis power with flange position .

Horn H3 , $2B = 60$, $F = 10$ GHz.

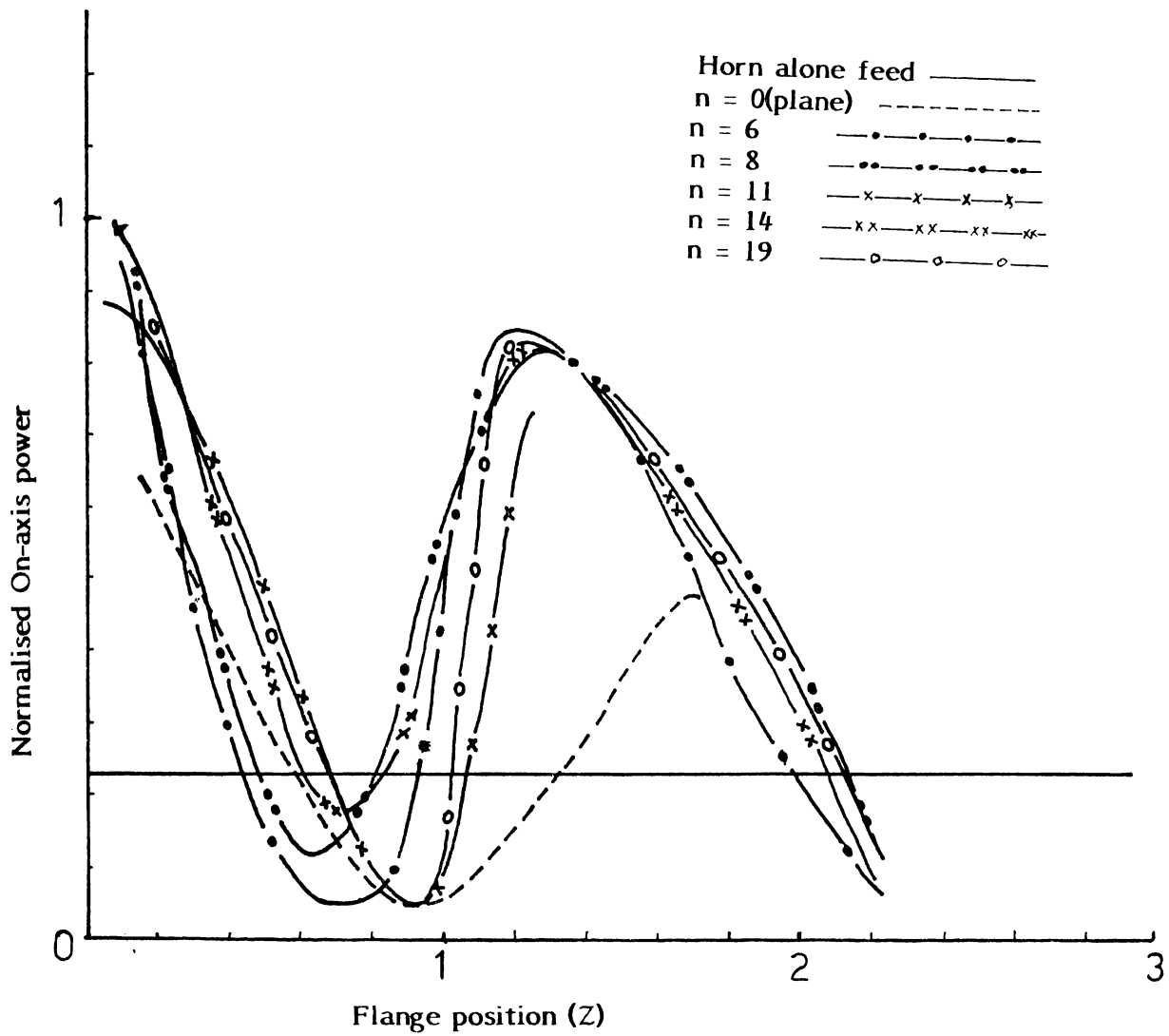


Fig. 4.2(i)(c); Variation of on-axis power with flange position .

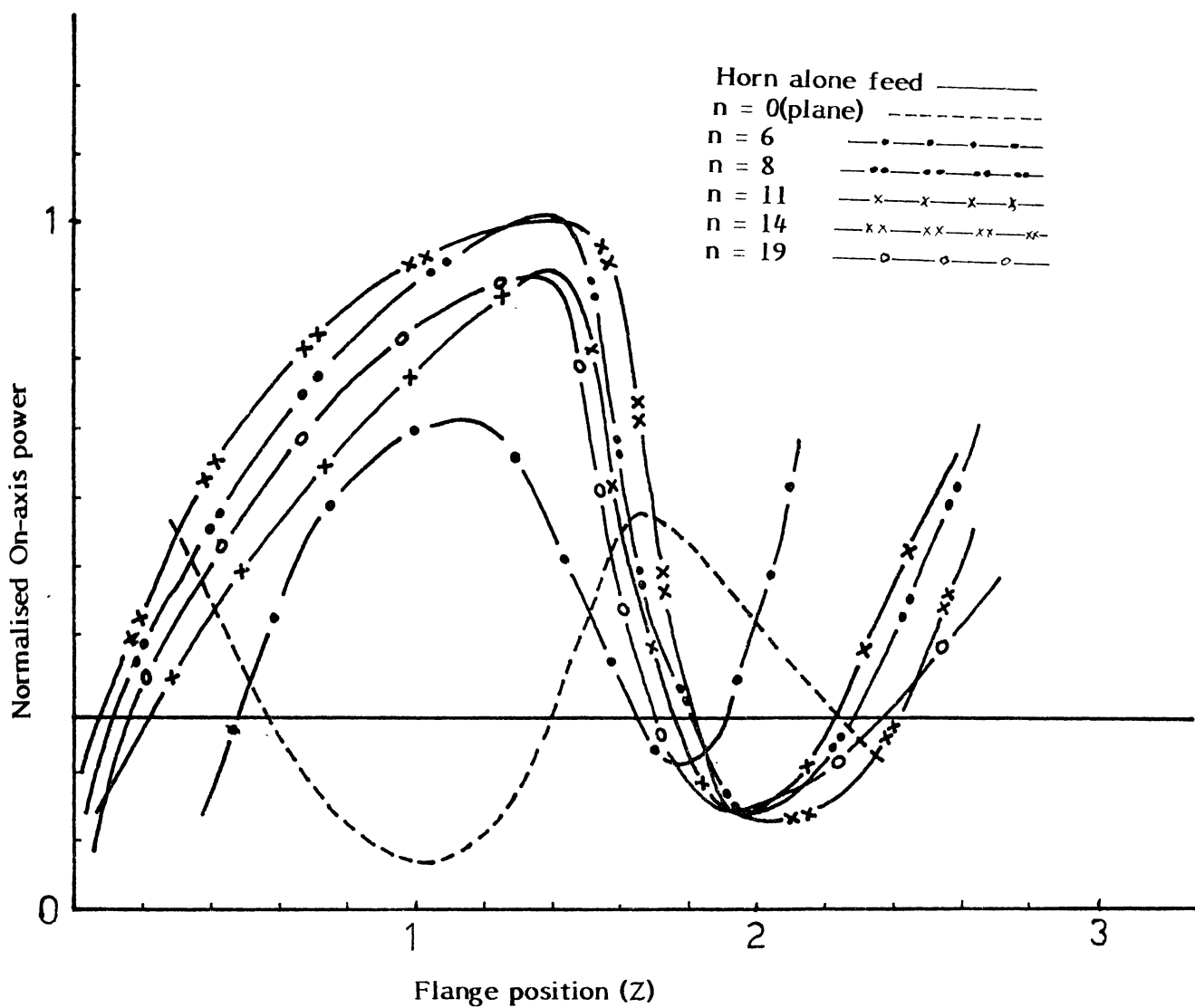


Fig. 4.2(i)(d): Variation of On-axis power with flange position .

Horn H3 , $2B = 60$, $F = 10.6$ GHz

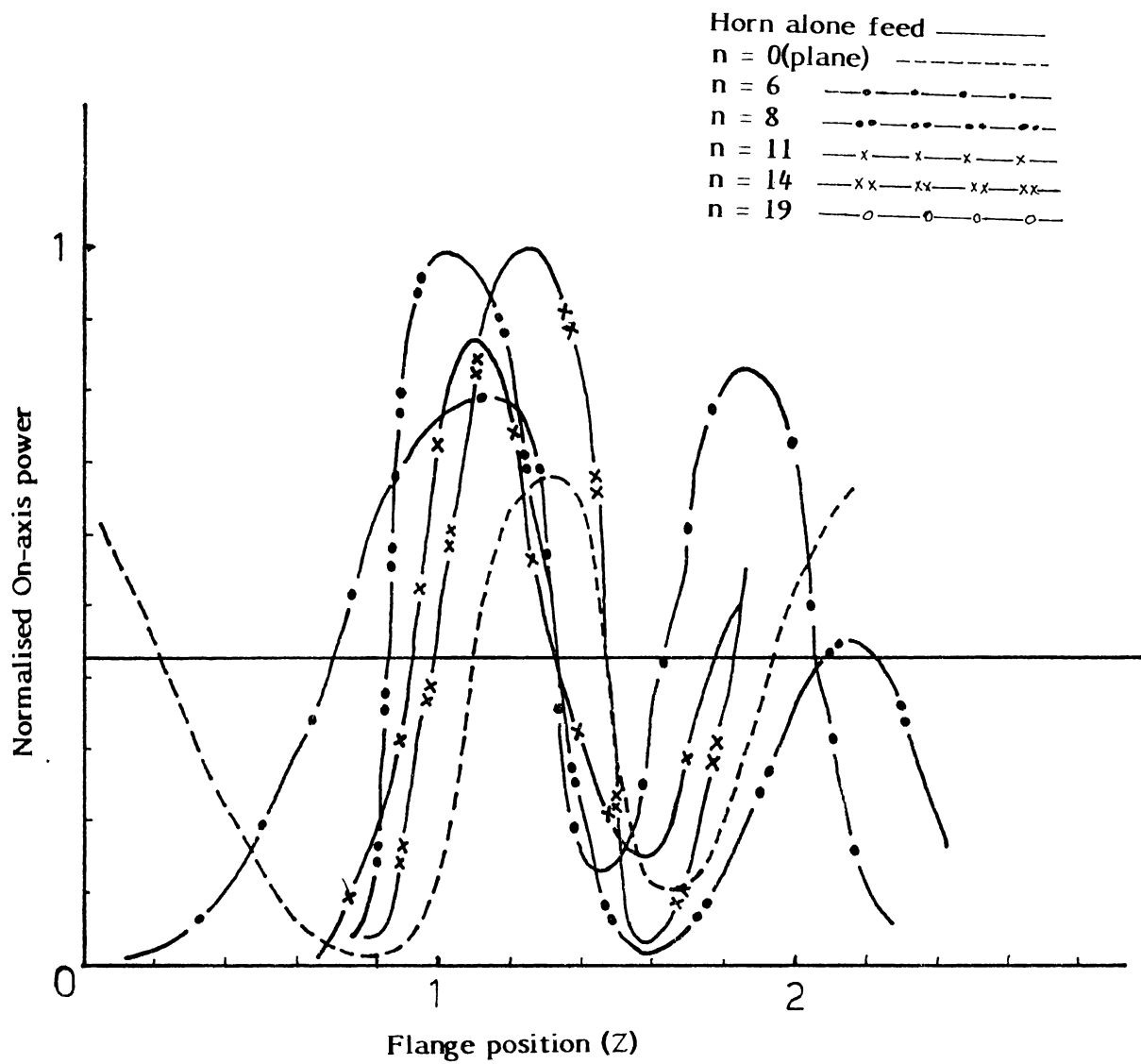


Fig. 4.2(i)(e): Variation of On-axis power with flange position .

Horn H3 , $2B = 90$, $F = 10$ GHz .

promising observation is that at the position where the on-axis power is maximum (O-position) the VSWR is found to be minimum. This is particularly more pronounced in the case of corrugated flanges than plane flanges. That is, the variation of on-axis power density and VSWR are almost reciprocal. This condition is ideal for antennas. Further as the flanges are moved through one wavelength the same phenomenon is found to repeat. But magnitudes of VSWR and on-axis power density are not same at every maxima and minima. In short, for a particular setting of the corrugated flanged feed, there is an optimum position where the VSWR is minimum (much lower than that with horn alone as the feed) and on-axis power density several times more than that of horn alone as feed. This is one of the most positive results of the corrugated flanges observed throughout the experiment.

4.3(i) Effect of flange position on beam shape

The shape of the beam emerging from the offset reflector depends very much on the position of the flanges on the feed horn. It is found that the flanges can serve to improve or worsen the beam shape. In fig.4.3(i)(a) and (b) the change of shape of the beam as the flanges are moved from the aperture to the back of the horn are shown. Both E- and H-plane patterns are plotted.

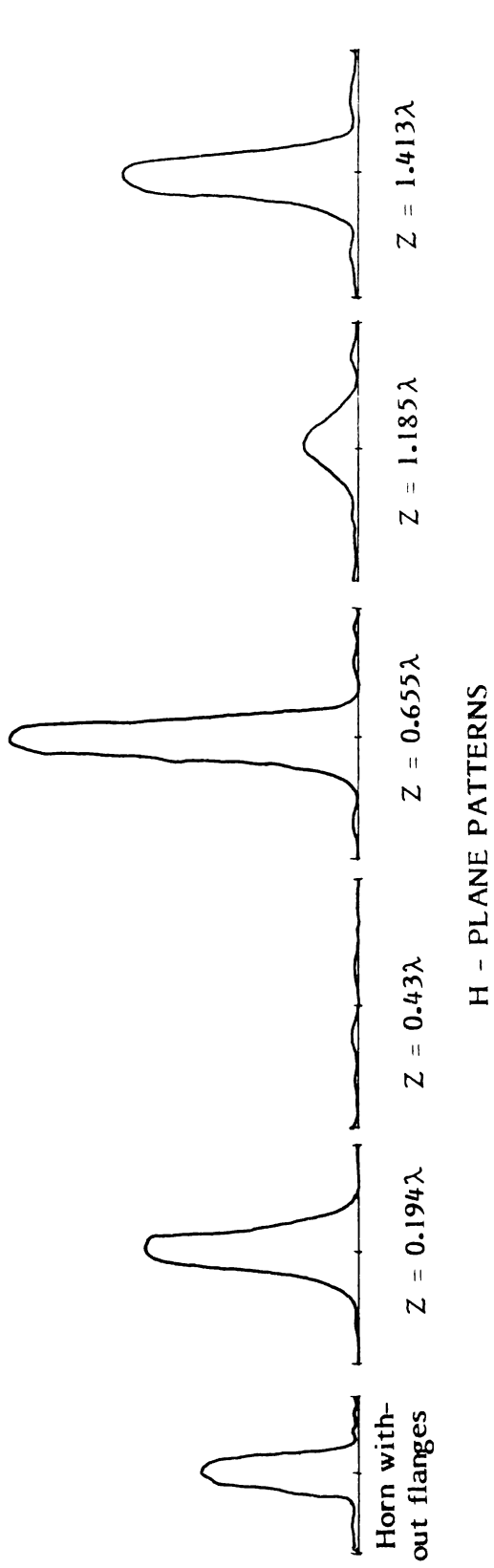


Fig. 4.3(i)(a): Variation of H - plane patterns as the flanges are moved back from the aperture of the horn

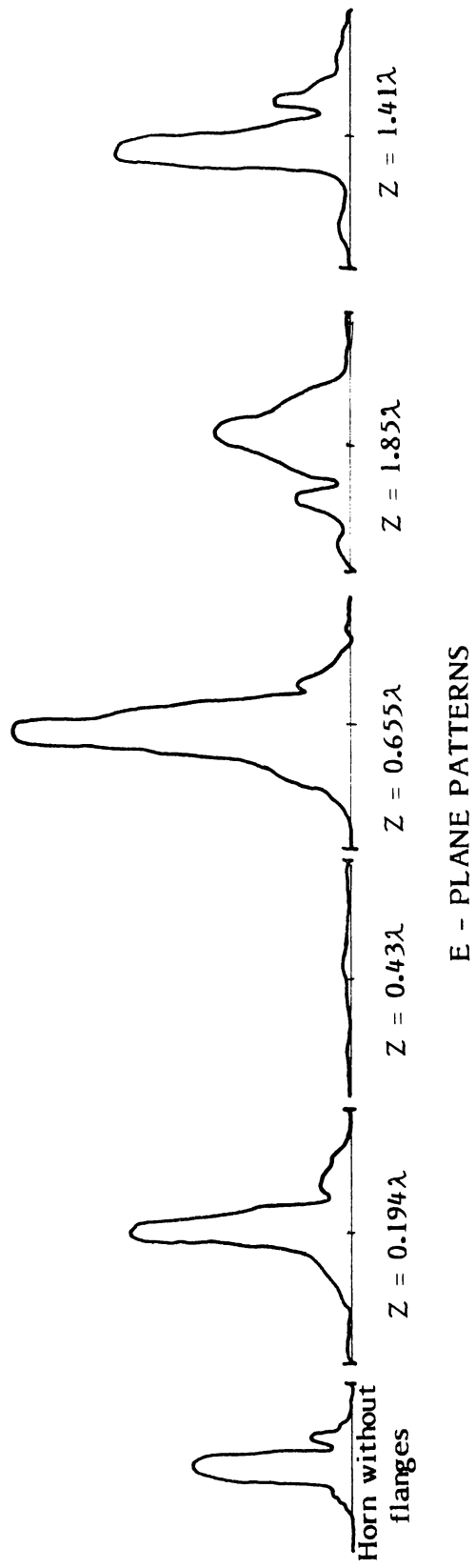


Fig. 4.3(i)(b): Variation of E - plane patterns as flanges are moved back from the aperture of the horn H3 , $2B = 90$, $n = 19$, $F = 10.6$ GHz .

A close study of the E- and H-plane patterns reveals that within experimental limitations of plotting the narrow beam the shape of H-plane patterns remains same irrespective of the position of the flanges. Only the amplitude of on-axis power changes. At the 'O' position of the flange the VSWR is minimum and on-axis power is maximum, at 'M' position the VSWR is maximum and on-axis power is minimum. It is consistent with the results obtained by Zachariah and Nair.

But the shape of E-plane patterns depend very much on the position of the flanges. When the flanges are kept at aperture, the resultant E-plane pattern is somewhat sharp; as the flanges reached the first 'O' position the E-plane patterns are further sharpened. At 'M' position the E-plane patterns are broadened and in some cases split with a null (or minimum power) at the centre. In this case sidelobes also are found to increase considerably. In between the 'O' and 'M' positions, the E-plane patterns first broaden and then begin to split with increase in sidelobes as we approach 'M' position. The same variation is repeated for every 'O' and 'M' positions. This result is particularly significant as it allows us to modify the E-plane pattern to any extent without adversely affecting the beam shape of the other plane.

It was found that generally a corrugated flange gives sharper beam than plane flange or horn without flange as feed.

But the introduction of flanges narrows down the frequency range in which the above observation holds true. In this sense it decreases the band-width as far as the HPBW is considered.

4.4 Antenna directive gain

As described in section (3.4) total directive gain of the antenna system is given by:

$$G_T = \frac{G_E G_H}{\pi}$$

where

G_E = Directive gain in E-plane

G_H = Directive gain in H-plane.

Since the E-plane and H-plane patterns are more or less independent of each other the directive gain in each plane is calculated separately and then the combined directive gain or total directive gain of the system in decibels is obtained as

$$G_{dB} = G_{EdB} + G_{HdB} - 20 \log_{10}$$

4.4(i) Dependence of directive gain on flange position

From previous sections it is obvious that the directive gain of the system depends very much on the position of the flanges with respect to the aperture of the feed horn. As the flanges are moved back from the aperture of the horn the directive gain of the system undergoes drastic changes. At the 'O' position the directive gain is maximum and at 'M' positions it is minimum. The directive gains are calculated only at these two positions as the intermediate positions are not of much practical importance judging from the radiation patterns.

It is found that the directive gain varies in the same manner as the on-axis power density, when the flange position is varied. The on-axis power density is maximum at positions of the flange where the directive gain in the plane is also usually high.

An outstanding feature of the radiation patterns with corrugated flanges at 'O' positions is the vanishing of the sidelobes with considerable increase of the on-axis power density. But the directive gain is not found to increase in all cases. The main lobe is broadened with a considerable reduction of sidelobes when directive gain is not increasing. This is an

expected result, since the flanges taper the amplitude from a maximum at the centre to a smaller value at the edges. According to Silver⁹, the variation will reduce the side-lobe level with widening of the main lobe and consequent reduction in directivity. Barring a few stray cases generally the directive gain remains constant or increased slightly as shown in fig.4.4(i)(a) and (b). This consistency of the directive gain is attributed to the lower sidelobe level obtained with the corrugated flanges.

4.4(ii) Dependence of directive gain on frequency

A study of directive gains at different frequencies for all the flanges and feed horn without flanges reveals that the directive gain of the system is found to be increased for frequencies around 10 GHz while it is decreased for the band edge frequency of 8.25 GHz and 11 GHz by the use of corrugated flanges. The maximum gain is obtained for the flange system with six corrugations (corrugation period $\approx \lambda/2$) The same was repeated for both the angles studied in detail. Another notable feature is that the directive gains are found to be complimentary to each other in the frequency domain. This is clearly brought out in figs.4.4(ii)(a) and (b). This may be explained as follows. The directive gain of the system

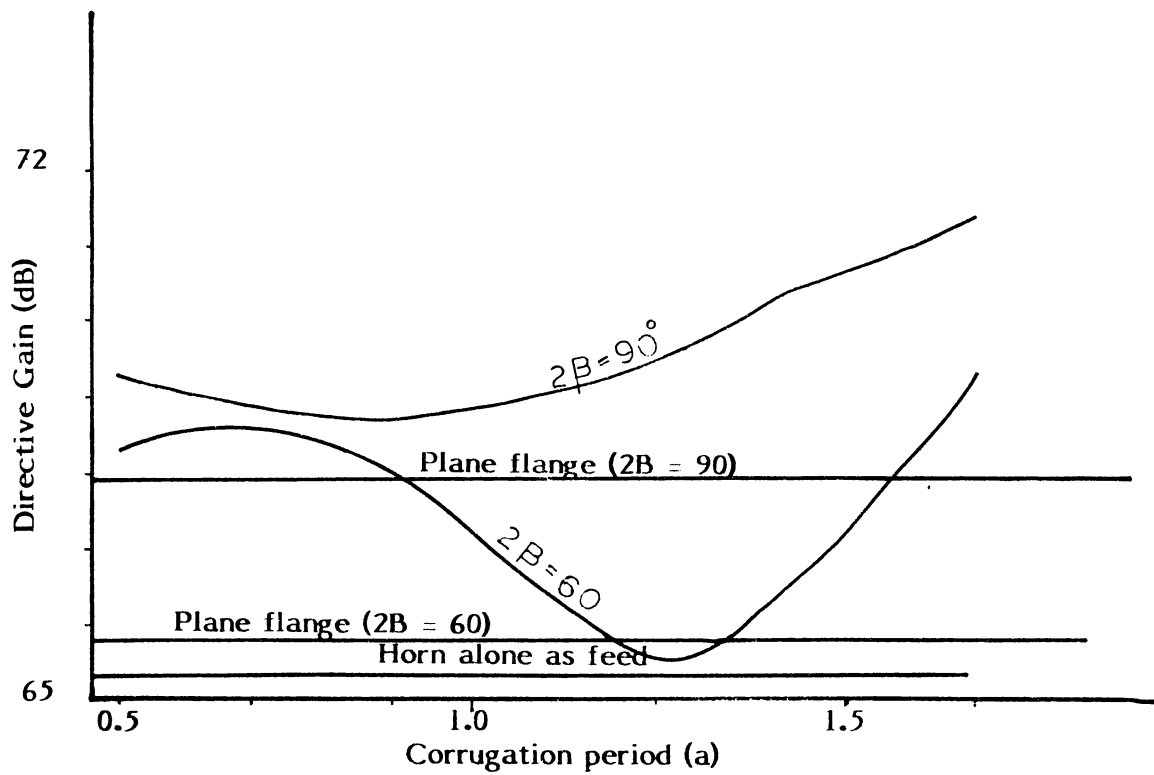


Fig.4.4(i)(a): Variation of Gain with corrugation period.

Horn H3, $F = 10$ GHz .

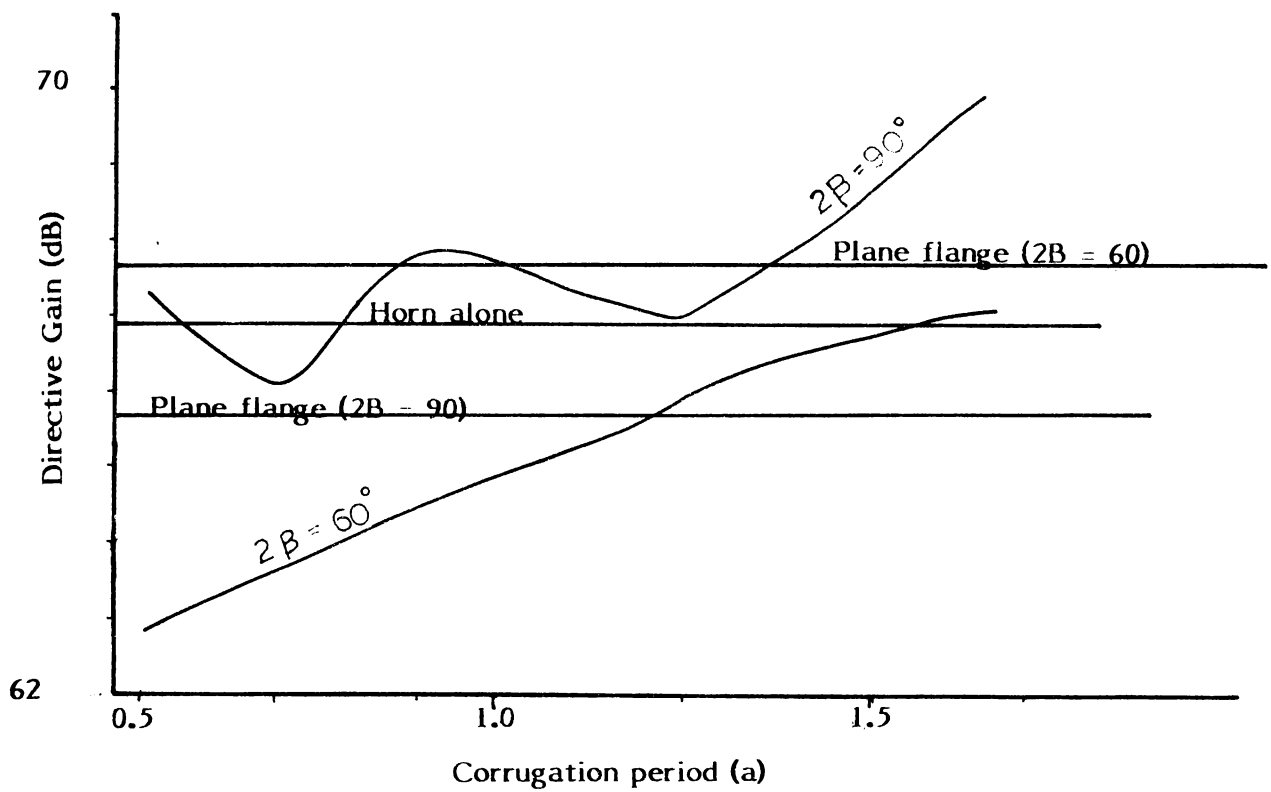


Fig.4.4(i) (b) ; Variation of gain with corrugation period .

Horn H3, $F = 10.6$ GHz .

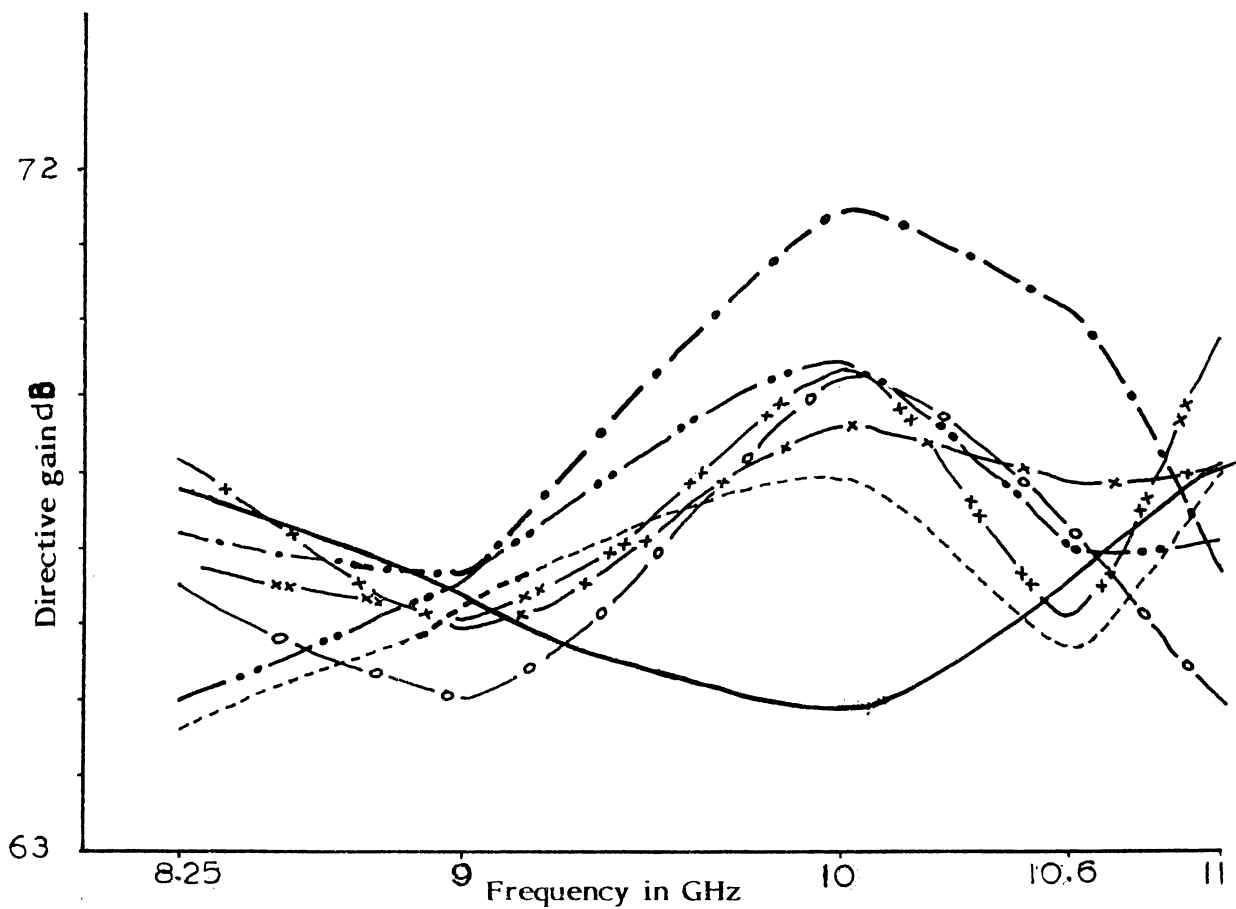


Fig. 4.4(ii)(a); Directive gain vs frequency characteristics of the system .
Horn H3 , $2\beta = 90^\circ$.

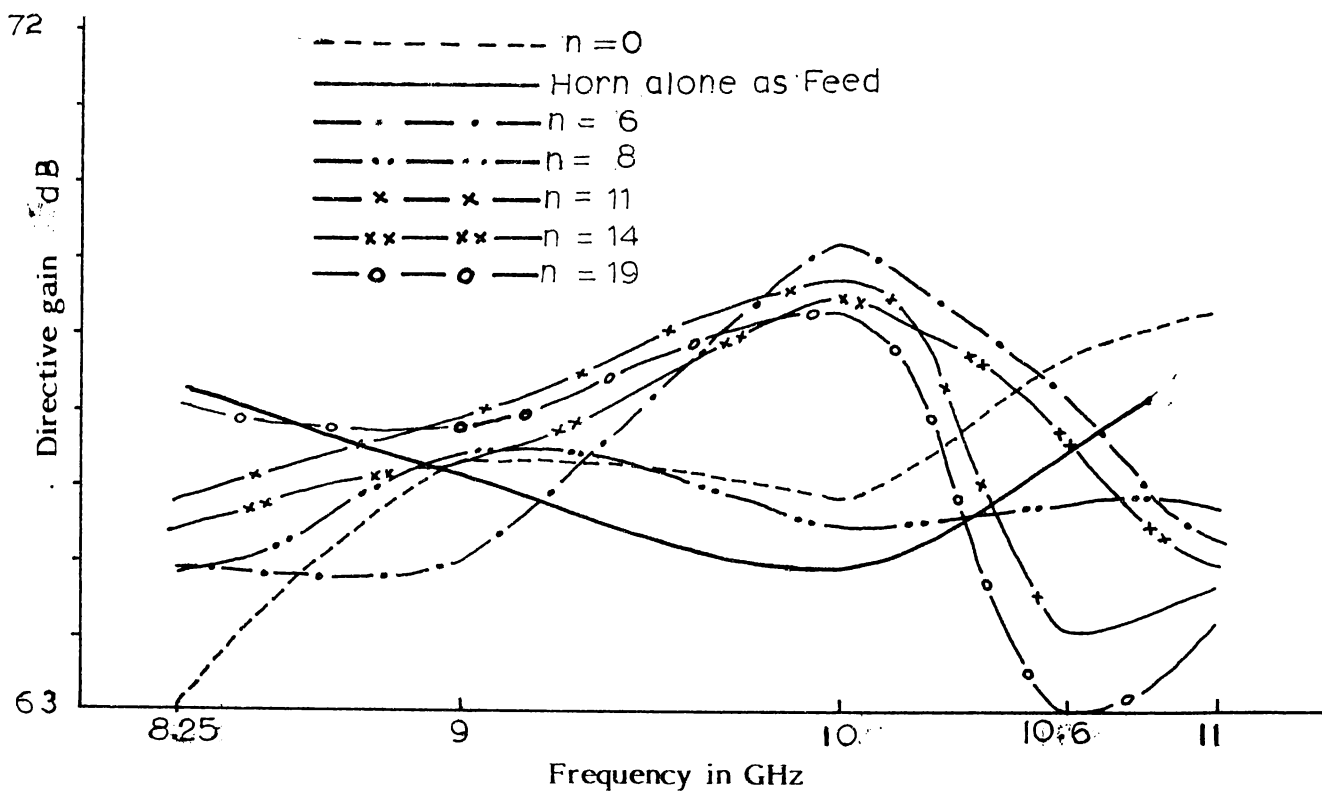


Fig.4.4(II)(b): Directive gain vs frequency characteristics of the system .
Horn H3 , $2\beta = 60^\circ$.

is determined by the width of the radiation patterns in the two planes. In the case of horn alone as feed the E-plane pattern is not modified at all and it is very broad. But for certain frequencies it is broader than usual. At these frequencies if corrugated flanges are used for modifying the E-plane pattern the interaction between the flange elements and the beam will be more and the beam will be modified for the better. For those frequencies where the E-plane patterns are not so broad the interaction will be less and the beam is not modified to the same extent. Thus the more uniform and narrower primary beam produced in the first case accounts for the better directive gain properties of the secondary reflector at the frequency.

4.5 Half power beam widths

All the patterns on both E-and H-planes plotted here are power patterns as mentioned earlier. The half power points or 3 dB points are the points on the pattern where the power falls to half the peak value.

4.5(i) Dependence of HPBW on various flange parameters

As mentioned in the previous sections, we are interested only in the HPBW at '0' positions. So, although patterns were

plotted for all 'O' and 'M' positions on both E and H-planes, HPBW of those patterns which give maximum gain only are considered here.

There are two HPBWs here. (1) The H-plane HPBW and (2) the E-plane HPBW. From these two we can visualize the three dimensional beam shape of the system. As the table 4.5(I) shows, it is observed that while the H-plane HPBW remains almost constant the E-plane HPBW varies considerably. This is because the E-plane pattern is most affected by the flange position as stated earlier. At the 'O' position, the half power beam width is minimum possible and at 'M' position it is very large due to beam broadening and splitting.

The variation of HPBW with the other parameters of flanged feed namely corrugation period, angle between flanges etc. follows almost the same pattern as that of gain of the corresponding parameters.

4.6 Cross polarization

Cross polarization is an important parameter of any reflector antenna. Experiments were carried out to see how the flange parameters affect the cross polarization level.

Table 4.5(I)

Horn H₃ - 'O' Position

| Frequency Angle in GHz | H-plane horn alone as feed | | n = 0 | | n = 6 | | n = 8 | | n = 11 | | n = 14 | | n = 19 | |
|---------------------------|-------------------------------|-------------|-------------|-------------|-------------|-------------|-------------|-------------|-------------|-------------|-------------|-------------|-------------|-------------|
| | E- plane | H- plane | E- plane | H- plane | E- plane | H- plane | E- plane | H- plane | E- plane | H- plane | E- plane | H- plane | E- plane | H- plane |
| 8.25 | 3.2 | 2.6 | 3.6 | 2.5 | 3.3 | 2.5 | 3.2 | 2.5 | 2.9 | 2.5 | 3.2 | 2.5 | 2.9 | 2.5 |
| 9 | 3.1 | 2.7 | 2.9 | 2.6 | 2.7 | 2.6 | 2.9 | 2.6 | 2.8 | 2.7 | 3.0 | 2.7 | 2.9 | 2.7 |
| 10.6 | 3.0 | 2.9 | 2.9 | 2.8 | 3.0 | 2.8 | 2.8 | 2.8 | 3.0 | 2.9 | 3.0 | 2.8 | 3.0 | 2.8 |
| 10.6 | 3.00 | 2.9 | 2.6 | 2.8 | 2.6 | 2.8 | 2.8 | 2.8 | 2.9 | 2.8 | 2.8 | 2.9 | 2.7 | 2.9 |

The ratio of the on-axis cross polarized power to co-polarized power is taken here as an indication of the cross polarization of the system. The cross polarized patterns are also plotted for all 'O' and 'M' positions and a comparative study is made with co-polar patterns.

4.6(i) Dependence of cross polarization on the position of flanges

It is seen that like co-polar patterns, cross-polar patterns are also very much dependent on the position of the flanges. Fig.4.6(i)(a) shows the variation of cross-polarized patterns as the flange is moved back from the aperture of the horn. It reveals that cross-polarized patterns are sharp in 'O' position and split in the 'M' positions almost identical to the dominant polarization.

4.6(ii) Comparison between the magnitudes of the cross polarization and co-polarization

In order to study the degree of cross-polarization the amplitude of co-polarized and cross-polarized patterns are measured at 'O' positions and a table is prepared as shown in 4.6(ii)(a,b,c). The table gives us a comparison between the maximum cross-polarization with flanged feed and

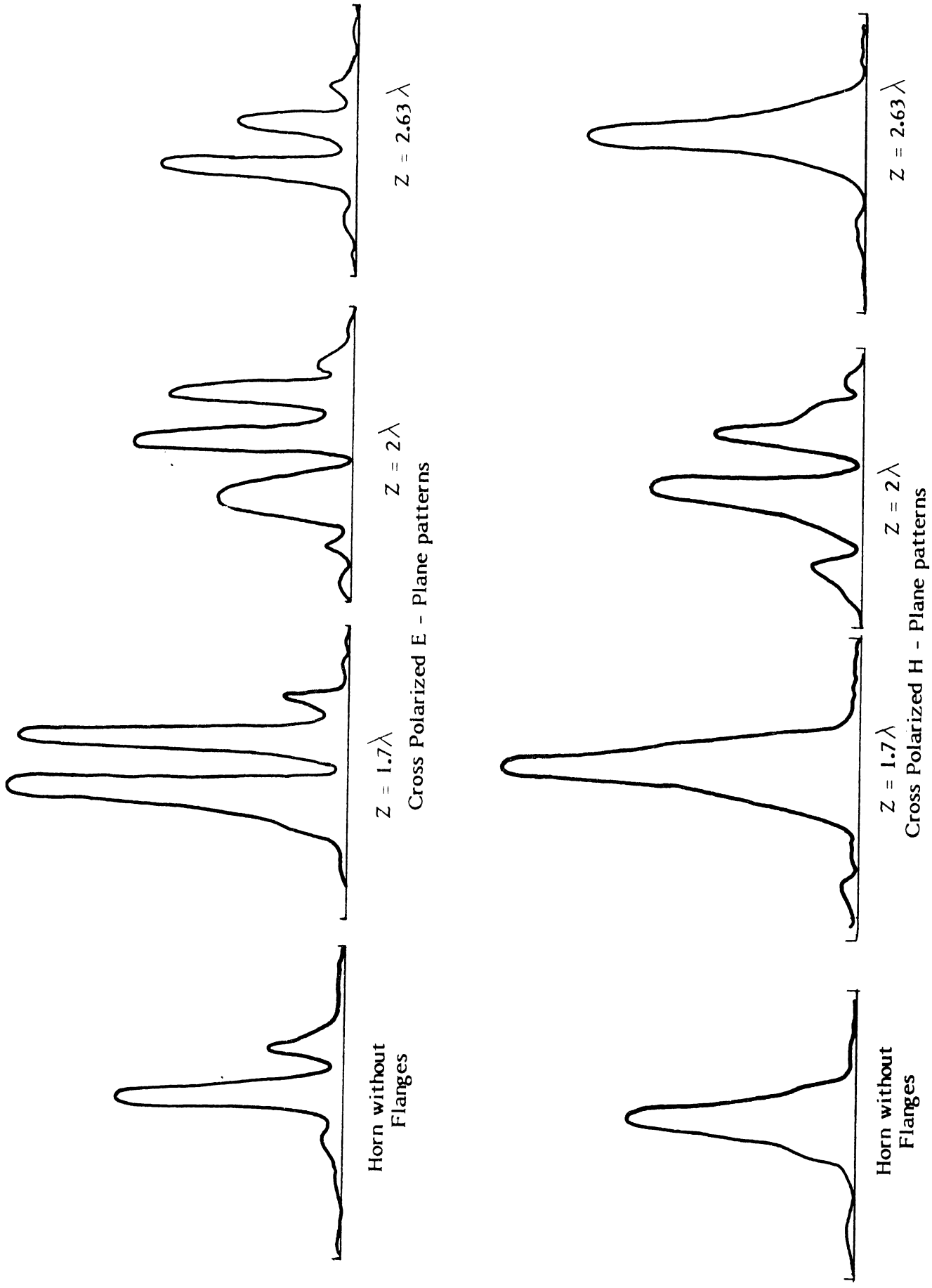


Fig . 4.6 (i) (a) ; The effect of flange position on the Cross polarized patterns .

Table 4.6(ii)(a)

Horn H_1 - Cross polarisation (Worst case)

| Frequency in GHz | 2θ | Number of corrugations 'n' | Cross polarisation dB |
|---------------------|----------------------|----------------------------------|-----------------------------|
| | Horn only as feed | Horn only as feed | -25.07 |
| 9 | 45° | 0 | -25.81 |
| | | 5 | -24.45 |
| | | 8 | -24.84 |
| | | 11 | -23.12 |
| | | 14 | -24.41 |
| | | 19 | -24.94 |
| | Horn only as feed | Horn only as feed | -25.07 |
| 9 | 90° | 0 | -26.02 |
| | | 6 | -22.28 |
| | | 8 | -23.10 |
| | | 11 | -23.49 |
| | | 14 | -22.64 |
| | | 19 | -23.19 |

Table 4.6(ii)(b)

Horn H₂ - Cross polarisation (Worst case)

| Frequency in GHz | 2θ | Number of corruga- tions 'n' | Cross polari- sation dB |
|---------------------|----------------------|---------------------------------------|----------------------------------|
| | Horn only as feed | Horn only as feed | -17.22 |
| | | 0 | -17.78 |
| | | 6 | -19.82 |
| 11 | 45° | 8 | -19.43 |
| | | 11 | -17.6 |
| | | 14 | -22.05 |
| | | 19 | -21.24 |
| | Horn only as feed | Horn only as feed | -17.22 |
| | | 0 | -17.53 |
| | | 6 | -17.88 |
| | | 8 | -17.75 |
| 11 | 60° | 11 | -20.58 |
| | | 14 | -19.77 |
| | | 19 | -18.86 |
| | Horn only as feed | Horn only as feed | -17.22 |
| | | 0 | -16.47 |
| | | 6 | -15.12 |
| 11 | | 8 | -16.63 |
| | | 11 | -18.05 |
| | | 14 | -15.78 |
| | | 19 | -17.20 |

Table 4.6(ii)(c)

Cross polarisation (Worst case)

| Frequency in GHz | 2β | Number of corruga- tions 'n' | Cross polari- sation dB |
|---------------------|----------------------|---------------------------------------|----------------------------------|
| | Horn only as feed | Horn only as feed | -25.30 |
| 11 | 90° | 0 | -27.4 |
| | | 6 | -28.37 |
| | | 8 | -26.57 |
| | | 11 | -27.61 |
| | | 14 | -25.87 |
| | | 19 | -27.58 |
| | Horn only as feed | Horn only as feed | -19.6 |
| 9 | 60° | 0 | -21.13 |
| | | 6 | -18.62 |
| | | 8 | -19.87 |
| | | 11 | -18.4 |
| | | 14 | -19.58 |
| | | 19 | -21.70 |
| | Horn only as feed | Horn only as feed | -14.02 |
| 10 | 60° | 0 | -15.29 |
| | | 6 | -14.78 |
| | | 8 | -17.18 |
| | | 11 | -17.28 |
| | | 14 | -17.23 |
| | | 19 | -17.83 |
| | Horn only as feed | Horn only as feed | -25.27 |
| 8.25 | 45° | 0 | -28.64 |
| | | 8 | -24.72 |
| | | 11 | -25.72 |
| | | 6 | -24.45 |
| | | | |

feed horn without flanges. It can be assumed from the tables that the flanges, under no circumstances contribute to the cross-polarization of the system on the other hand in some cases it improves the situation. This is found to be true for all the three horns used in the study.

This result is particularly significant since the two orthogonally polarized beams are used for doubling the number of channels (frequency re-use) available on a microwave circuit without installing another antenna. Hence this can be utilized to eliminate cross talk between the two orthogonal channels. In this case it is noted that the modified feed does not increase the cross-polarization. In some cases the overall cross-polarization decreases considerably.

The dependence of cross-polarization on the other parameters such as corrugation period, flange angle etc. is not so prominent as can be judged from the tables 4.6(ii)(a to c). The absolute magnitude of the cross-polarization of the system depends on the inherent cross-polarization of the system with horn alone as the feed.

THEORETICAL EXPLANATIONS

5.0 This chapter presents the theoretical interpretation of the results. First an attempt is made to derive the E-plane radiation pattern of the corrugated flanged H-plane sectoral horn feed. It may be recalled here that the secondary reflector antennas radiation patterns are controlled by the feed patterns. So, in order to derive the secondary antenna radiation patterns, it is essential to know the radiation patterns of the feed precisely. As mentioned earlier, a H-plane sectoral horn fitted with corrugated flanges is used as the feed of an offset paraboloidal reflector. The orientation of the flanges is such that corrugations are always parallel to the H-vector of the electromagnetic radiation from the H-plane sectoral horn. This arrangement serves only to modify the E-plane pattern of the H-plane sectoral horn.

5-1 E-plane pattern of H-plane sectoral horn feed fitted with corrugated flanges

The E-plane pattern is mainly determined by the flange parameters such as flange width, position relative to the horn

aperture, the number of corrugations inside the flanges, and angle between the flanges.

Zachariah et al⁸⁴ have derived an expression for the E-plane radiation pattern of the corrugated flanged H-plane sectoral horn. They have employed the line source theory and by the application of the method of images, derived the expression. A brief discussion of the method is given here for the sake of continuity.

The geometry of the flange mounted horn is as shown in fig.5.1(1). Here, M is the far field point, 'Z' the distance between the point where the two flanges meet and the aperture of the horn, β the half angle between the flanges, B_p the distance between the aperture and the p^{th} element of the corrugated flange, P_n the distance between the meeting point of the corrugated flanges and the p^{th} corrugation element.

It is assumed that the tips of the corrugation elements are excited by the primary horn. These elements then re-radiate the energy. This re-radiation adds up with the direct radiation from the horn aperture. The contribution of the corrugation elements of the two flanges to the field at any point 'M' is calculated as

$$E = [(K \sin \theta + K' \sin \theta')^2 + (K \cos \theta + K' \cos \theta')^2]^{\frac{1}{2}} \quad 5.1(1)$$

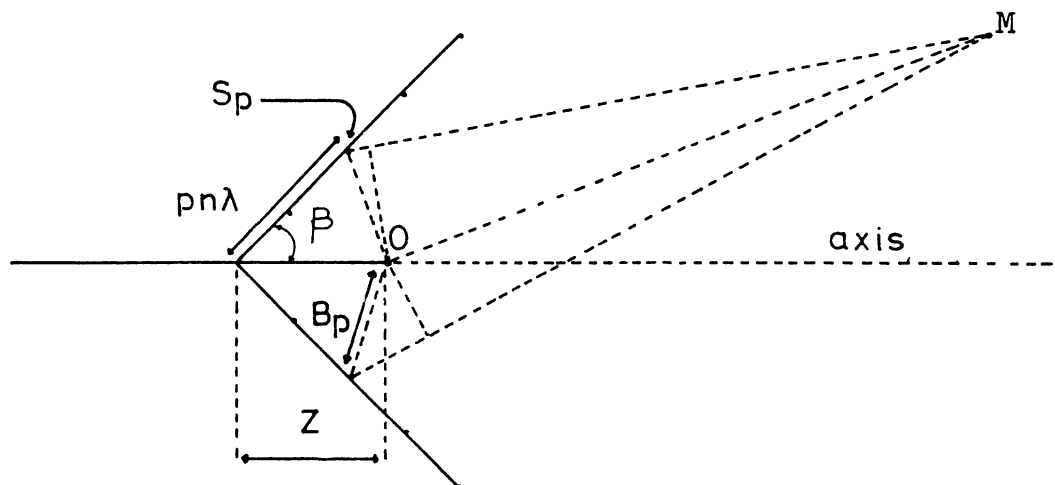


Fig.5.1(1)(a) Geometry of the corrugated flange mounted sectoral horn. O is the horn aperture. S_p is the p^{th} element on the flange surface. B_p is the distance of the p^{th} element from the horn aperture. Z is the distance between the point where the flanges are kept and the horn aperture.

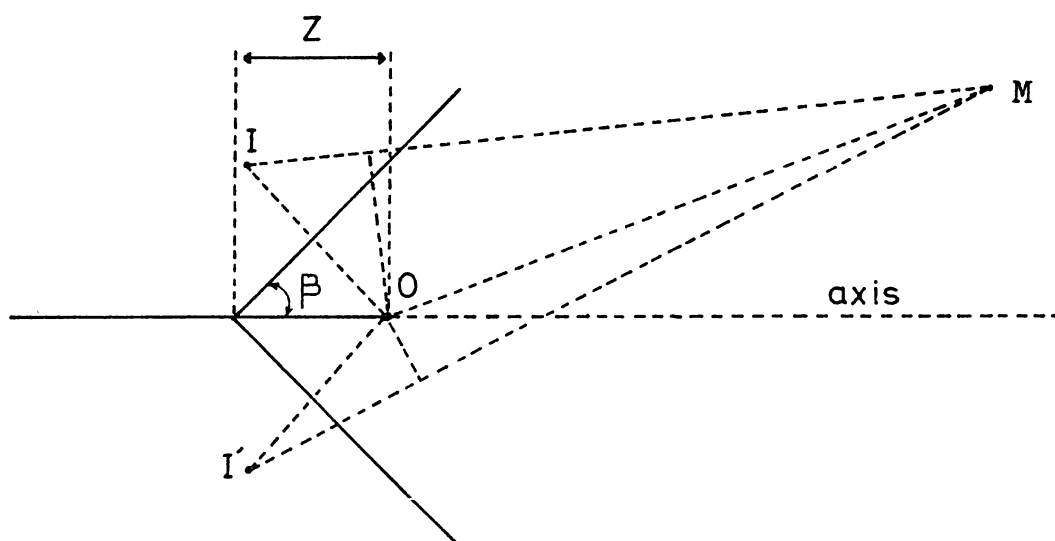


Fig.5.1(1)(b) Geometry of the flange mounted sectoral horn. O is the horn aperture. I and I' are the images of O cast by the flange elements.

To satisfy the limiting conditions, the expression is multiplied by an overall space directivity factor

$$\left(\frac{\cos \theta}{\cos \beta} - 1 \right)$$

Hence

$$E = \left\{ [(K \sin \theta + K' \sin \theta')^2 + (K \cos \theta + K' \cos \theta')^2] \times \left(\frac{\cos \theta}{\cos \beta} - 1 \right) \right\}^{\frac{1}{2}} \quad 5.1(2)$$

where 'K' is the amplitude of the resultant field at M due to the corrugation elements of one flange and ' θ ' the relative phase of this resultant. Similarly K' is the amplitude of the resultant field at 'M' due to the corrugation elements of the other flange and θ' its phase.

The distance $n\lambda$ between the corrugation elements used in this study is of the order of 0.25λ to 0.5λ . This allows the propagation of e.m. waves inside the slot formed by two adjacent corrugation elements. So we have also to take into account the contributions from the two images I and I' to get the total resultant field at M.

The contribution of the aperture, the image due to first flange I and second flange I' is calculated as follows.

$$\text{Amplitude } E_{\theta} = \left\{ 3 + 2[\cos(\delta - \delta') + 2[\cos \delta (1 + \cos(\delta - \delta'))] + \sin \delta \sin(\delta - \delta')] \right\}^{\frac{1}{2}} \quad 5.1(3)$$

and phase

$$\xi' = \tan^{-1} \frac{\sin \delta + \sin \delta'}{1 + \cos \delta + \cos \delta'} \quad 5.1(4)$$

where δ and δ' are the relative phases of I and I'. These can be evaluated as

$$\delta = \frac{2\pi}{\lambda} 2Z \sin \beta \sin(\beta - \theta) \quad 5.1(5)$$

$$\delta' = \frac{2\pi}{\lambda} 2Z \sin \beta \sin(\beta + \theta) \quad 5.1(6)$$

The total resultant field distribution at M due to all radiations is the vector sum of the fields given by the expressions 5.1(1), 5.1(2), 5.1(3), and 5.1(4).

The amplitude of the resultant power at M is given by

$$P_{\theta} = \left\{ [E_{\theta} \sin \xi + E_{\theta}' \sin \xi']^2 + [E_{\theta} \cos \xi + E_{\theta}' \cos \xi']^2 \right\} (1 + \cos \theta) \quad 5.1(7)$$

where $(1+\cos \theta)$ is the common directivity factor for all directions of antenna system.

This is the expression for the E-plane pattern of the corrugated H-plane sectoral horn

$$\text{But } E_{\theta} \propto \sqrt{P_{\theta}} \quad 5.1(8)$$

The H-plane electric field for the horn in the TE_{10} mode is ⁵⁰

$$E_{\theta} = \left\{ \left(\frac{\gamma}{K_0} \right)^2 + \cos \theta \right\} \frac{\cos (K_0 A \sin \theta \cos \phi)}{1 - \frac{(2K_0 A \sin \theta \cos \phi)^2}{\pi}} \frac{\sin K_0 B \sin \theta \sin \phi}{K_0 B \sin \theta \sin \phi} \cos \phi \quad 5.1(9)$$

$$\text{where } K_0 = \frac{2\pi}{\lambda}, \quad \gamma = \frac{2\pi}{\lambda_g}$$

A = E-plane half width of the rectangular horn

B = H-plane half width of the rectangular horn.

For evaluating the secondary radiation pattern we should know $P(\theta, \phi)$, i.e., the power density in any direction θ and ϕ . From the two known orthogonal plane patterns namely $P(\theta)$ & $P(\phi)$

the power pattern at any direction (θ, ϕ) , is taken as the geometrical mean of the two quantities.

$$\text{i.e., } P(\theta, \phi) = \sqrt{P_{\theta} \times P_{\phi}} \quad 5.1(10)$$

Substituting 5.1(8), and 5.1(9) for E_{θ} and E_{ϕ} in 5.1(10) we get

$$\begin{aligned} P(\theta, \phi) = & \left[\left\{ (E_{\theta} \sin \xi + E'_{\theta} \sin \xi')^2 + (E_{\theta} \cos \xi + E'_{\theta} \cos \xi')^2 \times (1 + \cos \theta) \right\} \right. \\ & \times \left[\left(\frac{\gamma}{K_0} \right)^2 + \cos \theta \right] \frac{\cos(K_0 A \sin \theta \cos \phi)}{1 - \left(\frac{2K_0 A \sin \theta \cos \phi}{\pi} \right)^2} \\ & \left. \times \frac{\sin K_0 B \sin \theta \sin \phi}{K_0 B \sin \theta \sin \phi} \cos \phi \right]^{\frac{1}{2}} \quad 5.1(11) \end{aligned}$$

This can be written as

$$\begin{aligned} P(\theta, \phi) = & \left[\left\{ (E_{\theta} \sin \xi + E'_{\theta} \sin \xi')^2 + (E_{\theta} \cos \xi + E'_{\theta} \cos \xi')^2 \right\} \times (1 + \cos \theta) \right]^{\frac{1}{2}} \\ & \times \left[\left\{ \left(\frac{\gamma}{K_0} \right)^2 + \cos \theta \right\} \frac{\cos(K_0 A \sin \theta \cos \phi)}{1 - \left(\frac{2K_0 A \sin \theta \cos \phi}{\pi} \right)^2} \right. \\ & \left. \times \frac{\sin K_0 B \sin \theta \sin \phi}{K_0 B \sin \theta \sin \phi} \cos \phi \right] \quad 5.1(12) \end{aligned}$$

This is the final feed power pattern.

5.2 Secondary radiation pattern

A number of approximations are made in finding the far field pattern of the offset paraboloid reflector. It is assumed that the currents on the shadow region of the reflector have negligible effect on the far field pattern since it is a fully solid surface. The edge effects are also neglected and the pattern on the shadow side of the reflector is not obtained. For the sake of simplicity of the analysis, the radiation fields of the paraboloid are separated into four regions.

- (1) Primary feed region near the focus containing the feed, giving rise to the feed pattern. $P_f(\theta, \phi)$, which is assumed not to be influenced by interactions with the reflector.
- (2) The reflector region with the surface currents due to the fields of the primary feed flowing only on the inner surface of the reflector, which is considered to be a perfect conductor.
- (3) An aperture region usually taken as a plane surface through the focus normal to the paraboloid as shown by the dotted circle in fig.5.2(1).

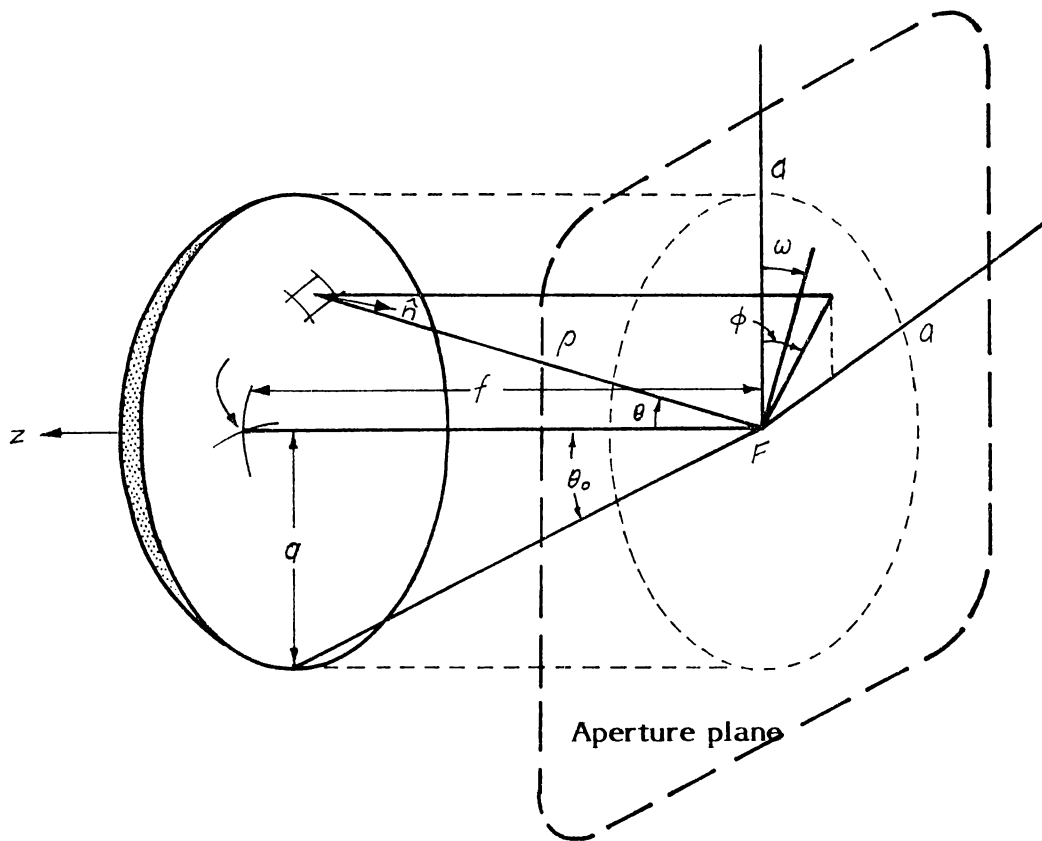


Fig. 5 . 2 (1) : Polar , cylindrical and rectangular coordinates defining paraboloid of revolution , reflector and its aperture plane (dotted circle) .

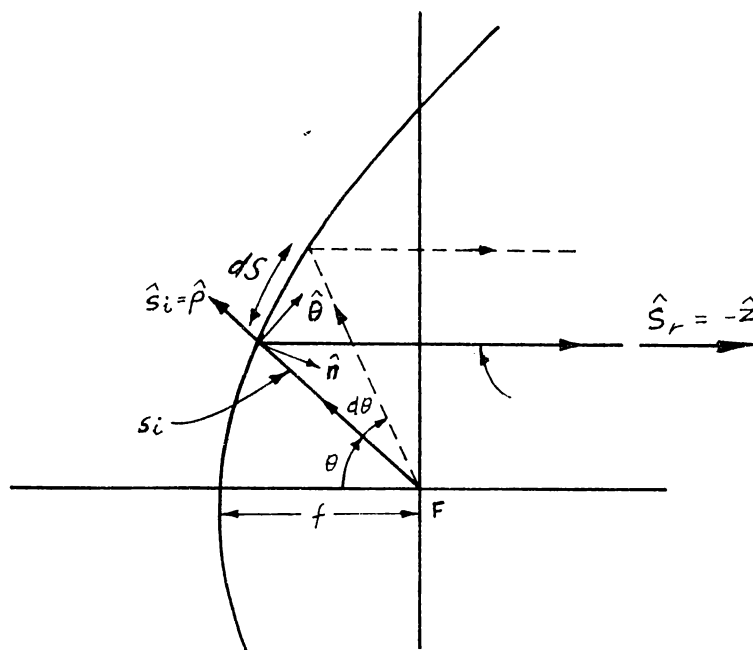


Fig. 5 . 2 (2) : Cross section of paraboloid showing optical rays .

- (4) The exterior region containing the diffraction fields including the Fresnel field (near-field) and Fraunhofer field (Far-field) region.

For all practical purposes, only the far field region is of any interest. So, here only the far field pattern of the offset paraboloid is derived.

Geometrical optics method⁵⁶ is employed here for the analysis of the reflector fields. Each differential area on the reflector is treated as a large conducting mirror and the Snell's law is applied. The geometry of the cross section of the paraboloid showing optical rays is as shown in fig.5.2(2).

Here \vec{S}_i is the direction of the incident ray and \vec{S}_r is the direction of the reflected ray, \vec{n} is the inner normal.

Applying Snell's law

$$\vec{n} \times (\vec{S}_i + \vec{S}_r) = 0 \quad 5.2(1)$$

$$\text{or } \vec{S}_r = \vec{S}_i - 2(\vec{S}_i \cdot \vec{n})\vec{n} \quad 5.2(1)$$

By applying the boundary conditions for a perfect conductor

$$\vec{n} \times (\vec{E}_r + \vec{E}_i) = 0$$

$$\vec{n} \cdot \vec{E}_r = \vec{n} \cdot \vec{E}_i$$

$$\text{or } E_r = 2(\bar{n} \cdot E_i)\bar{n} - E_i \quad 5.2(2)$$

For TEM waves the surface current density

$$J_s = \bar{n} \times (H_i + H_r) \quad 5.2(3)$$

where

$$H_i = \sqrt{\frac{\epsilon_o}{\mu_o}} (\bar{S}_i \times E_i) \quad 5.2(4)$$

$$H_r = \sqrt{\frac{\epsilon_o}{\mu_o}} (\bar{S}_r \times E_r) \quad 5.2(5)$$

Using 5.2(1), 5.2(2), 5.2(3), 5.2(4) and 5.2(5) we get

$$J_s = 2(\bar{n} \times H_i) = 2\sqrt{\frac{\epsilon_o}{\mu_o}} [\bar{n} \times (\bar{S}_i \times E_i)] \quad 5.2(6)$$

and also

$$J_s = 2(\bar{n} \times H_r) = 2\sqrt{\frac{\epsilon_o}{\mu_o}} [\bar{n} \times (\bar{S}_r \times E_r)] \quad 5.2(7)$$

The reflected electric field E_r can be written in terms of gain function, and total power radiated by the feed as

$$E_r = \sqrt{2\left(\frac{\mu_o}{\epsilon_o}\right)^{\frac{1}{4}} \left(\frac{P_f}{4\pi}\right)^{\frac{1}{2}}} \frac{[G_f(\theta, \phi)]}{e} e^{-jK_o r} \cdot \bar{e}_r \quad 5.2(8)$$

The gain function $G_f(\theta, \phi)$ of the feed can be evaluated as

$$G_f(\theta, \phi) = \frac{4\pi P_f(\theta, \phi)}{P_t} \quad 5.2(9)$$

To represent the far field radiation patterns, we denote the far field point P as (R, θ, ϕ) in spherical coordinates as shown in fig.5.2(3).

The far field scattered field intensity is

$$E = \frac{-j\omega\mu_0}{4\pi R} e^{-jk_0 R} \int_S [(J_s - J_s \cdot \bar{R}) \bar{R}] e^{jk_0 \bar{e} \cdot \bar{R}} ds \quad 5.2(10)$$

Since we are using a horn arrangement as feed the contribution to the far field by direct radiation can be neglected.

Now taking components of equation 5.2(10) we get

$$E_\theta = -\frac{j\omega\mu_0}{4\pi R} e^{-jk_0 R} \int_S \bar{\theta} \cdot J_s e^{jk_0 \bar{e} \cdot \bar{R}} ds \quad 5.2(11)$$

and

$$E_\phi = -\frac{j\omega\mu_0}{4\pi R} e^{-jk_0 R} \int_S \bar{\phi} \cdot J_s e^{jk_0 \bar{e} \cdot \bar{R}} ds \quad 5.2(12)$$

Using equation 5.2(8) in equation 5.2(7) and taking into

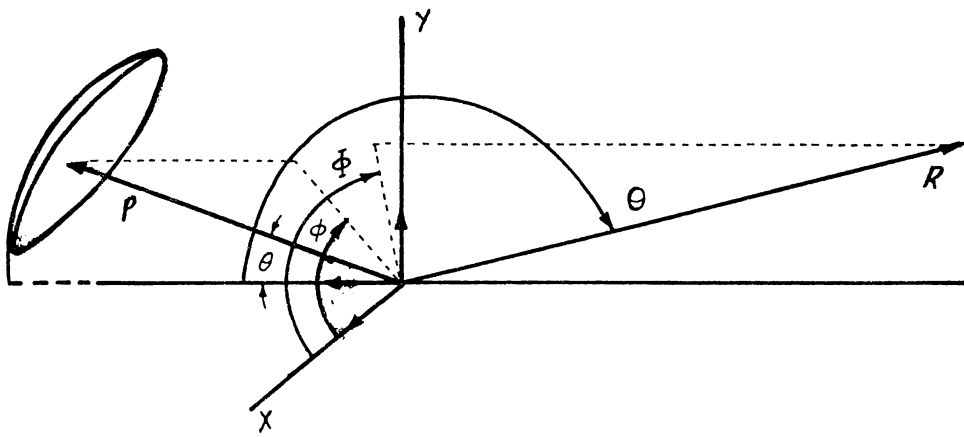


Fig. 5.2 (3) Coordinates used to express the far fields of a paraboloid .

consideration the fact that the reflected ray is in-Z direction, we get

$$J_s = 2\sqrt{2} \left(\frac{\epsilon_0}{\mu_0}\right)^{\frac{1}{4}} \left(\frac{P_t}{4\pi}\right)^{\frac{1}{2}} \frac{[G_f(\theta, \phi)]}{e} \bar{n} \times (-\bar{z} \times \bar{e}_r) e^{-jK_0 \rho} \quad 5.2(13)$$

To interpret the equation 5.2(11), we have to evaluate the

integral $\int_s J_s e^{jK_0 \rho \cdot \bar{R}} ds$ using the equation 5.2(13)

$$\begin{aligned} \text{i.e., } \int_s J_s e^{jK_0 \rho \cdot \bar{R}} ds &= 2\sqrt{2} \left(\frac{\epsilon_0}{\mu_0}\right)^{\frac{3}{4}} \left(\frac{P_t}{4\pi}\right)^{\frac{1}{2}} \\ &\times \int_0^{2\pi} \int_0^{\theta_0} \frac{[G_f(\theta, \phi)]}{e} \times \bar{n} \times (-\bar{z} \times \bar{e}_r) \\ &\times e^{-jK_0 \rho} [1 - \cos \theta \cos \theta - \sin \theta \sin \theta \cos(\phi - \phi)] \\ &\times e^2 \sin \theta \sec \frac{\theta}{2} d\theta d\phi \end{aligned} \quad 5.2(14)$$

This can be written as

$$\begin{aligned} 2\sqrt{2} \left(\frac{\epsilon_0}{\mu_0}\right)^{\frac{1}{4}} \left(\frac{P_t}{4\pi}\right)^{\frac{1}{2}} \int_0^{2\pi} \int_0^{\theta_0} \frac{[G_f(\theta, \phi)]}{e} \left[\cos \frac{\theta}{2} \bar{e}_r - (\bar{n} \cdot \bar{e}_r) \bar{z}\right] \\ \times e^{-jK_0 \rho} [1 - \cos \theta \cos \theta - \sin \theta \sin \theta \cos(\phi - \phi)] \\ \times e^2 \sin \theta \sec \frac{\theta}{2} d\theta d\phi \end{aligned}$$

We can simplify the term $\cos(\frac{\theta}{2}) \bar{e}_r - (\bar{n} \cdot \bar{e}_r) \bar{z}$ to $\cos(\frac{\theta}{2}) \bar{e}_r$ for narrow beams, and using the fundamental properties of parabola, the above equation becomes

$$2\sqrt{2} \left(\frac{\epsilon_0}{\mu_0}\right)^{\frac{1}{4}} \left(\frac{P_t}{4\pi}\right)^{\frac{1}{2}} \int_0^{2\pi} \int_0^a \frac{[G_f(\theta, \phi)]^{\frac{1}{2}}}{\rho} \bar{e}_r \quad 5.2(15)$$

$$\times e^{-jK_0 r \sin\theta \sin\phi} r d\phi dr$$

where $\rho = \frac{4f^2 + r^2}{4f}$ and $r = \rho \sin\theta$

'a' is the limit of the integration in the Y-plane which is the dimension of the paraboloid in that plane.

Hence

$$E_\theta = \frac{-j\omega\mu_0}{2\pi R} e^{-jK_0(R+2f)} \times 2\sqrt{2} \left(\frac{\epsilon_0}{\mu_0}\right)^{\frac{1}{4}} \left(\frac{P_t}{4\pi}\right)^{\frac{1}{2}} \\ \times \cos\theta \int_0^{2\pi} \int_0^a \frac{[G_f(\theta, \phi)]^{\frac{1}{2}}}{\rho} e_r e^{-jK_0 r \sin\theta \sin\phi} r d\phi dr$$

After simplification it becomes

$$E_\theta = \frac{-j}{\lambda R} \frac{\mu_0}{\epsilon_0} e^{-jK_0(R+2f)} \sqrt{2} \cos\theta \\ \times \int_0^{2\pi} \int_0^a \frac{[P_f(\theta, \phi)]^{\frac{1}{2}}}{\rho} \bar{e}_r e^{-jK_0 r \sin\theta \sin\phi} r d\phi dr \quad 5.2(16)$$

Referring to fig.5.2(2) we can evaluate \bar{e}_r as

$$\bar{e}_r = \frac{\bar{x} \sin \vartheta \cos \vartheta (1 - \cos \Theta) - \bar{y} (\sin^2 \vartheta \cos \Theta + \cos^2 \vartheta)}{\sqrt{1 - \sin^2 \vartheta \sin^2 \Theta}} \quad 5.2(17)$$

Since we are dealing here only with waves with dominant polarization along the Y-axis we can ignore the x-components in equation 5.2(17) hence

$$\bar{e}_{ry} = \frac{-(\sin^2 \vartheta \cos \Theta + \cos^2 \vartheta)}{\sqrt{1 - \sin^2 \vartheta \sin^2 \Theta}} \quad 5.2(18)$$

Substituting for e_r in equation 5.2(16) by equation 5.2(18), we get

$$E_\Theta = \frac{-j}{\lambda R} \left(\frac{\mu_0}{R_0} \right)^{1/4} e^{-jK_0(R+2f)} \sqrt{2} \cos \Theta \int_0^{2\pi} \int_0^a \left[\frac{P_f(\Theta, \vartheta)}{e} \right]^{1/2} \\ \times \frac{-(\sin^2 \vartheta \cos \Theta + \cos^2 \vartheta)}{\sqrt{1 - \sin^2 \vartheta \sin^2 \Theta}} e^{-jK_0 r \sin \Theta \sin \vartheta} r d\vartheta dr \quad 5.2(19)$$

Replacing $P_f(\theta, \phi)$ by the equation 5.1(12) we can get the final expression for the E-plane radiation pattern of the offset paraboloid.as

$$\begin{aligned}
 E_{\theta} = & \frac{-j}{\lambda R} \left(\frac{\mu_0}{\epsilon_0} \right)^{\frac{1}{4}} e^{-jK_0(R+2f)} \sqrt{2 \cos \theta} \int_0^{2\pi} \int_0^{103} \left\{ [E_{\theta} \sin \xi + E' \sin \xi']^2 + \right. \\
 & \left. + [E_{\theta} \cos \xi + E' \cos \xi']^2 \right\} (1 + \cos \theta)^{\frac{1}{4}} \\
 & \times \left[\left\{ \left(\frac{\gamma}{K_0} \right)^2 + \cos \theta \right\} \times \frac{\cos (K_0 A \sin \theta \cos \phi)}{1 - \left(\frac{2K_0 A \sin \theta \cos \phi}{\pi} \right)^2} \right. \\
 & \left. \times \frac{\sin (K_0 B \sin \theta \sin \phi)}{K_0 B \sin \theta \sin \phi} \cos \phi \right]^{\frac{1}{2}} \times \frac{1}{e} \\
 & \times \left\{ - \frac{(\sin^2 \phi \cos \phi + \cos^2 \phi)}{\sqrt{1 - \sin^2 \phi \cdot \sin^2 \theta}} \right\} e^{jK_0 r \sin \theta \sin \phi} r d\phi dr
 \end{aligned}$$

5.2(20)

The above integral was evaluated using numerical methods in Fortran language. The patterns obtained using the trapezoidal rule were not consistent and hence the more accurate Wedder's rule was adopted. Using this algorithm, the real part, imaginary part and absolute value of the integral were computed for different values of $\lambda, \gamma, N, Z, \mu,$ and β . For each combination of

these parameters, the integral was found varying from -90° to $+90^\circ$, in steps of 1° . The program took about 150 seconds on a P.S.I. micro computer to give one point on the curve with the minimum of 6×6 points in the domain of integration. This is the most approximated form of integration and even then the time of execution was found to be too long for any practical use. So, the program was run on a main frame NORX data 500 computer (one of the fastest available in India). The patterns obtained were highly symmetric but they were broader than the experimental ones. This is due to the approximation errors involved in the integration procedure on the machine. The machine can run at stretch for only a few hours, which is too short considering the time required to plot each point on the curve. With 175×175 points in the domain of integration, each point took more than one minute. Therefore, the plotting of the theoretical patterns using equation 5.2(20), was possible only in a restricted way. The generated theoretical patterns suggested further modification in the theoretical approach. This has been tried with various approximations and the computations were repeated. The disparity between the theoretical and experimental radiation pattern was conspicuous and efforts were made to reduce this to the minimum. A few theoretical patterns are presented with the experimental results in fig.5.2(4).

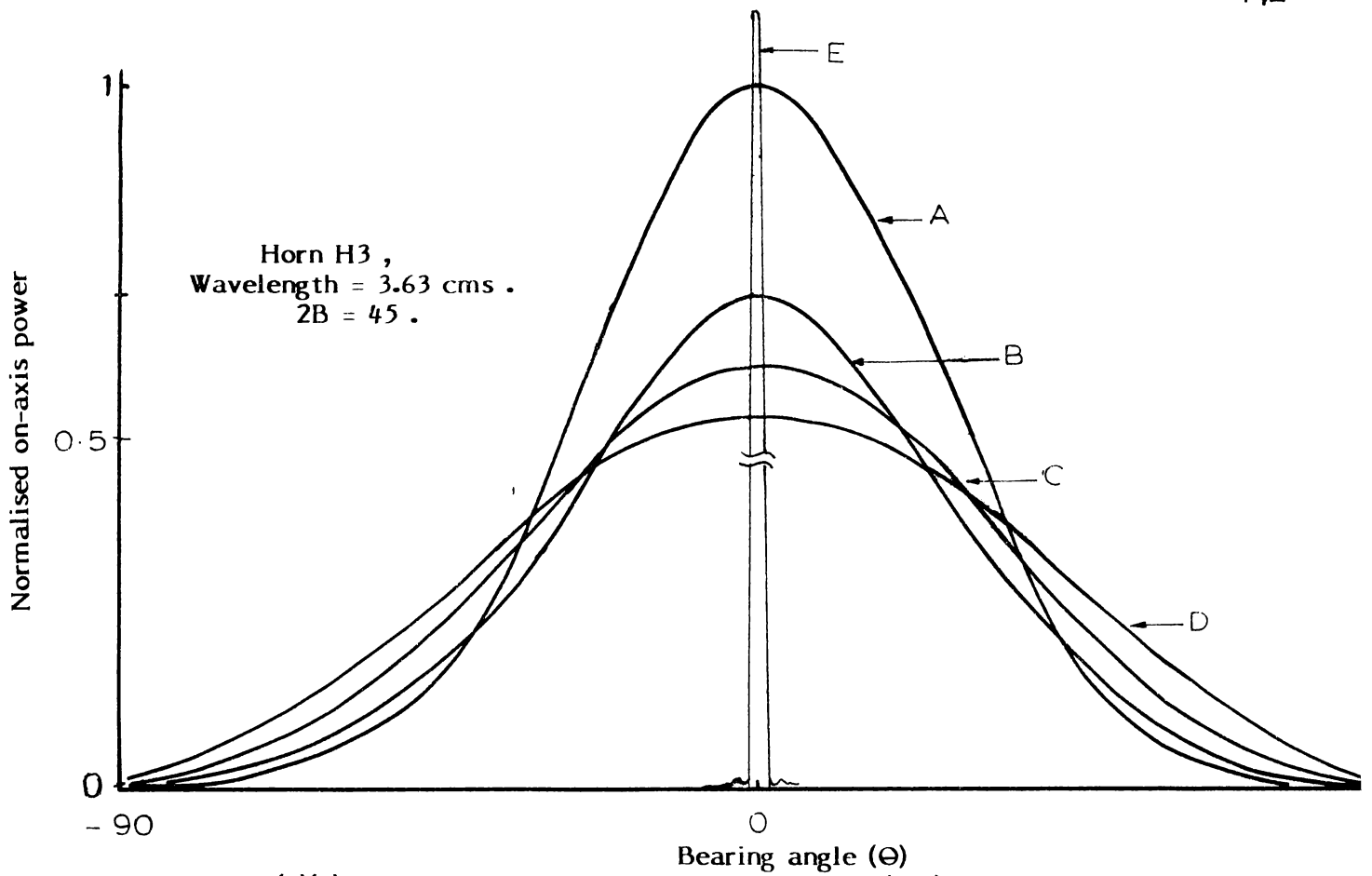


Fig. 5 . 2 (4)(a): Theoretical patterns with experimental (E) pattern for different steps of integrations A = 175 , B = 13 , C = 7 and D = 1

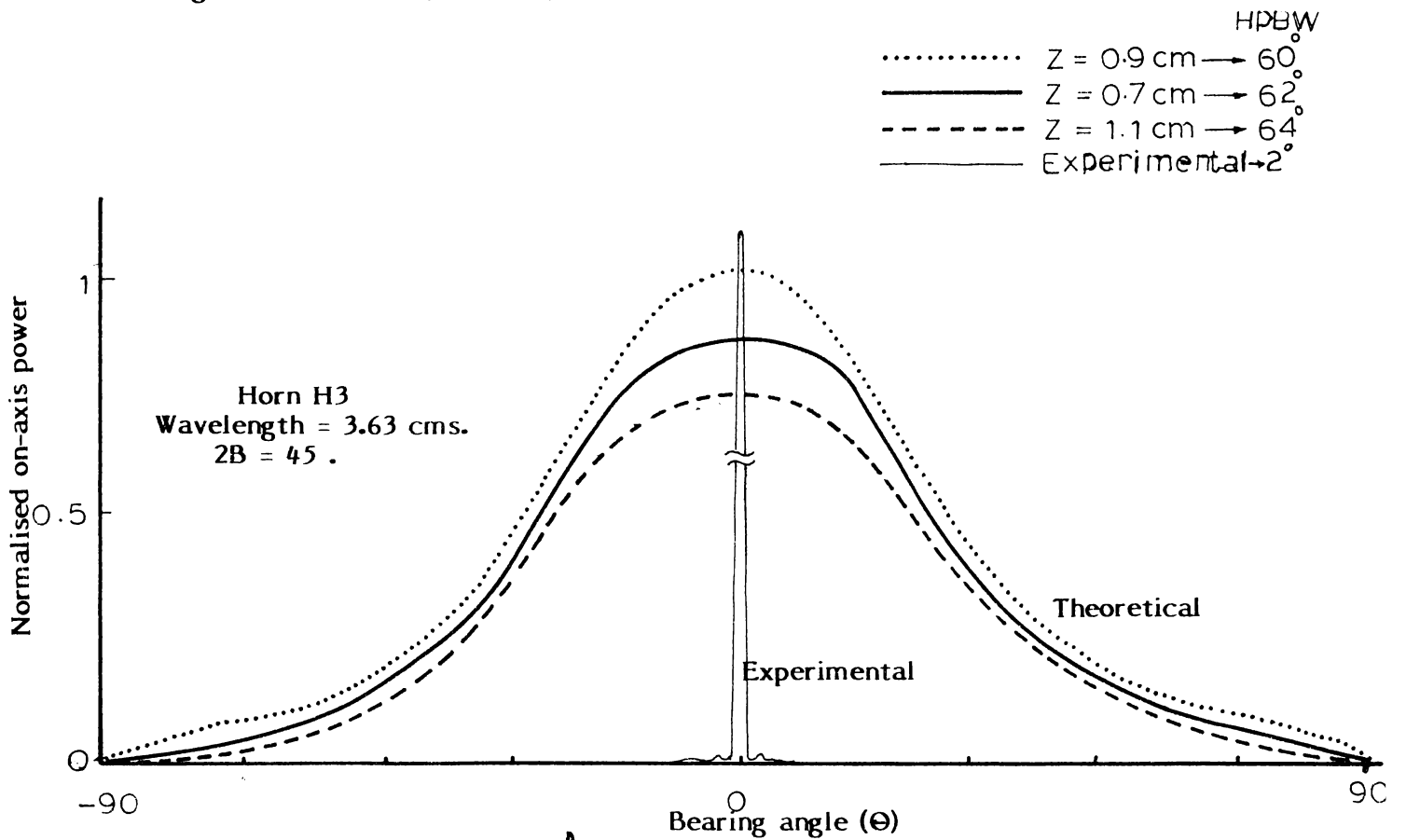


Fig. 5 . 2(4)(b) : Theoretical patterns along with experimental pattern as the flanges move away from the horn aperture

The basic expressions for the primary radiation pattern given in the equation 5.1(7) was derived by earlier workers using a combinational method of line source theory and method of images. There appears to be a little flaw in the approach. Once the line source corresponding to the corrugations are taken, it is questionable to consider their images.

The theoretical explanation of the results on the basis of a modified primary pattern using line source theory alone could be attempted as an extension of this work. This has been initiated by the author, but is not added as a part of this thesis.

Secondary radiation patterns from paraboloidal reflectors can be modified with considerable gain and precision by beam shaping of primary horn feeds using corrugated flanges. Theoretical explanation of these results on the basis of earlier work needs further modifications using appropriate approximations. The results obtained are applicable in large aperture antennas and reflectors.

Chapter VI

CONCLUSIONS AND SUGGESTIONS FOR FURTHER WORK

6.0 Here the results of the detailed experimental study of the effect of corrugated flanged feed horn, on the secondary pattern of the offset paraboloid is presented. The significance of the work in the present era of satellite communication is also highlighted.

6.1 Experimental conclusions

It may be recalled here that the effect of the various corrugated flange parameters on the VSWR of the system is described in sections 4.1(i), 4.1(ii), 4.1(iii) and 4.1(iv). From these it may be concluded that corrugated flanges give lower VSWR than plane flanges or simple horns for any frequency. But it is evident from the curves in the above sections that it is true only if the flange-parameters are controlled carefully.

Section 4.2(i) show how the on-axis power density varies with flange parameters. It may be safely inferred here that at the optimum positions (O-positions), the corrugated flanges give a much higher on-axis power density than plane

flanges on the horn. This is particularly significant since it is at the same position the VSWR is minimum. In short it may be concluded that corrugated flanges at the '0' positions give maximum on-axis power density with minimum of mismatch.

From section 4.3 it may be seen that at the '0' position of the flanges on the horn generally the antenna system gives a narrower beam.

Although it may be possible to obtain the above three conditions using a corrugated horn³⁰, the flanged feed horn stands unique in that it can be used to trim the antenna parameters to suit a number of applications. For example, to feed a paraboloid a broad beam with a sharp fall off near the edges with minimum of sidelobes is necessary. Further to illuminate a cheese mirror, a beam with null along the axis is needed. Using the flanged feed horn arrangement the above conditions can be easily realized.

6.2 Although the numerical evaluation of the radiation pattern did not coincide exactly with the experimental results, the pattern evaluated was symmetrical about the axis of the paraboloid and the '0' positions of the flanges were also more or less coinciding with the experimental results.

Since we have made an approximation that $(n.e_r)^2 \rightarrow 0$ for narrow beams⁵⁶, the final expression (5.2(20)) will not give the 'M' position patterns properly. The above simplification was mainly effected in order to make the final expression somewhat easier to deal with. Also, we are mainly interested in the 'O' position patterns for all practical purposes. It may be recalled here that an increase in the integration accuracy gives better half power beam-width. So it may be inferred here that one reason for the variation of the theoretical pattern from experimental results is the limit of maximum accuracy obtainable on the computer.

6.3 Suggestions for further work

The first suggestion is that a much more accurate theoretical expression may be derived taking into consideration the inadequacies in the flanged feed pattern. In the final expression the narrow beam approximation may be replaced by a much more general formulation so that any pattern with split beam, widely away from the axis, may also be accounted for. Further, any pattern deterioration due to the surface inaccuracies, alignment errors etc. may be incorporated in the theory. The computer program, as it stands now, consumes a lot of time. This time will only increase if the above modifications are

effected. So, a new algorithm may be developed which will drastically reduce the running time and hence we can have more points in the domain of integration for better accuracy.

Coming to the experimental side, only one offset paraboloid was used, just to establish the better flexibility of the flanged feed horn technique. Reflectors with varying f/D ratios, and surface contours may be used and an optimum relationship between the flanged feed horn parameters and the secondary reflector geometry may be established.

By using asymmetric corrugated flanges on the feed horn the system can be used to have a steerable beam.

The effect of circularly polarized corrugated flanged feed horns on the secondary radiation patterns is not studied here and it may be taken as an immediate follow up work.

The corrugated flanged feed horns may be used to illuminate the hyperboloid subreflector in a Cassegrain dual reflector system.

Corrugations may be made on the above hyperboloid and its effect on the total system may be studied. The

conclusions derived from above indicate wide scope for further work in the corrugated flanged horn fed secondary reflector system.

6.4 Significance of the results in modern communication and satellite links

The geosynchronous orbit is getting crowdier day by day as more and more countries own and operate satellites round the clock. An immediate consequence of the above is that the angular distance between adjacent satellites decreases. Therefore stringent restrictions are placed on the antenna beam characteristics to eliminate mutual interference between individual satellites and unnecessary wastage of energy by beam spreading.

Even on a single satellite two or more beams are simultaneously used to transmit information to different locations. Also it is a common practice to use two orthogonally polarized beams from a single reflector to accommodate two sets of independent channels beamed to the same geographic location.

All these requirements together with the limited space and power available as the satellite demand high efficiency and top performance from the antennas.

The leading satellite companies (Westar, Intelsat etc.) have found that only offset paraboloids can meet the stringent requirements of modern satellite systems. The most attractive properties of the offset paraboloid as mentioned by the satellite companies are the total elimination of aperture blocking due to the feed system thereby reducing the cross polarization, sidelobe levels and preservation of the maximum gain possible from the system.

In the light of this the work carried out here is significant as the above mentioned conditions are met to a fair degree of accuracy within the experimental resources available. A much more sophisticated experimental set up with fully automatic facilities for pattern recordings and analysis may be adopted and the enormous data thus obtained may be processed to find the optimum feed configurations suitable for particular applications.

APPENDIX - I

DEVELOPMENT OF A MICROWAVE ABSORBING MATERIAL

Microwave absorbing materials are used in anechoic chambers, antenna shrouds etc. For satisfactory performance of any anechoic chamber, it is very important that the absorber used should be of very high quality both electrically and mechanically. At present the supply of microwave absorbing material in India is very rare and production of the material is not announced by any industry. The material supplied by a local manufacturer is made of imported polyurethane form. This material is not ideal for the hot and humid atmosphere in our laboratories. Moreover, it is very costly. So an effort is made to develop a microwave absorber using indigenous materials. Natural rubber latex is chosen as the base material since it is stronger than the polyurethane form and available in large quantities at a very competitive price in this part of the country. Electrically also, natural rubber is a better absorber of microwaves than polyurethane form.

To increase the microwave absorption of rubber, materials like carbon and graphite are added to it. These materials are made into fine powder and then mixed with rubber

latex in different proportions to prepare test samples of the new absorbing material. It is found that if the total amount of the foreign materials (carbon, graphite etc.) are made more than 50% by weight of the sample, the mixture does not set. So in all cases the percentage of latex is kept fixed at 50% and remaining 50% is made up of carbon and graphite according to the table shown below (Table A.I(1)).

Table A.I(1) Total percentage by weight 50

| Sample | Carbon | Graphite |
|--------|--------|----------|
| 1 | 0 | 50 |
| 2 | 10 | 40 |
| 3 | 20 | 30 |
| 4 | 30 | 20 |
| 5 | 40 | 10 |
| 6 | 50 | 0 |

Measurement of absorption coefficient of the samples

Absorption coefficient is defined as the ratio of power absorbed by the sample to the power incident on it. But it is very difficult to measure the absolute powers directly so the VSWR method is used here.

In this method the absorber samples are cut in exact pyramidal shape very carefully. All the pyramids cut are of the same size and shape. This is introduced into a waveguide section shorted at one end using an aluminium sheet. The other end is connected to the microwave source through a slotted line and attenuator. The test set up is as shown in fig.A.I(1).

From the VSWR, 'S' the voltage reflection coefficient 'R' is obtained as

$$R = \frac{(S-1)}{(S+1)}$$

The power reflection coefficient $P = R^2$ and power reflection coefficient $\rho = R^2$ and power absorption coefficient is A.

$$\rho + A = 1.$$

So knowing the power reflection coefficient ' ρ ' the power absorption coefficient A is calculated.

The samples were both tested at S and X band microwave frequencies. A comparative analysis of results obtained is shown in Table A.I(2).

Table A.I(2)

| Sample | Frequency in GHz | Absorption coefficient |
|--------|---------------------|---------------------------|
| 1 | 2.5 | 0.6519 |
| | 3.9 | 0.6519 |
| | 4.2 | 0.7084 |
| | 9.3 | 0.6636 |
| 2 | 2.5 | 0.7690 |
| | 3.9 | 0.7599 |
| | 4.2 | 0.8775 |
| | 9.3 | 0.6975 |
| 3 | 2.5 | 0.7296 |
| | 3.9 | 0.6636 |
| | 9.2 | 0.8704 |
| | 9.3 | 0.7884 |
| 4 | 2.5 | 0.8236 |
| | 3.9 | 0.9375 |
| | 4.2 | 0.9559 |
| | 9.3 | 0.8556 |
| 5 | 2.5 | 0.8911 |
| | 3.9 | 0.9804 |
| | 4.2 | 0.9975 |
| | 9.3 | 0.9516 |
| 6 | 2.5 | 0.8631 |
| | 3.9 | 0.9559 |
| | 4.2 | 0.9600 |
| | 9.3 | 0.9271 |

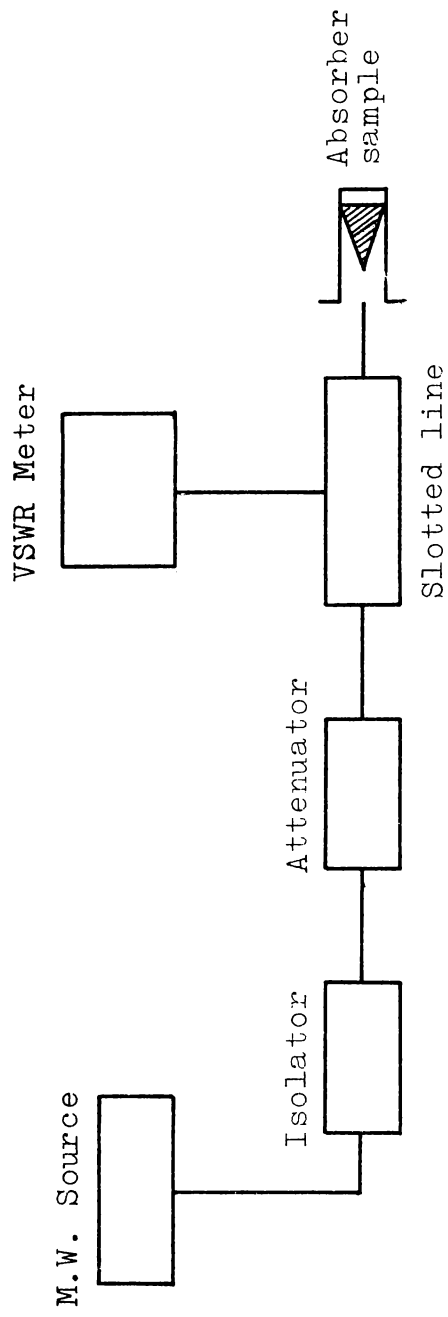


Fig.A.iCD Experimental set up used to measure the absorption coefficient of the different absorber samples.

It can be seen from the table that the sample with 50% rubber, 40% carbon and 10% graphite is the best one as far as absorption coefficient is concerned both in S and X band frequencies.

The results are conveniently displayed in Table A.I(2) The maximum absorption for all frequencies is when the ratio of carbon to graphite is 4:1 in proportion.

It is also found that the absorber samples are mechanically stable. So this samples can be cut into large pyramids (3 inch square base and 12 inches in height) and pasted to vertical walls of an anechoic chamber.

Some of the samples are also made into flat sheet type and its reflectivity is measured in the "Arch method" as shown in fig.A.I(3).

In the experimental set up the sample is a flat sheet of the absorbing material of size 2"x2"x1". This flat sheet is fixed to a plane aluminium sheet as shown in fig.A.I(3). Microwave radiations are directed on to the sheet from a distance of 6 feet at an angle of incidence 45° , and the reflected ray is received according to the laws of reflection in a direction 45° from the normal in the same plane on the

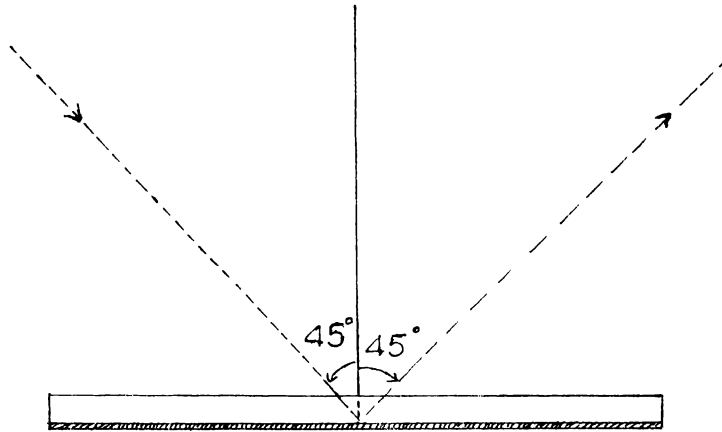


Fig. A I (3) : The 'Arc method' of measuring the reflectivity of a flat absorber sheet.

other side. After this the absorber sample is removed and the aluminium sheet is placed at the same position and the experiment is repeated. In each case the received powers are noted and the reflectivity is calculated as

$$P = 10 \log_{10} \frac{P_A}{P_S}$$

where P_A is the reflected power with absorber and back up plate and P_S is the reflected power with back up aluminium sheet alone.

In this case the measurements are only taken in the X-band frequency of 9.3 GHz. The average reflectivity is found to be more than that of pyramids. But it is found that the flat sheet absorber is an ideal base for sticking the pyramids.

APPENDIX - II

DESIGN, DEVELOPMENT AND PERFORMANCE EVALUATION OF AN ANECHOIC CHAMBER

To know exactly the characteristics of any antenna it is important that all the measurements should be carried out in an interference free environment. But it is practically impossible to get such a region inside an ordinary laboratory. Out-door open space testing of the antennas can only be carried out in favourable weather conditions. Moreover there is every possibility of unwanted signals interfering with the actual signals. So for all weather and round the clock antenna measurements special type of indoor rooms called "anechoic chambers" are constructed. By using absorbing materials and special type of shields a "free space" environment is artificially simulated inside the room. The word "anechoic" means "free of echoes" (referred here for microwave reflections).

The anechoic chamber as mentioned above is a big room well shielded from outside interferences and pasted inside with microwave absorbing materials of various shapes. This absorbing material helps to eliminate the unwanted reflections from the top, bottom and side walls. The performance of the chamber is essentially decided by the quality (absorption

coefficient) of the absorbing material used inside. Quiet zone is a region inside the chamber some distance in front of the back wall usually of spherical or cylindrical in shape, where the total reflection from the walls, roof and bottom of the chamber is below the direct radiation of the transmitting antenna by a certain specified amount⁶¹. Usually a chamber having a quiet zone of an average reflectivity of the order of -35 dB is considered to be fairly good. The antenna or any other device under test is kept at the centre of the quiet zone.

The anechoic chamber described here is of size 7.2 mtrs x 3.6 mtrs x 3 mtrs. The geometry of the chamber is as shown in fig.A.II(1). It is a tapered chamber with the microwave transmitter (Pyramidal horn) kept at the apex of the tapered portion. This shape is chosen with two objectives:

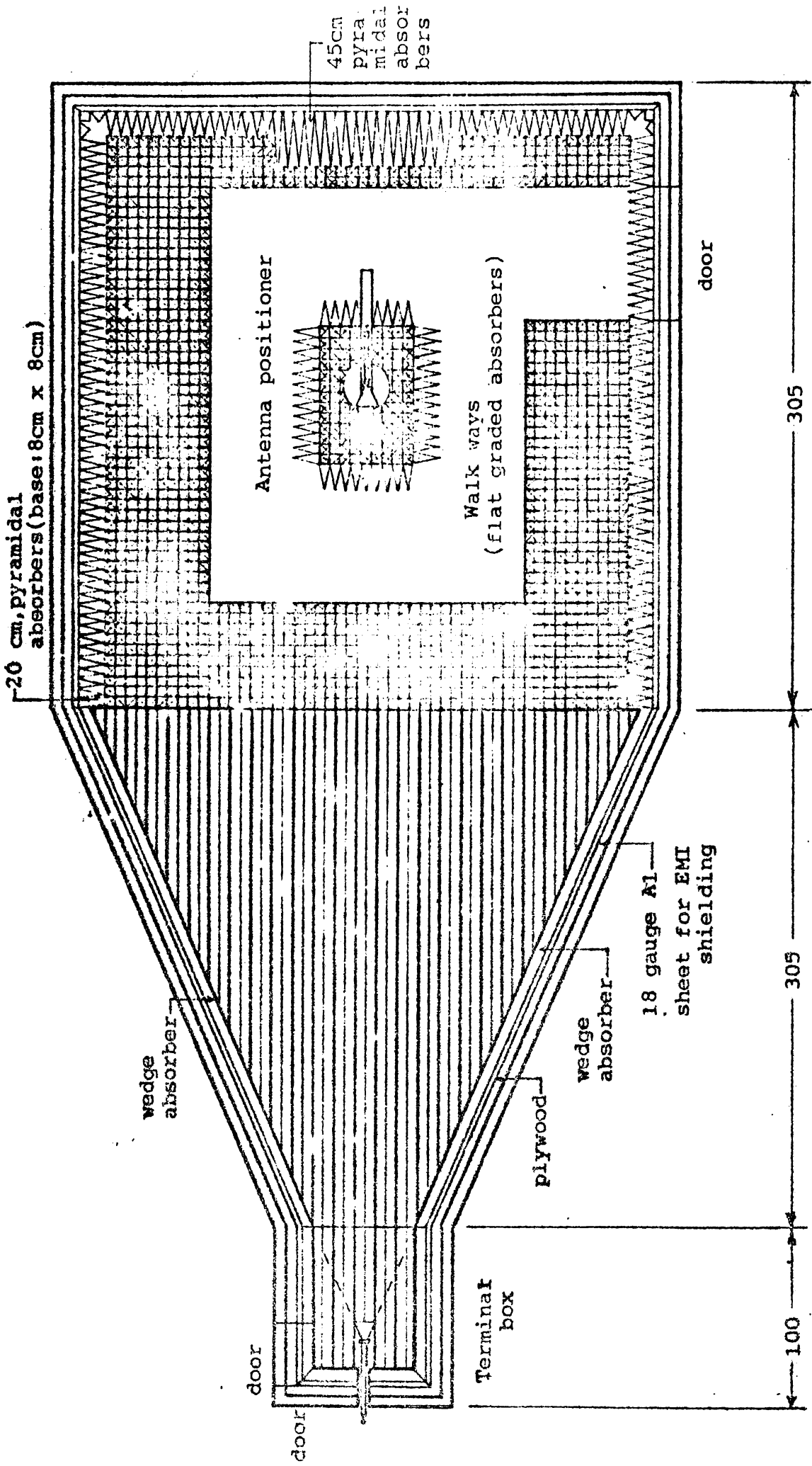
(1) It reduces the area to be covered with absorber which is a costly material.

(2) It gives a more uniform and quieter quiet zone than a rectangular one.

Mainly four types of absorbing materials are used inside the chamber.

COCHIN UNIVERSITY MICROWAVE ANECHOIC CHAMBER

[VIEW FROM THE TOP]



(All dimensions are in cm.)

Fig. A (II) (1)

(1) Small pyramids of base 3 inches square and height 6 inches. These are used to cover the rectangular portions of the chamber except the walk ways and central portion of back wall.

(2) Big pyramids of base 6 inches square and height 18 inches are used on the central portion of the back wall where the intensity of the direct ray is maximum.

(3) Wedges of triangular cross section of base width 4 inches and about 10 inches long having a height of 2 inches are used to cover the lateral sides of the chamber especially the tapered portions where the intensity of the direct ray is not much. The top and bottom sides of the tapered portions are also covered with the wedge shaped absorber.

(4) A graded multi-layered flat absorber of 2 feet square and thickness 8 inches is used to pave the walk ways. The most densely packed absorber going to the bottom and almost pure polyurethane form coming at the top.

The pyramids are pasted on a 2 feet square and 2 inch thick densely packed absorber sheet and these sheets are then finally pasted to the wooden walls using quick drying organic based adhesives.

To avoid interference from any strong external sources the chamber is given a metallic shielding. Aluminium sheets of 20 SWG are nailed over the wooden structure to serve as the shield. The shield is well earthed to prevent any possibility of fringing waves getting into the chamber. Mainly electrostatic shielding is provided by the aluminium shield. The magnetic fields usually encountered in the vicinity of the chamber are not strong enough to disturb the experiments inside the chamber.

The lowest frequency of waves that can be used in the chamber is calculated as 2 GHz. Waves below this frequency will undergo specular reflection from the walls. The chamber is usually used upto 12 GHz without any adverse effects. Since the laboratory is not having any source above 12 GHz it was not possible to test the upper frequency regions. The largest antenna that can be tested for farfield conditions (i.e. $R = \frac{2D^2}{\lambda}$, where 'R' is the distance between the transmitting antenna and antenna under test and 'D' is the largest aperture dimension of the antenna under test, and λ the operating wavelength), is 30 cms for X-band and 56 cms for S-band (R = 720 cms here).

The reflectivity of a chamber is usually measured using any one of the three methods given below, namely:

- (1) the "antenna-pattern comparison" technique,
- (2) "free space VSWR" technique, and
- (3) field probe method.

Out of these three, the first technique of "antenna-pattern comparison" was adopted here to measure the quality of "quiet zone". The average reflectivity determined by this method is about -32 dB at X-band, which is considered to be quiet good. Since almost all the work carried out here is in X-band, the measurements were not carried out on other bands.

Another important characteristic of the chamber determined is its termination VSWR. Usually the termination VSWR of the "anechoic" chambers is so small that conventional method of measuring the VSWR with a slotted section cannot be adopted since the mismatch in the section itself will be more than the chamber mismatch. So the "moving termination"⁶¹ technique was employed here to find the termination VSWR. It is found that the value of the termination VSWR measured using above method is 1.05 which is quite satisfactory.

Instrumentation

The 'anechoic chamber' is equipped with automatic facilities for plotting the radiation patterns. The heart of this is the remote controlled antenna positioner and X-Y plotter.

The antenna positioner was locally fabricated with heavy duty gear systems and a 1 H.P. 3-phase motor. A good quality linear potentiometer is used to get the information regarding angle of rotation. A brush and ring arrangement is used to take out the received power after rectification at the detector mount attached to the test antenna. The signal corresponding to the angle of rotation is fed to the X-axis of the plotter and the rectified microwave power to Y-axis. With this apparently simple arrangement it is possible to plot the radiation pattern for 180° at a stretch with a good degree of accuracy and repeatability.

The antenna positioner is controlled remotely by the control unit kept inside the control room adjacent to the chamber just behind the transmitting end. The control unit is having the following facilities:

- (1) Master ON/OFF switch
- (2) ON/OFF switch for the 3-phase motor
- (3) Forward/Reverse switch
- (4) Direction of rotation indicator
- (5) Position of the antenna indicator
- (6) Received power indicator

- (7) Limit switch with disabling facility
- (8) Provision for the DC signal to the angle indicating potentiometer.

All the signals to and from the chamber are routed only through the control unit. The signals corresponding to X- and Y-axes are taken out from the control unit via two UHF connectors fitted on the top of the panel. All the cables carrying AC, DC and detected power are doubly shielded from each other to avoid any mutual coupling between them and also with any outside disturbances.

Other instruments like VSWR meter, X-Y plotter, microwave power meter, power supply for the microwave source etc. are kept close to the control unit for easy accessibility and ease of operation.

It may be noted that the simple antenna positioner described here can plot patterns in only one plane. For the fear of added cost and complexity of fabrication, the above limitation was persisted upon.

APPENDIX - III

AXIALLY SYMMETRIC RADIATION PATTERNS FROM FLANGED E-PLANE SECTORAL HORN FEEDS

It is well known that flanges can shape the E-plane radiation patterns of H-plane sectoral horns. But very little work has been done on the effect of metallic flanges on the radiation patterns of E-plane sectoral horns. In this section, a brief report of the work done by the author in the above field is presented.

An antenna having equal E- and H-plane patterns was proposed by Kay³⁰. He showed that grooved walls in a horn would present the same boundary conditions for TM and TE waves and hence give symmetric radiation patterns. It was reported⁴⁹ that an E-plane sectoral horn fitted with plane metallic flanges can have a beam with adjustable characteristics. But it may be noted that no work has been so far done on the effect of corrugated flanges on E-plane sectoral horn. This chapter describes in brief the work initiated by the author in this direction.

The experimental arrangement is as shown in fig.A.III(1).

(1) is the microwave source (Gunn diode), (2) isolator which isolates the source from the rest of the circuit. (3) is the variable attenuator, (4) is the slotted line section used for the measurement of VSWR, (5) is the E-plane sectoral horn with corrugated metal flanges with corrugations parallel to the E-vector. The flange system can be slid back and forth along the length (Z) of the horn. A linear potentiometer attached to the Z-axis provides a DC voltage proportional to Z. This arrangement facilitates the automatic plotting of the Z vs. On-axis power density throughout the experiment.

The parameters of the different E-plane sectoral horns used in the study are as shown in Table A.III(1). Table A.III(2) gives the parameters of the various corrugated flanges used in the study.

Measurement techniques

The experiment is carried out in two steps: (1) The variation of the on-axis power and VSWR with the flange position, (2) Plotting the radiation patterns.

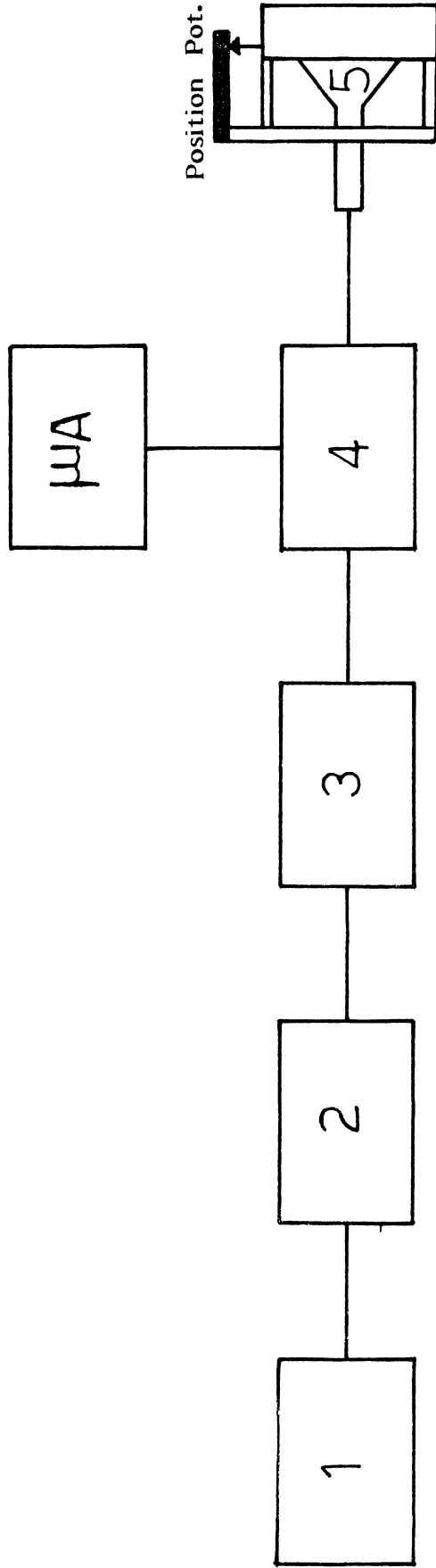


Fig. A III (1) : Experimental arrangement to study the variation of on-axis power and VSWR with position of the flanges on the E - plane horn .
 (1) Gunn diode source , (2) isolator , (3) variable attenuator , (4) slotted section for VSWR studies , (5) E - plane sectoral horn with flanges .

Table A.III(1)

| Horn | Flare angle (°) | Aperture width | |
|----------------|--------------------|----------------|----------------|
| | | H-plane cms | E-plane cms |
| E ₁ | 60 | 2.3 | 11 |
| E ₂ | 60 | 2.3 | 15.3 |
| E ₃ | 45 | 2.3 | 8.6 |

Table A.III(2)

Parameters of flanges
Flange width = 10 cms

| Flange No. | Number of corrugations (n) | Corrugation width (d) cms |
|------------|----------------------------|---------------------------|
| 1 | 0 (plane) | -- |
| 2 | 6 | 1.66 |
| 3 | 8 | 1.25 |
| 4 | 11 | 0.90 |
| 5 | 14 | 0.714 |
| 6 | 19 | 0.526 |

The flanged E-plane sectoral horn is used as the transmitter and a standard pyramidal horn as the receiver in the first part for measuring on-axis power and VSWR. A distance of greater than $(d_1^2 + d_2^2)/\lambda$ is maintained between the transmitter and receiver to get far field conditions, where d_1 and d_2 are the larger aperture dimensions of the transmitting and receiving horns respectively. The received power is rectified and fed to the Y-axis of the X-Y plotter and the DC signal corresponding to the flange position is fed to the X-axis. The flange system is then moved backwards from the aperture of the E-plane horn at a uniform slow speed and the variation of the on-axis power density with the position of the flanges is traced by the recorder. The VSWR at the point where the power is maximum is also measured using the slotted section and VSWR meter. This experiment is repeated for all the three E-plane horns and flanges mentioned in Tables A.III(1) and A.III(2). The VSWR of the E-plane horns without flanges and the corresponding on-axis powers are also noted for the comparative study.

The set up for plotting radiation pattern is as shown in fig.A.III(2).

Here the standard pyramidal horn is used as the transmitter and the flanged E-plane sectoral horn as the

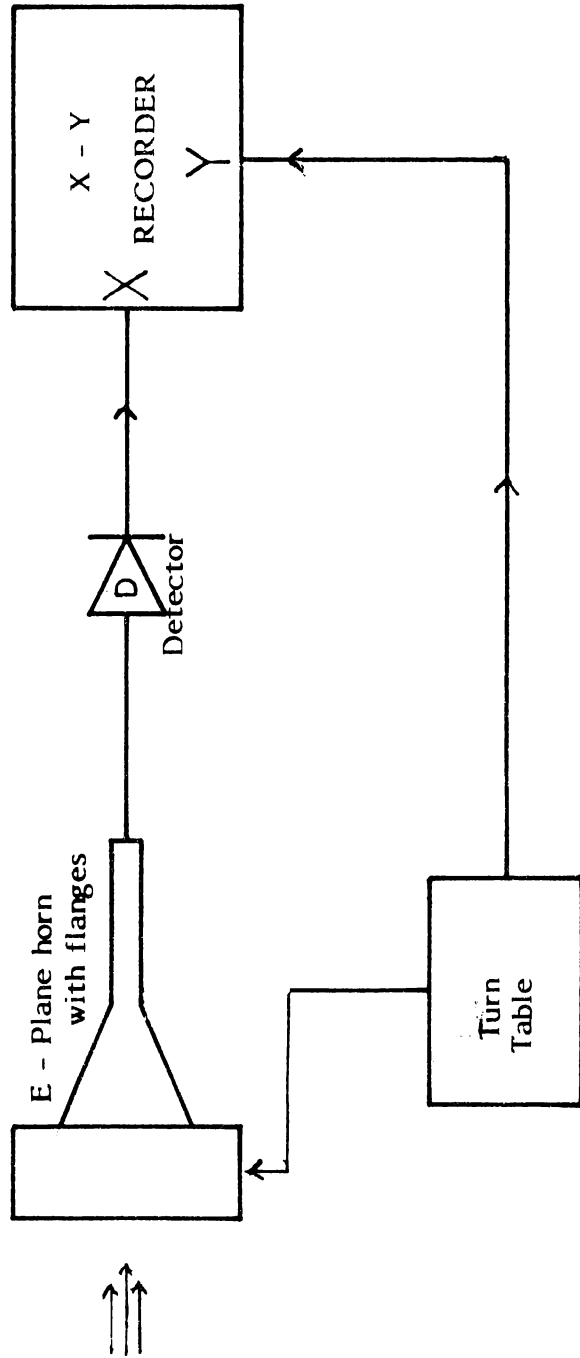


Fig. A (III) (2) ; Arrangement to plot the radiation patterns .

receiver. This part of the experiment is carried out inside an anechoic chamber in order to avoid strong reflections from walls and other objects. The received microwave power in the test antenna kept in the quiet zone is rectified using a crystal detector and fed to the Y-axis of the plotter and the DC signal corresponding to the angular position of the E-plane horn is fed to the X-axis. The radiation patterns of both E- and H-planes of the E-plane horn are plotted only for the corrugated flanged horn at the '0' position (i.e., maximum on-axis power) as we are only interested in making the beam sharper.

Experimental results

1. Variation of on-axis power with position of the flanges (Z)

As the flanges are moved towards the aperture, the on-axis power increases. Maximum on-axis power is obtained when flanges are near the aperture of the horn.

This was found to be true for all types of flanges, i.e., plane as well as corrugated as shown by the curves in fig.A.III(3). Table A.III(3) shows the improvement of on-axis power P_0 when flanges are fitted at the '0' position on the E-plane horn. Experimental data for three different E-plane horns with six different flange pairs and three angles is shown in Table A.III(3).

Table A.III(3)

| Flange Number | Horn E ₁ | | | Horn E ₂ | | | Horn E ₃ | | |
|------------------|---------------------|-------|-------|---------------------|-------|-------|---------------------|-------|-------|
| | Flange angle | | | Flange angle | | | Flange angle | | |
| | 30° | 45° | 60° | 45° | 60° | 90° | 30° | 45° | 60° |
| 1 | 11.64 | 15.95 | 11.68 | 16.15 | 16.18 | 6.57 | 12.38 | 12.69 | 11.71 |
| 2 | 10.53 | 12.81 | 10.81 | 18.39 | 17.21 | 10.88 | 12.28 | 15.69 | 11.50 |
| 3 | 11.10 | 10.55 | 10.81 | 18.40 | 15.01 | 7.23 | 13.70 | 13.68 | 10.76 |
| 4 | 7.00 | 15.32 | 6.49 | 11.47 | 15.36 | 9.59 | 11.69 | 14.97 | 8.82 |
| 5 | 10.76 | 15.80 | 12.97 | 19.62 | 15.50 | 8.53 | 11.93 | 14.47 | 10.76 |
| 6 | 11.69 | 15.25 | 13.73 | 19.22 | 13.40 | 9.91 | 13.52 | 13.84 | 11.87 |

Reference E-plane horns without flanges (0 dB).

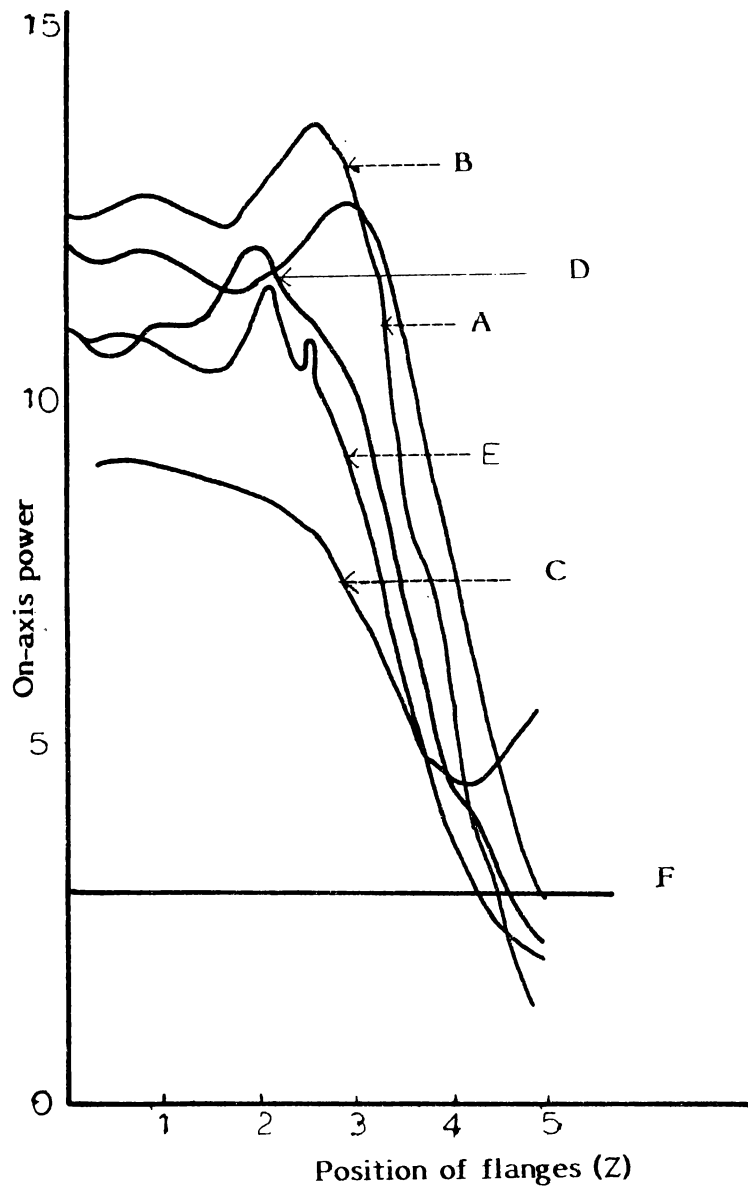


Fig. A III (3) : The effect of position of flanges on the on-axis power .
E - Plane horn .

$2B = 60$, corrugation nos. A = 19, B = 14 , C = 11 ,
D = 8 , E = 6 , and F horn alone .

2. Variation of VSWR with position of the flange

It is noted that the effect of the flanges on the VSWR of the system is not so much pronounced for all flanges and horns.

3. Effect of the number of corrugations (n) on the on-axis power P_o

For a particular horn and flange angle (2β), the on-axis power varies with the number of corrugations ' n ' as shown in fig.A.III(4). The frequency is fixed.

4. Variation of on-axis power P_o with flange angle

The on-axis power density P_o varies considerably with the flange angle 2β . A number of curves for plane and corrugated flanges are shown in fig.A.III(5). The optimum flange angle depends on the particular flange in use. For example, the flange with eleven corrugations, the maximum power is for a flange angle of 45° . It may be mentioned here that all other parameters like frequency, flange width etc. are kept constant.

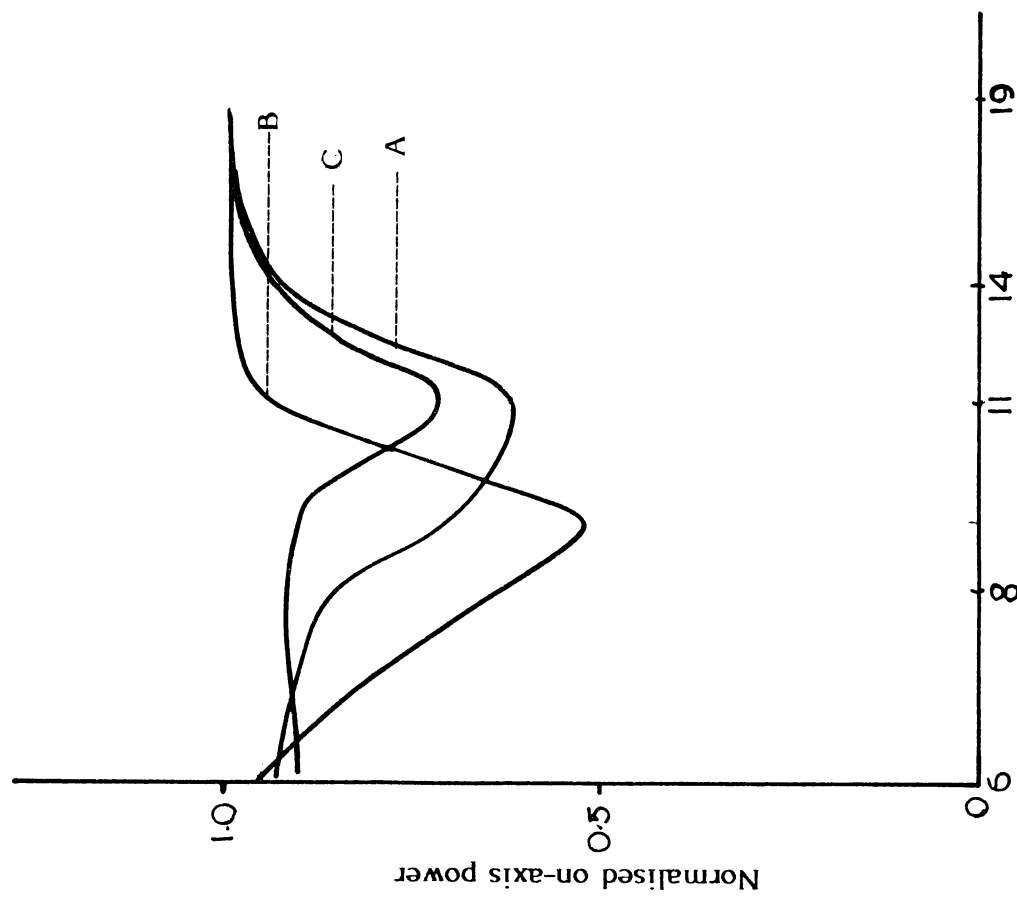


Fig. A (III) (4) : Effect of number of corrugations on the on-axis power (Curves A,B,C are for 2B = 30,45, and 60 respectively)

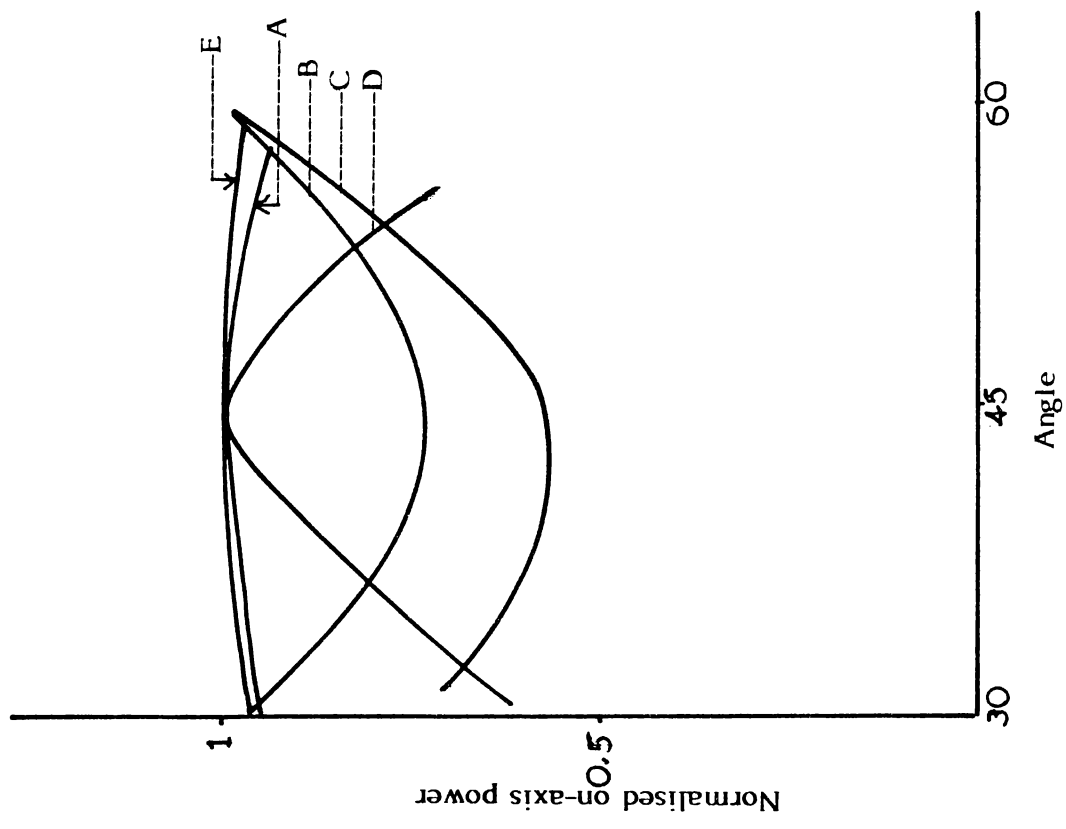


Fig. A (III) (5) : Variation of on-axis power with flange angle (Curves A,B,C,D and E are for corrugation numbers 0,6,8,11 and 14 respectively .)

5. Effect of flanges on radiation patterns

The flanges particularly corrugated ones affect the H-plane radiation pattern of the E-plane horn as shown in fig.A.III(6).

This radiation pattern was taken by keeping the flange system at the '0' position. The curves 'b' and 'c' are the H- and E-plane patterns of the E-plane sectoral horn after modification. From the figure it is clear that the flange system can be used to get axially symmetric patterns from a highly asymmetric sectoral horn antenna. The typical data before and after modification is as shown below:

| | |
|----------------------------------|------------|
| Gain of the natural E-plane horn | = 17.25 dB |
| E-plane HPBW before modification | = 21.79° |
| H-plane HPBW before modification | = 74.35° |
| E-plane HPBW after modification | = 21.79° |
| H-plane HPBW after modification | = 22.26° |
| Gain of the modified system | = 24.97 dB |

From the data, it is clear that the flanges on the E-plane horn serves only to modify the H-plane pattern just like the H-plane aperture of a pyramidal horn.

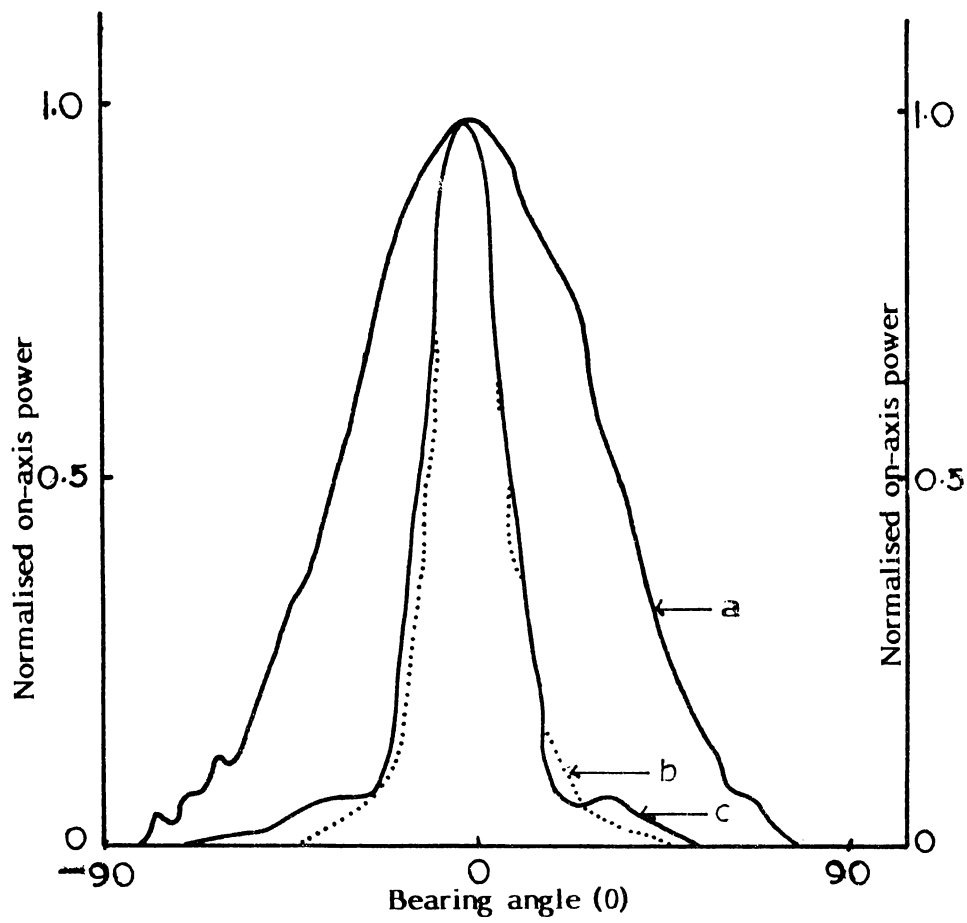


Fig. A III (6) : Effect of flanges on the radiation patterns of the E - plane horn.
 (a) radiation pattern without flanges (H - plane) , (b) shaped H - plane pattern
 (c) E - plane pattern of the E - plane horn .

From the experiment, it is noted that corrugated flanges with the corrugation distance of the order of $\lambda/2$ is the most effective.

Conclusion

It has been found that the metallic corrugated flanges satisfying certain conditions are very effective in modifying the H-plane patterns of E-plane sectoral horns. By a judicious choice of various parameters, it is very easy to trim the H-plane pattern almost close to the E-plane pattern so as to get an axially symmetric pattern suitable to feed a circular parabolic antenna. This development gives a flexibility which is unattainable with the fixed corrugated horn feeds.

REFERENCES

1. K.G.Jansky, "Electrical disturbances apparently of extra-terrestrial origin", Proc.IRE, 21(10), 1933, pp.1387-1398.
2. G.Reber, "Cosmic static", Astrophys.J, 100(3), 1944, pp.279-287.
3. J.Ashmead and A.B.Pippard, "The use of spherical reflectors as microwave scanning aeri-als", J.Inst.Elec.Engg., Part IIIA, 93(4), 1946, pp.627.
4. A.R.G.Owen and L.G.Reynolds, "The effect of flanges on the radiation patterns of small horns", J.Inst.Elec.Engg., Vol.93, 1946, pp.1528-1535.
5. C.C.Cutler, "Parabolic antenna design for microwaves", Proc.IRE, Vol.35, Nov.1947, pp.1284-1294.
6. R.C.Spencer, "A least square analysis of the effect of phase errors on antenna gain", Air Force Cambridge Research Laboratories, Ref.E5025, 1949.
7. R.C.Spencer, C.J.Sletten and J.E.Walsh, "Correction of spherical aberration by a phased line source", Proc. of the National Electronics Conference, Vol.5, 1949, pp.320-333.
8. C.G.Montgomery, "Techniques of microwave measurements", McGraw-Hill Book Company Inc., New York, 1949.

9. Samuel Silver, "Microwave antenna theory and design", McGraw-Hill Book Company Inc., New York, 1949.
10. John D.Kraus, "Antennas", McGraw-Hill Book Company Inc., 1950.
11. J.Ruze, "The effect of aperture errors on the antenna radiation pattern", Nuovo Cimento Suppl.,9(3), 1952, pp.364-380.
12. S.A.Schelkunoff and H.T.Friis, "Antennas : theory and practice", Wiley, New York, 1952.
13. E.M.T.Jones, "Paraboloid reflector and hyperboloid lens antennas", IRE Trans.Antennas Propagat, Vol.2, July 1954, pp.119-127.
14. D.K.Cheng, "Effect of arbitrary phase errors on the gain and beam width characteristics of radiation pattern", IRE Trans.Antennas Propagat, July 1955, pp.145-147.
15. David Carter, "Phase centres of microwave antennas", IRE Trans.Antennas Propagat, Vol.4, Oct. 1956, pp.597-600.
16. J.Robieux, "Influence de la precision de fabrication dune antenne Sur ses performance", Ann.Radio Electricite, 11(43), 1956, pp.29-56.

17. D.K.Cheng, "On the simulation of Fraunhofer radiation patterns in the Fresnel region", IRE Trans.Antennas Propagat. Vol.5, Oct. 1957, pp.399-402.
18. R.H.Brown and A.C.B.Lowell, "The exploration of space by radio", John Wiley, 1957, New York.
19. J.F.Ramsey, "Microwave antenna and waveguide techniques before 1900", Proc.IRE, 46(2), 1958, pp.405-415.
20. P.C.Butson and G.T.Thomson, "The effect of flanges on the radiation patterns of waveguides and sectoral horns", J.Inst.Elec.Engg. Vol.106, Pt.B, 1959, pp.422-426.
21. R.N.Bracewell, "Tolerance theory of large antennas", IRE Trans.Antennas Propagat. 9(1), 1961, pp.49-58.
22. Peter U.Hannan, "Microwave antennas derived from the Cassegrain telescope", IRE Trans. Antennas Propagat. Vol.9, March 1961, pp.140-153.
23. S.Hariharan and K.Gopalakrishnan Nair, "An experimental investigation of the change in the radiation patterns in the Fresnel's region of sectoral electromagnetic horn antennas due to shorting grills", J.Inst.Telecom.Engg., Vol.7, 1961, pp.189-196.
24. S.Hariharan and K.Gopalakrishnan Nair, "Impedance matching of sectoral electromagnetic horn antennas by shorting grills", J.Inst.Telecom.Enggrs., Vol.8, 1962, pp.246-251.

25. W.V.T.Rusch, "Scattering from a hyperboloidal reflector in a Cassegrainian feed system", IEEE Trans.Antennas Propagat. Vol.11, July 1963, pp.414-421.
26. A.C.Schell, "The diffraction theory of large aperture spherical reflector antennas", IEEE Trans.Antennas Propagat. July 1963, pp.428-432.
27. P.D.Potter and A.C.Ludwig, "Beam shaping by use of higher order modes in conical horns", North East Electronics Research and Engineering Meeting, Boston, Massachusetts, Vol.5, 1963, pp.92-93.
28. P.A.Jensen, "A low-noise multimode Cassegrain monopulse feed with polarisation diversity", North-East Electronics Research and Engineering Meeting, Boston, Massachusetts, Vol.5, 1963.
29. F.S.Holt and E.L.Bouche, "A Gregorian corrector for spherical reflectors", IEEE Trans.Antennas Propagat. Vol.12, Jan.1, 1964, pp.44-47.
30. A.E.Kay, "The scalar feed", Air Force Cambridge Research Laboratories Report No.64-347, 1964.
31. Victor Galindo, "Design of dual reflector antennas with arbitrary phase and amplitude distributions", IEEE Trans. Antennas Propagat. Vol.AP-12, July 1964, pp.403-408.

32. W.H.Watson, "The field distribution in the focal plane of a paraboloidal reflector", IEEE Trans.Antennas Propagat. Vol.12, Sept.1964, pp.561-569.
33. The Bao Vu, "The effect of phase errors on the forward gain", IEEE Trans.Antennas Propagat. Vol.13, Nov. 1965, pp.981-982.
34. William F.Williams, "High efficiency antenna reflector", Microwave Journal, Vol.8, July 1965, pp.79-82.
35. John Ruze, "Antenna tolerance theory - A review", Proc. IEEE, Vol.54, April 1966, pp.633-640.
36. Irwin Koffman, "Feed polarization for parallel currents in reflectors generated by conic sections", IEEE Trans. Antennas Propagat. Vol.14, Jan. 1966, pp.37-40.
37. H.C.Minnett and B.Mac A.Thomas, "A method of synthesizing radiation patterns with axial symmetry", IEEE Trans. Antennas Propagat. Vol.14, No.5, 1966, pp.654-656.
38. V.H.Rumsey, "Horn antennas with uniform power patterns around their axes", IEEE Trans.Antennas Propagat. Vol.14, No.5, 1966, pp.656-658.
39. R.E.Lawrie and L.Peters Jr., "Modifications of horn antennas for low sidelobe levels", IEEE Trans.Antennas Propagat. Vol.14, No.5, 1966, pp.605-610.

40. Mehdi S.Zarghamee, "On antenna tolerance theory", IEEE Trans.Antennas Propagat. Vol.15, 1967, pp.777-781.
41. G.C.McCormick, "A line feed for a spherical reflector", IEEE Trans.Antennas Propagat. Vol.15, Sept.1967, pp.639-645.
42. K.G.Nair and G.P.Srivastava, "Beam shaping of H-plane sectoral horns by metal flanges", J.Inst.Telecom.Engrs. Vol.13, Feb.1967, pp.76-82.
43. Edward C.Jordan, "Electromagnetic waves and radiating systems", Prentice Hall India (Pvt) Ltd., 1967.
44. E.V.Jull, "On the behaviour of electromagnetic horns", Proc.IEEE, Vol.56, Jan. 1968, pp.106-108.
45. K.G.Nair, V.K.Koshy and G.P.Srivastava, "E-plane sectoral horns yield to flange technique", Int.J.Electronics, Vol.24, 1968, pp.93-98.
46. K.G.Nair, G.P.Srivastava, S.B.Singh and V.K.Koshy, "A study of the effect of the relative position of metal flanges on the radiation pattern of H-plane sectoral horn", Int.J.Electronics, Vol.25, 1968, pp.153-164.
47. M.A.K.Hamid, "Diffraction by a conical horn", IEEE Trans. Antennas Propagat. Vol.16, Sept.1968, pp.520-528.

48. K.G.Nair, G.P.Srivastava and S.B.Singh, "Some effects of metal flanges on the radiation pattern of H-plane sectoral horns", J.Inst.Telecom.Engrs., Vol.14, 1968, pp.352-358.
49. V.K.Koshy, K.G.Nair and G.P.Srivastava, "An experimental investigation of the effect of conducting flanges on the H-plane radiation patterns of E-plane sectoral horns", J.Inst.Telecom.Engrs., Vol.14, 1968, pp.519-527.
50. D.Herbison-Evans, "Optimum paraboloid aerial and feed design", Proc.Inst.Elec.Engg. Vol.115, Jan.1968, pp.87-90.
51. T.B.Vu, "Influence of correlation interval and illumination taper antenna tolerance theory", Proc.Inst.Elec.Engg., 116(2), 1969, pp.195-202.
52. M.E.J.Jeuken, "Experimental radiation pattern of the corrugated conical horn antenna with small flare angle", Electronics Letters, Vol.5, No.20, 1969, pp.484-485.
53. K.G.Nair, G.P.Srivastava and S.Hariharan, "Sharpening of E-plane radiation patterns of E-plane sectoral horns by metallic grills", IEEE Trans.Antennas Propagat. Vol.17, Jan. 1969, pp.91-93.

54. J.S.Yu and R.C.Ruddock, "H-plane pattern of a pyramidal horn", IEEE Trans.Antennas Propagat. Vol.17, Sept.1969, pp.651-652.
55. K.G.Nair, G.P.Srivastava and S.Hariharan, "Effect of conducting grills on the E-plane radiation patterns of E-plane sectoral horns", Int.J.Electronics, Vol.26, 1969, pp.561-572.
56. Robert E.Collin and Francis J.Zucker, "Antenna theory Part I and II", Vol.7, McGraw-Hill Book Company, New York, 1969.
57. K.G.Nair, "A modified theory for the radiation pattern of an aperture antenna and two secondary sources excited by the primary", Int.J.Elec. Vol.28, 1970, pp.459-462.
58. M.S.Narasimhan and B.V.Rao, "Hybrid modes in corrugated conical horns", Electronics Letters, Vol.6, No.(2), 1970, pp.32-34.
59. S.B.Cohn, "Flare angle changes in a horn as a means of pattern control", Microwave Journal, Vol.13, No.10, 1970, pp.41-46.
60. V.K.Koshy, K.G.Nair, and G.P.Srivastava, "Analysis of radiation from a flanged aperture antenna", IEEE Trans.Antennas Propagat. Vol.AP-18, May 1970, pp.407-411.

61. Steven Galagan, "Understanding microwave absorbing materials and anechoic chambers Part III & IV", *Microwaves*, April 1970, pp.47-50, and May 1970, pp.69-73.
62. P.J.B.Clarricoats and P.K.Saha, "Propagation and radiation behaviour of corrugated feeds", *Proc.Inst.Elect.Eng.*, 118(9), 1971, pp.1167-1186.
63. V.K.Koshy, K.G.Nair and G.P.Srivastava, "Gain improvement of flanged sectoral horn antennas by flange angle variations", *Indian Journal of Pure and Applied Physics*, Vol.9, July 1971, pp.476-478.
64. L.L.Tsai, D.R.Wilton, M.G.Harrison and E.H.Wright, "A comparison of geometric theory of diffraction and integral equation formulation for analysis of reflector antennas", *IEEE Trans.Antennas Propagat.* Vol.20, Nov.1972, pp.705-712.
65. M.Mizusava and T.Kitsuregawa, "A beam waveguide feed having a symmetric beam for Cassegrain antennas", Paper presented at the International IEEE G-AP Symposium, College of William and Mary, Williamsbury, 1972.
66. T. Shing Chu and R.H.Turin, "Depolarization properties of offset reflector antennas", *IEEE Trans.Antennas Propagat.* Vol.2, May 1973, pp.339-345.

67. Grame L. James and Vassilios Kerdemeldis, "Reflector antenna radiation pattern analysis by equivalent edge current", IEEE Trans. Antennas Propagat. Vol. 21, Jan. 1973, pp. 19-24.
68. A. W. Love, "Scale model development of a high efficiency dual polarised line feed for the Arecibo spherical reflector", IEEE Trans. Antennas Propagat. Vol. 21, No. 5, 1973, pp. 628-639.
69. John R. Cogdell and John H. Davis, "Astigmatism in reflector antennas", IEEE Trans. Antennas Propagat. Vol. 21, July 1973, pp. 565-567.
70. William M. Truman and Constantine A. Balanis, "Optimum design of horn feeds for reflector antennas", IEEE Trans. Antennas Propagat. Vol. 22, July 1974, pp. 585-586.
71. Alan W. Rudge, "Multiple-beam antennas: Offset reflectors with offset feeds", IEEE Trans. Antennas Propagat. Vol. 23, May 1975, pp. 317-322.
72. Alan W. Rudge and N. A. Adatia, "New class of primary-feed antennas for use with offset parabolic reflector antennas", Electronics Letters, Vol. 11, Nov. 27, 1975, pp. 597-599.

73. J.F.Kauffman, William F.Croswell and Leonard J.Jowers,
"Analysis of the radiation patterns of reflector
antennas", IEEE Trans.Antennas Propagat. Vol.24,
Jan. 1976, pp.53-65.
74. J.C.Bennett, A.P.Anderson, P.A.McInnes and A.J.T.Whitaker,
"Microwave holographic meteorology of large reflector
antennas", IEEE Trans.Antennas Propagat. Vol.24,
May 1976, pp.295-303.
75. G.P.Srivastava, K.K.Bhan and R.Baldwin, "Experimental study
of a flange mounted waveguide as a device for square
radiation pattern", IEEE Trans.Antennas Propagat.
Vol.24, Mar. 1976, pp.242-244.
76. K.G.Nair, K.Mohanachandran and K.T.Mathew, "Beam shaping
of sectoral horn by dielectric flanges", Indian J.
Radio Space Phys., Vol.5, Sept. 1976, pp.254-256.
77. S.I.Ghobrial, "Co-polar and cross-polar diffraction images
in the focal plane of paraboloidal reflectors : A
comparison between linear and circular polarisations",
IEEE Trans.Antennas Propagat. Vol.24, July 1976,
pp.418-424.

78. Mehmet Safak and Paul P. Delogne, "Cross-polarization in in Cassegrainian and front-fed paraboloidal antennas", IEEE Trans. Antennas Propagat. Vol. 24, July 1976, pp. 497-501.
79. K.G. Nair and K.T. Mathew, "Effect of flanged sectoral horn primary feeds on the radiation patterns of secondary reflector antennas", J. IETE, Vol. 23, 1977, pp. 148-149.
80. K.G. Nair and P.A. Mathews, "Metallic flanges on sectoral horns as corner reflectors", IEEE Trans. Antennas Propagat. Vol. 25, May 1977, pp. 431-435.
81. C. Dragone, "Characteristics of a broad band microwave corrugated feed : A comparison between theory and experiment", Bell. Syst. Tech. J., Vol. 56, July-Aug. 1977, pp. 869-888.
82. P.K. Agrawal, J.F. Kauffman and U.F. Croswell, "Calculated scan characteristics of a large spherical reflector antenna", IEEE Trans. Antennas Propagat. Vol. 27, No. 3, May 1979, pp. 430-431.
83. E.J. Zachariah, K. Vasudevan and K.G. Nair, "Beam shaping and impedance matching of sectoral electromagnetic horn antennas using corrugated flanges", Indian J. Radio & Space Phys., Vol. 8, Feb. 1979, pp. 24-28.

84. E.J.Zachariah, K.Vasudevan and K.G.Nair, "Metal flanges with more parameters for beam shaping", IEEE Trans. Antennas Propagat. Vol.27, Sept.1979, pp.708-710.
85. Raj Mittra, Yahya Rahmat Samii, Victor Galindo-Israel and R.Norman, "An efficient technique for the computation of vector secondary patterns of offset paraboloid reflector", IEEE Trans.Antennas Propagat. Vol.27, No.3, May 1979.
86. Ovidio M.Bucci, Giuseppe Di Massa and Catello Savarese, "Control of reflector antennas performance by rim loading", IEEE Trans.Antennas Propagat. Vol.29, No.5, Sept.1981, pp.773-779.
87. K.Vasudevan and K.G.Nair, "An analysis of radiation patterns of corrugated corner reflector antenna systems", Indian Journal of Radio & Space Physics, Vol.II, Aug.1982, pp.156-158.
88. Per-Simon Kildol, "Combined E- and H-plane phase centers of antenna feeds", IEEE Trans.Antennas Propagat. Vol.31, No.1, Jan. 1983, pp.199-201.
89. John Huang, Yahya Rahmat-Samii and K.Woo, "A GTD study of pyramidal horns for offset reflector antenna applications", IEEE Trans.Antennas Propagat. Vol.31, No.2, March 1983, pp.305-309.

90. Alan G. Cha and D.A. Bathken, "Preliminary announcement of an 85 percent efficient reflector antenna", IEEE Trans. Antennas Propagat. Vol.31, No.2, March 1983, pp.341-342.

PAPERS PUBLISHED BY THE AUTHOR

1. "Microwave absorbing material using rubber and carbon",
Indian Journal of Pure and Applied Physics, Vol.18,
No.3, 1980, pp.216-218.

2. "Corrugated flanged horn feed for offset paraboloidal
reflectors",
Indian Journal of Radio and Space Physics, Vol.10,
December 1981, pp.246-247.

3. "Axially symmetric radiation patterns from flanged E-plane
sectoral horn feeds",
Indian Journal of Radio and Space Physics, Vol.11,
June 1982, pp.112-115.

4. "Design, development and performance evaluation of an
anechoic chamber for microwave antenna studies",
Indian Journal of Radio and Space Physics, Vol.13,
February 1984, pp.29-31.